

---

# Tropical-cyclone evolution in a minimal axisymmetric model

Christoph Wolf Dieter Jakob Schmidt

---



München 2011



---

# **Tropical-cyclone evolution in a minimal axisymmetric model**

**Christoph Wolf Dieter Jakob Schmidt**

---

Dissertation  
an der Fakultät für Physik  
der Ludwig–Maximilians–Universität  
München

vorgelegt von  
Christoph Wolf Dieter Jakob Schmidt  
aus Fürstenfeldbruck

München, den 27.05.2011

Erstgutachter: Prof. Dr. Roger Smith

Zweitgutachter: Prof. Dr. George Craig

Tag der mündlichen Prüfung: 25.07.2011

# Contents

<b>Abstract</b>	<b>ix</b>
<b>1 Introduction</b>	<b>1</b>
1.1 Overview of tropical cyclones . . . . .	1
1.2 The basic physics of tropical cyclones . . . . .	3
1.3 Paradigms of tropical-cyclone spin-up . . . . .	6
1.3.1 The CISK-paradigm . . . . .	6
1.3.2 The cooperative-intensification paradigm . . . . .	8
1.3.3 The WISHE-paradigm . . . . .	9
1.3.4 The role of vortical hot towers . . . . .	11
1.4 The hurricane boundary layer . . . . .	13
1.5 Motivation . . . . .	15
1.6 Structure of the thesis . . . . .	17
<b>2 Description of the model</b>	<b>19</b>
2.1 Governing equations . . . . .	19
2.2 Parameterization of turbulence . . . . .	20
2.2.1 Surface turbulent fluxes . . . . .	20
2.2.2 Subgrid-scale diffusion . . . . .	21
2.3 Parameterization of convection . . . . .	22
2.4 Explicit moist processes . . . . .	22
2.5 Parameterization of radiative cooling . . . . .	23
2.6 Boundary and initial conditions . . . . .	23
2.7 Numerical methods . . . . .	24
<b>3 Control experiment</b>	<b>25</b>
3.1 Overview of vortex evolution . . . . .	26
3.2 Some details on vortex evolution . . . . .	28
3.3 Spin-up in the model . . . . .	31
3.4 Inertial instability . . . . .	39
3.5 Summary . . . . .	45

<b>4</b>	<b>Rotational influences on the intensity and size of tropical cyclones</b>	<b>47</b>
4.1	The Turner-Lilly-Morton ideas . . . . .	47
4.2	The calculations . . . . .	49
4.3	Dependence on the Coriolis parameter . . . . .	49
4.3.1	Vortex intensity . . . . .	49
4.3.2	Vortex size . . . . .	50
4.3.3	Intensity versus size . . . . .	51
4.3.4	Trajectories . . . . .	52
4.4	Effective forcing . . . . .	53
4.5	An appraisal of the TLM ideas . . . . .	54
4.5.1	Relevance to intensity . . . . .	55
4.5.2	Relevance to size . . . . .	55
4.6	Summary . . . . .	56
<b>5</b>	<b>Rotational influences on the intensity and size - fixed forcing</b>	<b>59</b>
5.1	The calculations . . . . .	59
5.2	Results . . . . .	60
5.3	Interpretation . . . . .	61
5.3.1	Constraints on the secondary circulation . . . . .	62
5.3.2	Factors controlling size . . . . .	64
5.3.3	The role of the boundary layer . . . . .	65
5.3.4	Factors controlling intensity . . . . .	65
5.4	Summary . . . . .	66
<b>6</b>	<b>Sensitivity studies on model parameters and physical processes</b>	<b>69</b>
6.1	Radial resolution . . . . .	69
6.1.1	Introduction . . . . .	69
6.1.2	The calculations . . . . .	70
6.1.3	Results and interpretation . . . . .	70
6.2	Radial diffusion . . . . .	72
6.2.1	Introduction . . . . .	72
6.2.2	The calculations . . . . .	73
6.2.3	Results and interpretation . . . . .	74
6.3	Surface drag coefficient . . . . .	77
6.3.1	Introduction . . . . .	77
6.3.2	The calculations . . . . .	78
6.3.3	Results and interpretation . . . . .	79
6.4	Capped surface enthalpy flux . . . . .	83
6.4.1	Introduction . . . . .	83
6.4.2	The calculations . . . . .	83
6.4.3	Results and interpretation . . . . .	83
<b>7</b>	<b>Summary and conclusions</b>	<b>87</b>

<b>Contents</b>	<b>vii</b>
<b>Appendix</b>	<b>93</b>
<b>Bibliography</b>	<b>95</b>
<b>Acknowledgements</b>	<b>95</b>
<b>Lebenslauf</b>	<b>98</b>





# Zusammenfassung

Diese Arbeit untersucht mithilfe eines axisymmetrischen numerischen Modells die Prozesse, die zur Intensivierung tropischer Zyklone führen. Das Modell ist hydrostatisch, die Modellgleichungen sind in Sigmakoordinaten auf einer  $f$ -Ebene formuliert. Es besteht aus drei Schichten: einer für die Grenzschicht und zwei für die freie Troposphäre.

Insbesondere wird der Einfluss des Coriolisparameters  $f$  auf die Intensität und Größe von tropischen Zyklonen untersucht. In der ersten von zwei Experimentreihen zeigt sich, dass sich die stärksten Stürme bei mittleren Werten von  $f$  entwickeln. Ebenso gibt es einen optimalen Wert von  $f$  im mittleren Bereich, bei dem die größten Stürme entstehen. Diese Ergebnisse scheinen zunächst mit klassischen Laborexperimenten von Turner und Lilly übereinzustimmen. Eine mögliche Analogie dieser Laborexperimente zu tropischen Zyklonen wird eingehend untersucht. Dabei zeigt sich, dass diese Analogie unter anderem aufgrund des in der Grenzschicht stattfindenden Intensivierungsprozesses begrenzt ist. Zum weiteren Verständnis wird eine zweite Experimentreihe durchgeführt. Die modellierten Stürme werden hierbei durch ein vorgeschriebenes Profil der diabatischen Erwärmungsrate angetrieben. Andere Feuchtprozesse werden ausgeschlossen. Es ergibt sich nun kein optimaler Wert von  $f$  für die Intensität der Stürme. Die Beziehung zwischen der Stärke des Antriebs und der Stärke der Rotation ist somit ein wichtiger zusätzlicher limitierender Faktor bei tropischen Zyklonen. Dennoch gibt es einen optimalen Breitengrad für die Größe der Zyklone, vergleichbar mit dem in der ersten Experimentreihe.

Außerdem wird die Sensitivität des Modells bezüglich der horizontalen Auflösung, des Eddy-Diffusions- und Reibungskoeffizienten und der Windgeschwindigkeitsabhängigkeit des Bodenflusses von Enthalpie untersucht. Die Intensität nimmt geringfügig mit größerer horizontaler Auflösung zu, die Größe des Sturms bleibt nahezu unverändert. In Übereinstimmung mit anderen Ergebnissen in der Literatur ist die Intensität stark abhängig vom horizontalen Eddy-Diffusionskoeffizienten. Erhöht man den Reibungskoeffizienten und lässt den Wärmeaustauschkoeffizienten konstant, bewirkt dies eine erhöhte Feuchtekonvergenz und damit einen früheren Beginn der schnellen Intensivierung. Die Intensität am Ende der Simulation nimmt, im Unterschied zu neuesten Ergebnissen von Montgomery *et al.*, jedoch ab. Kappt man die Windgeschwindigkeitsabhängigkeit des Bodenflusses von Enthalpie bei kleinen Werten von  $10 \text{ m s}^{-1}$ , so simuliert das Modell dennoch Stürme mit Intensitäten, die Hurrikanstärke übersteigen. Dies zeigt, dass der in weiten Kreisen akzeptierte ‘Verdunstungs-Wind-Rückkopplungsmechanismus’ nicht wesentlich für die Intensivierung tropischer Zyklone ist.



# Abstract

The processes that lead to the intensification of a weak initial vortex to a mature tropical cyclone are studied using a minimal axisymmetric numerical model. The model is hydrostatic and is formulated in  $\sigma$ -coordinates on an  $f$ -plane. It has three layers in the vertical: one for the boundary layer, and two to represent the free troposphere.

The influence of ambient rotation on the intensity and size of tropical cyclones is investigated. In the first of two sets of experiments, the same initial baroclinic vortex is spun up in a quiescent environment with different levels of ambient rotation, characterized by the Coriolis parameter. It is found that the strongest vortices, as characterized by their final intensity, develop in environments with intermediate ambient rotation. It is found also that there exists a similar optimum ambient rotation rate to obtain the largest storm as measured by the radius of gale-force winds. These results appear to be in line with those of classical laboratory experiments by Turner and Lilly, an analogy that will be explored in this study. The analogy is found to have certain limitations, including the fact that spin up of the inner-core winds in the model takes place in the boundary layer. As an aid to understanding the foregoing results, a second set of calculations is carried out with the vortex forced by a prescribed radial profile of diabatic heating rate typical of that in the first set and other moist processes excluded. For this distribution of heating rate, there is no optimum ambient rotation for intensity within a realistic range of values for the Coriolis parameter, implying that the relationship between the forcing strength and rotation strength is an important additional constraint in tropical cyclones. However, there is an optimum latitude for size, comparable with that in the first set of experiments.

The sensitivity of the model to the radial resolution, the eddy diffusivity, the surface drag coefficient, and the wind-speed dependence of the surface enthalpy flux is examined. The maximum intensity increases only slightly as the horizontal resolution is increased, but the vortex size hardly changes. The maximum intensity is strongly sensitive to the radial eddy diffusivity, consistent with other results in the literature. An increase of the surface drag coefficient while keeping the enthalpy exchange coefficient fixed, leads to an enhanced moisture convergence, and thereby to an earlier onset of rapid intensification. However, the final intensity is reduced, contrary to recent results of Montgomery *et al.* When the wind-speed dependence of the surface enthalpy flux is capped at nominal values as small as  $10 \text{ m s}^{-1}$ , the model is able to produce storms that reach maximum intensities greater than hurricane-strength. Thus, the widely-accepted ‘evaporation-wind’ feedback mechanism is not essential for tropical-cyclone spin-up.



# Chapter 1

## Introduction

### 1.1 Overview of tropical cyclones

A tropical cyclone is the generic term for a non-frontal synoptic scale low-pressure system that forms over warm tropical or sub-tropical oceans with organized convection and definite cyclonic surface wind circulation (Holland 1993). Based on the maximum sustained surface winds<sup>1</sup> as the intensity metric, tropical cyclones are called *tropical depressions* if the intensity is less than  $17 \text{ m s}^{-1}$ . Once the maximum sustained surface winds attain at least  $17 \text{ m s}^{-1}$ , they are termed *tropical storms*. Two regionally specific names are used for tropical cyclones with surface winds of at least  $33 \text{ m s}^{-1}$ : *hurricanes* in the Atlantic and East Pacific and *typhoons* in the Western North Pacific. In this thesis, the terms hurricane and tropical cyclone will be used interchangeably. The main characteristics of a tropical cyclone in its mature stage are the violent rotating winds in an annular region around an inner warm-core region, where the winds are light. The light wind region is termed *the eye* as it is often free of deep clouds. The eye contains the axis of rotation and has a typical radius of about  $15 - 30 \text{ km}$ . The air is slowly subsiding in the eye, which gives rise to adiabatic warming and consequently low surface pressure and low values of humidity. The eye is surrounded by an annular ring of deep convective clouds, named *the eyewall*, which extends through the depth of the troposphere. The strongest tangential wind speeds are found near the surface usually within the eyewall, that extends from the outer edge of the eye radially outwards another  $20 - 50 \text{ km}$  (Emanuel 2003). The tropical cyclone is accompanied by torrential rainfall in the regions of strong convection, *i.e.* in the eyewall and in spiral rainbands. The kinematic structure of the tropical cyclone, including the eye, the eyewall, and spiral rainbands can be seen in the satellite image of Hurricane Katrina (2005) in Fig. 1.1.

Based on the maximum sustained surface (total) wind speed (averaged over one minute) at the standard meteorological 10-m level, a 1 to 5 categorization is used as a tool for

---

<sup>1</sup>In theoretical studies, the maximum tangential wind is usually the preferred intensity metric. In operational communities, however, intensity is defined as a sustained horizontal wind speed at the surface or anemometer level (e.g. 10 m) over some time interval, either a one minute or ten minute average. To keep with the basic research theme of this study, the former definition of intensity will be used.

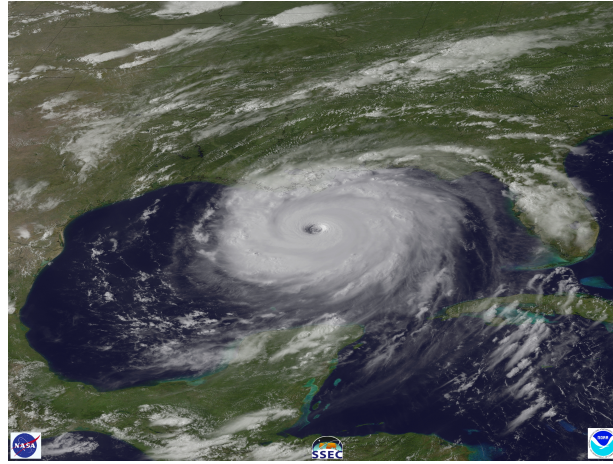


Figure 1.1: High-resolution satellite image of Hurricane Katrina as it hits land on 29 August 2005 (from NOAA/AOML Hurricane Research Division, Miami, FL, USA.)

Table 1.1: Saffir-Simpson Scale.

Saffir-Simpson Scale	Max. Wind speed (mph [ $ms^{-1}$ ])	Damage
1	74-95 [33-42]	Minimal
2	96-110 [43-49]	Moderate
3	111-130 [50-58]	Extensive
4	131-155 [59-69]	Extreme
5	> 156 [ $> 70$ ]	Catastrophic

alerting the public and estimating the potential flooding and damage a hurricane might cause. This so-called Saffir-Simpson Scale (see Table 1.1) is used for the Atlantic and Northeast Pacific basins by the USA (Simpson and Riehl 1981, pp398). Being defined by an intensity metric only, this scale does not refer to other storm characteristics important for considering the possible damage like storm surge, rainfall-induced floods, or the size of the storm, *i.e.* the horizontal extent of strong wind speeds. In theoretical studies (and in this thesis), the size of a tropical cyclone is often defined as the radial extent of gale-force winds ( $17 \text{ m s}^{-1}$ ) near the surface.

Tropical cyclones of Category 3, 4 and 5 are collectively termed as major (or intense), and cause 83 % of the damage in the USA, but they account for only 21 % of all tropical cyclones making landfall (Pielke and Landsea 1998). Although only a Category 3 hurricane at landfall, Hurricane Katrina (2005) caused the most damage with 81 billion US dollars in total loss and more than 2500 lost lives. Until Hurricane Katrina, the list of the costliest mainland US tropical cyclones was topped by Hurricane Andrew (1992). Even though Andrew was a Category 5 hurricane at landfall over Florida, it caused only a third of the damage of Hurricane Katrina.

Being well known from observations, a typical tropical storm initially intensifies gradually before a period of rapid intensification follows. Nearly all major hurricanes, *i.e.* those

that reach Category 3, 4 or 5 on the Saffir-Simpson scale, become major through rapid intensification (Willoughby *et al.* 2007). To date, the skill of forecasting intensity (see footnote 1) by the operational hurricane forecast models still lags behind the skill of forecasting hurricane track (DeMaria *et al.* 2007). In particular, the operational prediction of rapid intensification remains difficult (Elseberry *et al.* 2007, NOAA 2006). Given the threatening impacts of hurricanes that undergo rapid intensification, the Tropical Prediction Center/National Hurricane Center (TPC/NHC) has declared rapid intensification as its top forecast priority (NHC 2008). The reason why rapid intensification remains difficult to forecast is the fact that there is still a general lack of understanding of the physical processes involved (Kaplan *et al.* 2009).

The aim of this thesis is to investigate the mechanisms that are responsible for the intensification process of tropical cyclones. In particular, it will be examined what processes lead to changes in the intensity, as measured by the maximum tangential wind speed, and which mechanisms govern the size, as measured by the radial extent at which the tangential wind speed reaches gale-force ( $17 \text{ m s}^{-1}$ ).

## 1.2 The basic physics of tropical cyclones

A scale analysis of the equations of motion by Willoughby (1979) reveals that the radial and vertical momentum equations governing the azimuthally-averaged motions within a tropical cyclone can be approximated to a good degree by gradient wind balance (except in the boundary layer) and hydrostatic balance, respectively. Hydrostatic balance means, that the upward-directed pressure gradient force is balanced by the gravitational force acting downwards:

$$\frac{1}{\rho} \frac{\partial p}{\partial z} = -g, \quad (1.1)$$

where  $\rho$  is the moist air density,  $p$  is the (total) pressure,  $z$  is the geometric height, and  $g$  is the acceleration due to gravity. This force balance is not valid in regions where small-scale motions such as gravity waves and convection are important. However, the hydrostatic balance assumption is a good approximation for the macro-scale motions of the hurricane.

Provided that the azimuthal-mean tangential wind component squared is very much larger than the corresponding radial component squared and if the frictional force terms are negligible, the gradient wind approximation is valid, which means that the inward-directed radial pressure gradient force is nearly balanced by the sum of the centrifugal and Coriolis forces acting outwards, *i.e.*,

$$\frac{1}{\rho} \frac{\partial p}{\partial r} = \frac{v^2}{r} + fv, \quad (1.2)$$

where  $r$  is the radius from the vortex centre,  $v$  is the tangential velocity component, and  $f$  is the Coriolis parameter,  $2\Omega \sin\phi$ , where  $\Omega$  is the Earth's rotation rate and  $\phi$  is the latitude. Figure 1.2 shows a schematic diagram that illustrates the gradient wind force balance.

The tangential quasi-axisymmetric flow is referred to as the *primary circulation* of the tropical cyclone. Aircraft measurements (Willoughby 1990, Bell and Montgomery 2008) support the validity of gradient wind balance in the lower and middle free troposphere. The gradient wind approximation is disrupted in the (hurricane) boundary layer, that has a typical depth of 500 m to 1 km, as the friction terms can no longer be neglected. In section 1.4, more details on the unbalanced dynamics in the boundary layer are presented highlighting its important role in the spin-up process of tropical cyclones.

Superposed on the primary circulation is the so-called *secondary circulation* depicted also schematically in Fig. 1.2. It describes a thermally-direct transverse (overturning) circulation or “in-up-and-out circulation”. It consists of low and middle level inflow, slant-wise upflow in the eyewall and outflow in the upper troposphere. Combining the primary and secondary circulation, the overall picture is one in which air parcels spiral cyclonically inwards at lower levels, turn upwards in the convective updraughts of the eyewall, and eventually flow outwards in the upper troposphere, forming an upper-level anticyclone. The reason why an anticyclone forms in the upper troposphere is given in due course. The secondary circulation is termed thermally-direct since the rising air in the eyewall is warmer than the subsiding air at large radii. Consequently, potential energy is released (Holton 2004, p339).

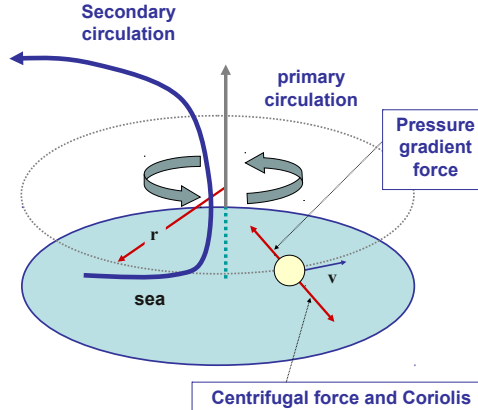


Figure 1.2: Schematic diagram illustrating the primary circulation associated with gradient wind force balance and the secondary circulation. Adapted from Montgomery and Smith (2011).

Another important equation can be derived by cross-differentiating Equations (1.1) and (1.2) and eliminating the pressure. The resulting first-order partial differential equation, termed the *thermal wind equation*, relates the radial and vertical density gradients to the vertical derivative of the tangential wind component:

$$g \frac{\partial \ln \rho}{\partial r} + C \frac{\partial \ln \rho}{\partial z} = - \frac{\partial C}{\partial z}, \quad (1.3)$$



where

$$C = \frac{v^2}{r} + fv \quad (1.4)$$

denotes the sum of the centrifugal and Coriolis forces per unit mass (Smith *et al.* 2005, Smith 2006). The thermal wind equation, which is basically a twin constraint of gradient wind and hydrostatic balance, constitutes a strong constraint on the evolution of a tropical cyclone in regions where these balances are satisfied.

The secondary circulation is just that required to maintain thermal wind balance in the presence of processes (e.g. diabatic heating, azimuthal momentum sources) trying to drive the flow away from such balance. An important diagnostic equation in balance theories that governs the secondary circulation is the so-called *Sawyer-Eliassen equation*. A derivation of the equation for an axisymmetric flow is given by Smith *et al.* (2005) assuming strict gradient wind and hydrostatic balance. The Sawyer-Eliassen equation can be solved for a streamfunction,  $\psi$ , for the overturning circulation satisfying the two relationships:  $u = -1/(r\rho)\partial\psi/\partial z$  and  $w = 1/(r\rho)\partial\psi/\partial r$ , where  $u$  and  $w$  are the radial and vertical velocity components. It takes the following form:

$$\begin{aligned} & \frac{\partial}{\partial r} \left[ -g \frac{\partial\chi}{\partial z} \frac{1}{\rho r} \frac{\partial\psi}{\partial r} - \frac{\partial}{\partial z} (\chi C) \frac{1}{\rho r} \frac{\partial\psi}{\partial z} \right] + \\ & \frac{\partial}{\partial z} \left[ \left( \xi\chi(\zeta + f) + C \frac{\partial\chi}{\partial r} \right) \frac{1}{\rho r} \frac{\partial\psi}{\partial z} - \frac{\partial}{\partial z} (\chi C) \frac{1}{\rho r} \frac{\partial\psi}{\partial r} \right] = \\ & g \frac{\partial}{\partial r} (\chi^2 \dot{Q}) + \frac{\partial}{\partial z} (C\chi^2 \dot{Q}) - \frac{\partial}{\partial z} (\chi C F_\lambda), \end{aligned} \quad (1.5)$$

where  $\chi$  is the inverse of the potential temperature ( $\chi = 1/\theta$ ),  $\xi = 2v/r + f$  is twice the local absolute angular velocity at radius  $r$ ,  $\zeta = (1/r)(\partial(rv)/\partial r)$  is the vertical component of relative vorticity at radius  $r$ ,  $\dot{Q} = d\theta/dt$  is the diabatic heating rate, and  $F_\lambda$  is the tangential component of the azimuthally-averaged force per unit mass (including surface friction). Details of the derivation of the Sawyer-Eliassen equation can be found in Smith *et al.* (2005) and Bui *et al.* (2009). It can be seen from this equation that, in a balanced vortex, the streamfunction is forced both by diabatic heat and tangential momentum sources. Solutions of the Sawyer-Eliassen equation given prescribed point sources of heat and momentum are presented in Shapiro and Willoughby (1982).

In an axisymmetric perspective, vortex spin-up can be illustrated from the equation for absolute angular momentum per unit mass

$$M = rv + \frac{1}{2}fr^2 \quad (1.6)$$

given by

$$\frac{\partial M}{\partial t} + u \frac{\partial M}{\partial r} + w \frac{\partial M}{\partial z} = F, \quad (1.7)$$

where  $F = rF_\lambda$  is the torque per unit mass acting on a fluid parcel in association with frictional, nonaxisymmetric eddy processes, or turbulent forces. If this torque is zero, then the absolute angular momentum per unit mass is materially conserved, *i.e.*  $DM/Dt = 0$ , where  $D/Dt = \frac{\partial}{\partial t} + u\frac{\partial}{\partial r} + w\frac{\partial}{\partial z}$  is the material derivative, *i.e.* the derivative following an air parcel. The axisymmetric dynamics of the spin-up process can be understood, when solving Eq. (1.6) for  $v$ :

$$v = \frac{M}{r} - \frac{1}{2}fr. \quad (1.8)$$

When  $M$  is materially conserved, it is clear that both terms contribute to an increase in  $v$  as  $r$  decreases, that is when air parcels converge inwards. Similarly, as air parcels move outwards, the vortex spins more slowly. The radial convergence of air in the boundary layer, which is induced by friction, leads to radial divergence just above the boundary layer on account of mass continuity. From the arguments above, this explains why the vortex weakens in the early stage of development. Clearly, there must be radial convergence above the boundary layer induced by the diabatic heating, which more than offsets the frictionally-induced divergence there, in order for vortex spin-up to occur (Ooyama 1969, 1982, Smith 2000).

Even though absolute angular momentum is not materially conserved in the boundary layer, because some angular momentum is lost due to surface friction, the inner core of the vortex can be spun up significantly by radial convergence of air parcels in this frictional layer (see section 1.4). The fact that an air parcel loses a fraction of its absolute angular momentum as it spirals inwards in the boundary layer explains also why the flow becomes anticyclonic in the upper troposphere as it moves outwards at some radius from the vortex axis. This air parcel eventually turns upwards into the eyewall and as it diverges outwards in the upper layers, it conserves its (somewhat reduced) absolute angular momentum. Referring to Eq. (1.8), it is clear that  $v$  eventually becomes negative beyond some radius in the upper troposphere.

The aim of this thesis is to provide additional insight on certain dynamical aspects of the tropical-cyclone intensification process. Therefore, it is pertinent to review briefly the paradigms of tropical-cyclone spin-up that have been suggested over the last five decades. Different paradigms for tropical-cyclone spin-up have been proposed. Each of these paradigms has enjoyed wide acceptance for a while, before being replaced by a new one.

## 1.3 Paradigms of tropical-cyclone spin-up

### 1.3.1 The CISK-paradigm

At about the same time, Charney and Eliassen (1964) and Ooyama (1964) proposed independently an axisymmetric balance theory for the cooperative interaction between the cumulus- and cyclone-scale motions of an incipient cyclonic vortex, with the cumulus

clouds supplying the necessary latent heat energy to the cyclone and the cyclone, in turn, supplying the moisture (the ‘fuel’) to the clouds. Charney and Eliassen addressed the question why tropical cyclones develop in a conditionally-unstable tropical atmosphere. The authors explain that conventional conditional instability cannot be considered for the tropical-cyclone intensification process, as this instability explains rather small-scale cumulus convection, but not larger-scale convectively-induced circulations. Using a two-level axisymmetric, quasigeostrophic model and applying a perturbation technique, Charney and Eliassen found unstable modes at sub-synoptic scales shorter than a few hundred kilometers. This newly discovered instability was later termed *Conditional Instability of the Second Kind* (CISK), in order to distinguish it from the conventional conditional instability (‘of the first kind’), which is responsible for the formation of individual small-scale cumulus clouds. In common with the cooperative-intensification paradigm by Ooyama (see subsection 1.3.2), Charney and Eliassen’s theory emphasizes the role of surface friction which acts not only to spin the vortex down, as was perceived hitherto, but has a rather dual character. It acts not only to dissipate kinetic energy, but, since it is responsible for low-level moisture convergence in the boundary layer, it acts also to supply latent heat energy to the cyclone. The idea of the cooperative interaction between the cyclone and the cumulus convection encroaches on the closure assumption of CISK, which states that the rate of latent heat release by deep cumulus convective clouds is proportional to the convergence of moisture in the boundary layer. The positive feedback cycle can be closed recalling that, in a balanced vortex, the strength of the secondary circulation is proportional to the radial gradient of the net diabatic heating rate (see Eq. (1.5) in section 1.2). The diabatic heating rate in deep cumulus clouds is largest in the middle and upper troposphere, and leads to inflow below this maximum and outflow above. According to arguments given in section 1.2, convergence then leads to an acceleration of the tangential wind. Consequently, the boundary-layer inflow and moisture convergence increase also. The positive feedback cycle is completed recalling that the closure assumption in CISK then implies an increase in the diabatic heating rate as well as in its radial gradient.

Charney and Eliassen’s paper was highly influential on tropical-cyclone research in subsequent years, and the CISK-theory is still entrenched in many meteorological textbooks (e.g. Holton, 2004, section 9.7.2; James, 1994, pp 279-281). However, CISK has been subject to much criticism, e.g. by Ooyama (1982) and Emanuel (1994), who both developed new paradigms of tropical-cyclone intensification, which are presented in the next two subsections. Ooyama (1982) noted that the closure made in CISK by Charney and Eliassen (1964) is not realistic during the early stage of tropical-cyclone development, since at this stage, cumulus convection is not under the control of the parent vortex. Ooyama was aware of the limitations of the linear CISK-paradigm already in 1964, and it was this insight that led to the cooperative-intensification paradigm (see subsection 1.3.2). Emanuel (1994) pointed out that the closure made in CISK completely ignores the surface moisture fluxes in remoistening the hurricane boundary layer. The necessity of the oceanic heat source has also been recognized by Ooyama (1969) who showed that in the absence of sea-air heat fluxes, only weak intensification of an incipient cyclonic vortex occurs provided that some initial ambient CAPE is present. The CISK-paradigm merely assumes that the latent heat

release in the regions of deep convection is proportional to the vertically-integrated radial moisture flux, and completely ignores the moisture source from the ocean. In fact, if the CISK-paradigm would be essential for tropical-cyclone intensification, the latter would be as likely to occur over land as over sea. Further fundamental flaws of the theory of CISK when applied to tropical cyclones are discussed in Raymond and Emanuel (1993), Craig and Gray (1996), and Smith (1997).

### 1.3.2 The cooperative-intensification paradigm

The papers by Charney and Eliassen (1964) and Ooyama (1964) are often treated under the same umbrella when reviewing the linear CISK-paradigm. However, Ooyama recognized the shortcomings in this hypothesis soon after it was articulated and he subsequently developed the so-called cooperative-intensification theory (Ooyama 1969, 1982). In his seminal paper of 1969, Ooyama presents a simple nonlinear axisymmetric balance model for hurricane intensification. This model already incorporated the roots of the new theory, including a simple bulk aerodynamic representation of the surface moisture flux, he discovered to be essential for the intensification process. The basic mechanism of the cooperative-intensification paradigm starts with a weak cyclonic vortex, which organizes convection in the region where there is convergence due to surface friction. Differential heating due to this area of organized convection generates a secondary circulation in the free atmosphere. As described in section 1.2, the secondary circulation keeps the motion of the vortex in balance with the pressure field. Provided that the equivalent potential temperature of the boundary layer is sufficiently high, so that the atmosphere is conditionally unstable to moist convection, the convergence in the lower troposphere will bring in more absolute angular momentum than is lost to the sea surface. Since absolute angular momentum is materially conserved in the free atmosphere, the cyclonic circulation increases, which, together with the decreased pressure due to the convective heating, will cause the boundary-layer inflow to increase. This, in turn, gives rise to more intense convective activity, so that the positive feedback is closed. Of course, this is not a runaway process, since the atmosphere becomes less unstable to deep convection as the troposphere warms due to condensational heating.

In contrast to Charney and Eliassen's CISK-paradigm, Ooyama's model explicitly represents surface moisture fluxes by a simple bulk aerodynamic formula. To a certain extent, the inclusion of surface moisture fluxes can be regarded as a first step towards another paradigm shift, pushed forward by a series of papers by Emanuel and collaborators in the late 1980s and early 1990s. Emanuel developed a theory for tropical-cyclone intensification, which found wide acceptance in the field until today (see subsection 1.3.3). Although Ooyama recognized the importance of the surface moisture fluxes, he did not discuss the potential importance of their wind-speed dependence. However, this dependence forms an essential part of the paradigm proposed by Emanuel. The necessity of the wind-speed dependence of the surface fluxes for tropical-cyclone intensification has been questioned again very recently by Montgomery *et al.* (2009). This issue is more detailed in subsection 1.3.4. However, Ooyama notes that saturation equivalent potential temperature (or the

saturation mixing ratio) at the surface sharply increases with decreasing surface pressure in the inner core, which raises the moisture disequilibrium at the sea surface accompanied with increased surface fluxes augmenting the amount of moisture in boundary layer of the inner-core region. This pressure dependence is, in fact, incorporated in the parameterization of the thermodynamical energy flux in Ooyama's model. Of course, the moisture disequilibrium eventually decreases as water vapour mixing ratio in the boundary layer increases, which, in addition to the warming of the middle troposphere by condensational heating, sets a limit to the feedback process between the parent vortex and the organized deep convection.

In summary, one may point out two aspects that both Charney and Eliassen's CISK-paradigm and Ooyama's cooperative-intensification theory have in common. These aspects may be referred to as the *conventional view* of tropical-cyclone spin-up as they have been regarded as essential prerequisites for intensification:

- the main spin-up of the vortex occurs by the convectively-induced convergence of absolute angular momentum above the boundary layer, which must be large enough to more than offset the frictionally-induced divergence, and
- the important role of the boundary layer lies in converging moisture to sustain deep convection, but from the dynamical point of view, it acts to spin the vortex down.

Section 1.4 discusses the possibility that gradient wind imbalance in the boundary layer on account of surface friction may lead to a stronger vortex rather than a weaker one. This possibility was put forward by Anthes as long ago as 1971, but was resurrected by Smith *et al.* (2009). These authors suggested a different perspective of the dynamical role of the boundary layer that will be investigated in detail in Chapter 3. In particular, a study of the sensitivity of tropical-cyclone spin-up to the surface drag coefficient is carried out, with the aim of assessing the second item of the conventional view of tropical-cyclone spin-up highlighted above.

### 1.3.3 The WISHE-paradigm

The two paradigms described in the previous subsections ascribe the mechanism of vortex intensification to the positive feedback between the convective-scale and cyclone-scale motions, whereby the low-level moisture convergence in the boundary layer supports the cumulus convection. Early numerical simulations by e.g. Kleinschmidt 1951, Riehl 1954, Malkus and Riehl 1960, and Ooyama (1969) reveal that the latent (and possibly also the sensible) heat flux from the sea surface is essentially important for tropical cyclones to develop. However, it was Emanuel (1986) who turned the focus on these fluxes, and hypothesized that they are not only essentially important, but are exclusively responsible for the development and maintenance of tropical cyclones. The highly influential paper by Emanuel (1986) presents an analytic axisymmetric model, which is based on the assumption that air parcels upon exiting the boundary layer rise to the upper troposphere along surfaces of constant absolute angular momentum and constant saturation moist entropy.

These surfaces flare outwards with height and eventually become quasi-horizontal in the upper troposphere. Another assumption of Emanuel’s model, which has come under large criticism recently (Smith *et al.* 2008, 2009, Montgomery *et al.* 2009) is the assumption of gradient wind balance everywhere, including the boundary layer (see section 1.4).

Emanuel (1986) suggests that if the linear instability mechanism CISK was essentially important, provided that it does exist in nature at all, the occurrence of tropical cyclones would not be confined to maritime environments, but should be expected over land also. The newly developed air-sea interaction theory by Emanuel (1986) suggests that tropical cyclones develop and are maintained exclusively by self-induced anomalous fluxes of moist enthalpy, *i.e.* fluxes of latent and sensible heat, at the sea surface. The positive feedback mechanism between the system-scale tangential wind speed of the vortex and the surface fluxes of moist enthalpy was later given the acronym WISHE by Yano and Emanuel (1991), which stands for “wind-induced surface heat exchange”. Emanuel (1986) showed further that convective available potential energy (CAPE) is generated in situ by virtue of this positive feedback, so that any ambient initial CAPE is not necessary for tropical cyclones to develop. Until this time, all numerical simulations of tropical cyclones started with a conditionally-unstable environment. In a companion paper, Rotunno and Emanuel (1987) present a full primitive-equation numerical model and show that a tropical cyclone can develop from a weak-amplitude vortex in a conditionally neutral environment, *i.e.* without preexisting CAPE. These authors describe the nature of the paradigm shift by emphasizing that “the truly important thermodynamic interaction, *even in the developing stage*, is between vortex and ocean (as distinct from vortex and convection sustained by preexisting conditional instability as in the CISK theory) with cumulus convection rapidly redistributing heat acquired at the oceanic source upward and outward to the upper tropospheric sink.”

A comprehensive review of the details of the WISHE-mechanism is given by Montgomery *et al.* (2009), who question whether WISHE is actually *necessary* for the intensification of tropical cyclones, and show that it is not (see subsection 1.3.4). The WISHE-mechanism for intensifying the inner-core tangential wind speed owes its existence to the fact that the surface enthalpy flux is dependent on the near-surface wind speed. The details of this feedback process are illustrated schematically in Fig. 1.3. Except near the centre, the near-surface wind speed,  $V_{sfc}$ , of a tropical cyclone increases with decreasing radius. The near-surface humidity,  $\bar{q}_v$ , increases with increasing near-surface wind speed due to enhanced evaporation rates from the underlying ocean that leads to an enhanced negative radial gradient of  $\bar{q}_v$ . This, in turn, produces an enhanced negative radial gradient of equivalent potential temperature,  $\bar{\theta}_e$ , near the surface and, by vertical mixing, also throughout the boundary layer. In the inner-core region, air parcels exiting the boundary layer rise upwards and outwards to the upper troposphere and, since equivalent potential temperature is a materially-conserved quantity, they carry an imprint of the negative radial gradient of  $\bar{\theta}_e$  from the surface into the interior of the vortex. The rising air rapidly saturates, thereby producing a negative radial gradient of virtual temperature, which explains that the vortex is warm cored. The vortex aloft is assumed to remain in thermal wind balance, and hence an increased negative radial gradient of virtual temperature leads to an increased negative

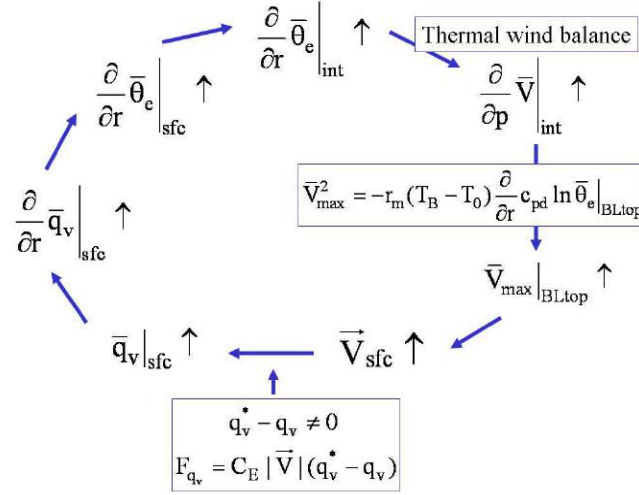


Figure 1.3: Schematic of the wind-induced surface heat exchange mechanism, WISHE. The variables are defined in the text. An overbar refers to an azimuthal mean of the corresponding variable. From Montgomery *et al.* (2009).

vertical shear of the tangential wind speed. Referring here to arguments given in Emanuel (1986), this increase leads to an increase in the maximum tangential wind speed at the top of the boundary layer. On account of turbulent mixing processes in the boundary layer, the increased tangential wind speed is communicated down to the surface. Larger near-surface wind speed enhances the sea-to-air moisture fluxes,  $F_{q_v}$ , leading to increased near-surface humidity, and so the circle of the positive feedback process is closed. The increase in near-surface humidity, however, tends to reduce the thermodynamic disequilibrium in specific humidity between the ocean surface and the near-surface air ( $q_v^* - q_v$ ). The thermodynamic disequilibrium could be maintained, however, if there is an associated reduction of surface pressure, which would increase the saturation specific humidity,  $q_v^*$ , at the sea surface temperature.

This thesis focuses on important dynamical aspects of tropical-cyclone intensification that are not included in the WISHE-paradigm, *i.e.* the role of the boundary layer, where the flow is not in gradient wind balance (see section 1.4). A particular sensitivity study investigates whether the WISHE-mechanism is essential for tropical-cyclone intensification in the three-layer axisymmetric model used in this thesis.

### 1.3.4 The role of vortical hot towers

The three paradigms presented so far have assumed that the broad-scale features of tropical cyclones, and in particular the intensification process, can be described by an axisymmetric theory. However, observations show, that tropical cyclones are highly asymmetric in the stage of rapid development, with bursts of intense convection, presumably possessing significant local buoyancy. This raises the question, to which extent axisymmetric theories

are applicable to the tropical-cyclone intensification process, or if the latter is rather intrinsically asymmetric in reality. In various simulations performed with the three-dimensional version of the minimal tropical-cyclone model used in this study, flow asymmetries were found to emerge during the stage of rapid intensification, even though the problem as posed was axisymmetric and the simulations were carried out on an  $f$ -plane (Zhu *et al.* 2001). Even earlier, Kurihara and Tuleya (1974) described the development of flow asymmetries on an  $f$ -plane in their calculations, however, it was not until the last few years, that the role of these features in the spin-up process of a tropical cyclone was attempted to be understood.

A comprehensive numerical study by Nguyen *et al.* (2008), using the non-hydrostatic model MM5<sup>2</sup>, investigated the role of the flow asymmetries in the prototype intensification problem<sup>3</sup> on an  $f$ -plane. Horizontal cross-sections of vertical velocity and vertical vorticity fields (see their Figures 4 - 6) reveal the formation of deep, but localized rotating updraughts, termed *vortical hot towers* (VHTs) by Hendricks *et al.* (2004), which coincides with the stage of rapid development. Embedded in the parent cyclonic vortex with lifetimes on the order of an hour, the VHTs rotate cyclonically around the centre. As they develop, the VHTs stretch and hence intensify the local vorticity field. This leads to an initially ring-like distributed field of highly asymmetric vorticity dipoles (strong cyclonic vorticity and much weaker anticyclonic vorticity anomalies).

In the simulations by Nguyen *et al.* (2008), the VHT-distribution shows a dominant azimuthal wavenumber-12 pattern in the early stage of rapid intensification. By the end of this process however, the number of VHTs has decreased to no more than three. The cyclonic vorticity anomalies grow horizontally, a result of the merger and axisymmetrization with neighbouring cyclonic vorticity anomalies. It is known from vortex-motion theory (McWilliams and Flierl 1979, Smith and Ulrich 1990, Schecter and Dubin 1999) that intense vorticity anomalies generally “move up the ambient vorticity gradient”. Therefore, the cyclonic vorticity anomalies move slowly towards the vortex centre, while the anticyclonic anomalies move outwards relative to the mean radial flow recalling that the VHTs are embedded in the parent vortex, which is characterized by a negative vorticity gradient. This segregation mechanism would not be possible if the opposite-sign vorticity anomalies were simply advected by the secondary circulation. As the anticyclonic vorticity anomalies move outwards, they decrease in amplitude, which makes them susceptible for axisymmetrization by the parent vortex. The cyclonic vorticity anomalies on the other hand are not easily axisymmetrized as they are at least one order of magnitude larger in amplitude than the vorticity of the parent vortex. For this reason, axisymmetrization is never complete, and even at the end of the rapid intensification period, the relative vorticity field of the inner core often exhibits a wavenumber-one or wavenumber-two structure. However, by the merger, segregation and axisymmetrization process during the period of rapid intensification, the VHTs directly contribute to the system-scale spin-up of the vor-

<sup>2</sup>MM5 refers to the Pennsylvania State University-National Center for Atmospheric Research fifth-generation Mesoscale Model.

<sup>3</sup>The prototype intensification problem examines the evolution of a prescribed, initially cloud-free, axisymmetric, baroclinic vortex over a warm ocean on an  $f$ -plane.



tex (Montgomery *et al.* 2006). It is interesting that the maximum total wind speed sharply increases earlier and more rapidly than the azimuthal-mean tangential wind speed. As the former coincides with the formation of the VHTs, the foregoing fact indicates that the flow intensifies first on the convective scale, and subsequently on the system scale (Nguyen *et al.* 2008).

Based on the new insights, which emerged from the calculations by Nguyen *et al.* (2008), Montgomery *et al.* (2009) posed the challenging question whether the widely-accepted paradigm for tropical-cyclone intensification, WISHE, is essentially important for this process, or if a vortex in the prototype intensification problem is spun up by the VHT-pathway only. In fact, these authors could show that, if the surface wind-speed dependence in the formulae for the sea-to-air vapour fluxes is capped at a nominal (trade-wind) value, vortex intensification still occurs by a pathway which involves the locally buoyant VHTs and by the near-surface convergence that is induced by these convective structures.

## 1.4 The hurricane boundary layer

The boundary layer of a mature hurricane is an important feature of the storm as it controls the radial distribution of vertical motion, absolute angular momentum and moisture at the top of this layer (Smith and Vogl 2008, Smith and Montgomery 2008, Vogl and Smith 2009, Smith and Montgomery 2010). In his influential paper, Emanuel (1986) emphasized that there is also an important thermodynamical constraint of the boundary layer. It is this layer, where the sea-to-air sensible and latent heat fluxes take place. The dependence of these fluxes on the near-surface wind speed plays a key role in the WISHE-paradigm for tropical-cyclone intensification (see subsection 1.3.3). Emanuel's steady-state tropical-cyclone model (Emanuel 1986) and his time-dependent models (Emanuel 1989, 1995b, 1997, 2004) focus largely on thermodynamic processes, making drastic simplifications to the dynamics through the assumption of gradient wind balance and hydrostatic balance. It was only recently that the tacit assumption of gradient wind balance in the boundary layer and its implication were noticed (Smith *et al.* 2008). The azimuthal momentum equation is used explicitly only in the boundary layer and only then to determine the radial *sic* inflow there. The assumption of strict gradient wind balance in the boundary layer, or even quasi-balanced dynamics associated with a generalized Ekman layer, is not supported by a scale analysis of the equations of motion (Smith and Montgomery 2008, Vogl and Smith 2009). The unbalanced dynamics in the inner-core region are generally important for determining the maximum radial and tangential wind components that can be attained, and therefore important in determining the azimuthal-mean intensity of the vortex (Smith *et al.* 2008, 2009). The strong inflow that is a prominent feature of the inner-core boundary layer owes much of its magnitude to gradient wind imbalance (Bui *et al.* 2009).

While the question of what constraints determine the size of a tropical cyclone (measured, e.g., by the radius of gale force winds) seems largely unanswered, recent progress has been made in understanding the reasons for the apparent lack of a strong relationship

between their intensity and size (Smith *et al.* 2009). Building on recent studies of tropical-cyclone intensification in a three-dimensional numerical model by Nguyen *et al.* (2008) and Shin and Smith (2008), these authors showed that, from an axisymmetric perspective, there are two mechanisms for vortex intensification in this framework, both involving the radial convergence of absolute angular momentum.

- The first mechanism is associated with the radial convergence of absolute angular momentum *above the boundary layer* in conjunction with its material conservation. The convergence is produced by a system-scale radial gradient of diabatic heating rate associated with deep, inner-core convection in the presence of enhanced surface moisture fluxes. This mechanism has been articulated previously by many authors (e.g. Willoughby 1979, Schubert and Hack 1983). It explains why the vortex expands in size and may be interpreted in terms of balance dynamics.
- The second mechanism is associated with radial convergence of absolute angular momentum *within the boundary layer* and becomes important in the inner core. Although absolute angular momentum is not materially conserved in the boundary layer, large wind speeds can be achieved there if the radial inflow is sufficiently large to bring the air parcels to small radii with minimal loss of angular momentum. This mechanism is tied fundamentally to the dynamics of the boundary layer, where the flow is not in gradient wind balance and deviations therefrom are significant over a substantial radial stretch.

The existence of these two mechanisms provides a plausible physical explanation for the long-standing observations of typhoons by Weatherford and Gray (1988), which indicate that inner-core changes in the azimuthal-mean tangential wind speed often occur independently from those in the outer core. The statement in Smith *et al.* (2009) that these mechanisms are independent is too strong: there must be a degree of coupling between them through boundary-layer dynamics as discussed by Montgomery and Smith (2011). The second mechanism of vortex spin-up described above ascribes the hurricane boundary layer a dynamical role, which is opposite to that in the conventional view of tropical-cyclone spin-up. In the latter view, the dynamical role of the boundary layer is that it acts to spin the vortex down on account of surface friction. According to Smith *et al.* (2009) surface friction acts to reduce the tangential wind speed beyond some radius outside the radius of maximum gradient wind, and hence acts also to reduce the centrifugal and Coriolis forces, so that the flow becomes subgradient. The agradient force, however, drives air parcels inwards towards the inner core of the storm with minimal loss of absolute angular momentum as described above. Eventually, the tangential wind speed becomes so large, *i.e.* the flow becomes supergradient, rapidly decelerates and turns upwards into the eyewall. Calculations by Smith and Vogl (2008) with a simple slab model of the boundary layer show that the development of supergradient winds in this layer is a ubiquitous feature of their solutions.

This thesis revisits the interpretation of spin-up in the axisymmetric model used herein in the light of these new insights.

## 1.5 Motivation

There is observational evidence to suggest that there is little relationship between the intensity of a tropical cyclone and its size, measured, for example, by the maximum near-surface tangential component of wind speed and the radius of gale-force winds, respectively (see e.g. Merrill 1984, Weatherford and Gray 1988). Since these observations were reported they have remained a puzzle and it has not been until recently that an explanation has been offered to account for them (see section 1.4). Much theoretical work has been focused on estimating the maximum possible intensity that a storm can achieve in a particular environment (Emanuel 1986, 1988, 1995b, Holland 1997, Bister and Emanuel 1998). A critique of these theories and list of references is given by Camp and Montgomery (2001), who concluded that Emanuel's theory comes closest to providing a useful calculation of maximum intensity. However, they noted also several shortcomings in the theory, arguing for the need for more basic research on the axisymmetric and asymmetric dynamics of hurricanes.

There do not appear to be any theories to account for the range of sizes of tropical cyclones that are observed in nature. More fundamentally, there is a lack of understanding of what governs the size of a storm through its life cycle. Some early numerical simulations by Yamasaki (1968) showed that storms tend to be larger at higher latitudes, consistent with observations by Merrill (1984) and with later calculations by DeMaria and Pickle (1988). The latter authors showed using an idealized, axisymmetric three-layer model that low-latitude storms are smaller than high-latitude storms, but low-latitude storms intensify more rapidly initially. In addition, they showed that the final intensity of storms does not vary appreciably (they say rapidly) with latitude. These authors suggested that "the effect of latitude appears to be related to the radial positioning of the diabatic heating", and argued that "the boundary-layer convergence and thus the diabatic heating occur much closer to the storm centre as the latitude is decreased". They go on to speculate how the foregoing result might be generalized in a three-dimensional simulation, noting that "if the absolute vorticity of the synoptic-scale flow had an effect similar to latitude, the initial formation of tropical cyclones might be favoured in regions where the large-scale vorticity of the surrounding flow is small". They speculated also that the absolute vorticity of the synoptic-scale flow may be a factor that influences the size of tropical cyclones.

While the question of what constraints determine a tropical-cyclone's size (measured, e.g., by the radius of gale-force winds) seems largely unanswered, recent progress has been made in understanding the reasons for the apparent lack of a strong relationship between their intensity and size (see section 1.4). Given these new insights it is natural to investigate to what extent the intensity and size are constrained by the level of ambient rotation, characterized, e.g., by the background vertical rotation rate. The existence of the two spin-up mechanisms raises questions also concerning Emanuel's steady-state tropical-cyclone model (Emanuel 1986) and his time-dependent models (Emanuel 1989, 1995b, 1997, 2004). In these models, the tacit assumption of gradient wind balance in the boundary layer forbids the development of supergradient winds in this layer. Thus, the mechanism for vortex intensification within the boundary layer, as described in the previous section,

cannot occur in such models.

The foregoing studies indicate an incomplete understanding of the processes that determine the intensity and size of tropical cyclones. Motivated by this situation, this thesis aims to explore the effects of the ambient rotation rate on tropical-cyclone intensity and size using the minimal axisymmetric numerical model. A possible conceptual framework for this investigation is provided by some early studies of geophysical vortices. These are discussed in Chapter 4 together with an assessment of their applicability to tropical cyclones.

The thesis investigates also some sensitivities of the minimal model to certain parameters and physical processes. First, the sensitivity of the model to the horizontal resolution is examined, followed by a study of the sensitivity to the radial eddy diffusivity. The issue of diffusivity was raised by Bryan and Rotunno (2009), who showed that, in the context of a more sophisticated axisymmetric model, the maximum tangential wind speed is strongly sensitive to the radial component of turbulent diffusivity. The remaining sensitivity studies concern the dual role of surface friction in the intensification process and the ‘evaporation-wind’ feedback mechanism as discussed in the next two paragraphs.

In subsection 1.3.2, it has been pointed out that both Charney and Eliassen’s CISK-paradigm and Ooyama’s cooperative-intensification theory ascribe the boundary layer a dual role. These authors emphasize that the thermodynamical role of the boundary layer lies in converging moisture to sustain deep convection, however, from the dynamical point of view, it acts to spin the vortex down. This dual role of the boundary layer is one of the two aspects that have been referred to as the conventional view of tropical-cyclone spin-up. The perception that surface friction acts only to spin the vortex down has prevailed until recently (e.g. Raymond *et al.* 1998, 2007, Kepert 2010). However, already early in the 1970s, Anthes (1971) discussed “... the paradox of the dual role of surface friction yielding more intense circulation ...” As opposed to the dual role of the boundary layer as envisaged in the conventional view of tropical-cyclone spin-up, the dual role of this layer as conceived by Anthes (1971) is purely dynamical. In fact, using a three-dimensional high-resolution numerical model, Montgomery *et al.* (2010) show that the vortex intensity *increases* as the surface drag increases up to large values that are more typical of those over land. The sensitivity of intensification to the surface drag in the present model is examined here to see whether it shows a similar behaviour to that described by Montgomery *et al.*

Montgomery *et al.* (2009) question whether the ‘evaporation-wind’ feedback mechanism (WISHE) is actually *necessary* for the intensification of tropical cyclones (see subsections 1.3.3 and 1.3.4). In fact, these authors show that, if the surface wind-speed dependence in the formula for the sensible and latent surface heat fluxes is capped at a nominal (trade-wind) value, vortex intensification still occurs. They conclude that their findings are independent of an axisymmetric or three-dimensional configuration. Motivated by these results, a set of experiments are carried out to investigate the extent to which vortex spin-up can occur in the minimal axisymmetric model used here if the surface heat fluxes are capped as in Montgomery *et al.* (2009).

Recent studies (Nguyen *et al.* 2008, Shin and Smith 2008) have shown that tropical-cyclone intensification is intrinsically a three-dimensional process in which deep convective

vortex structures, or “vortical hot towers” (VHTs), play a central role (see subsection 1.3.4). Despite the important role of the VHTs, one can usefully apply arguments based on the evolution of the axisymmetric mean fields as in Smith *et al.* (2009) and Bui *et al.* (2009). In order to retain maximum simplicity, a minimal axisymmetric model, that has only three layers in the vertical, has been chosen for the present study. Avoiding complexity is desired when the aim is to understand the underlying dynamics and/or thermodynamics of atmospheric phenomena. This spirit is supported by Ian James who, in reference to the Held-Hou model for the Hadley circulation, states: “This is not to say that using such [simple] models is folly. Indeed the aim of any scientific modelling is to separate crucial from incidental mechanisms. Comprehensive complexity is no virtue in modelling, but rather an admission of failure” (James 1994, p93).

## 1.6 Structure of the thesis

The next chapter gives a brief description of the minimal axisymmetric numerical model used in this study and the behaviour of the vortex in a control experiment is discussed in Chapter 3. In particular, this chapter revisits the interpretation of spin-up in the model in the light of new insights described in section 1.4 and examines also the development of regions where a necessary criterion for inertial instability is satisfied. Chapter 4 investigates the rotational influences on the tropical-cyclone size and intensity by varying the Coriolis parameter,  $f$ . In order to suppress the implicit dependence of the effective forcing on the vortex intensity, results of a set of similar, but more simplified calculations is presented in Chapter 5. In these calculations moist processes are absent and an approximately equivalent diabatic heating rate is prescribed. The results of these calculations are easier to interpret, and provide a basis for understanding the results of the more complex “moist” calculations. A paper by Smith *et al.* (2011b) based on Chapters 4, 5 and parts of Chapter 3 is currently in press. Chapter 6 examines the sensitivity of the model to certain parameters and physical processes. These studies include the model sensitivity to the radial resolution, the eddy diffusivity, the surface drag coefficient, and to the wind-speed dependence of the surface enthalpy flux. A summary and conclusions are given in Chapter 7.



# Chapter 2

## Description of the model

### 2.1 Governing equations

The model used for this study is the axisymmetric version of the minimal three-layer hurricane model described by Zhu *et al.* (2001), as developed by Nguyen *et al.* (2002). It is based on the hydrostatic primitive equations in cylindrical  $\sigma$ -coordinates ( $r, \lambda, \sigma$ ) on an  $f$ -plane, where

$$\sigma = \frac{p - p_{top}}{p^*}, \quad (2.1)$$

$p^* = p_s - p_{top}$ ,  $p_s$  and  $p_{top}$  are the surface and top pressures, respectively,  $p_{top}$  is a constant (taken here to be 100 mb), and  $f$  is the Coriolis parameter. The upper and lower boundary conditions require that  $\dot{\sigma} = 0$  at  $\sigma = 0$  and  $\sigma = 1$ , where  $\dot{\sigma} = D\sigma/Dt$  is the ‘vertical’  $\sigma$ -velocity and  $D/Dt$  is the material derivative. The radial and tangential momentum equations and the hydrostatic equation are:

$$\begin{aligned} \frac{\partial u}{\partial t} = & -u \frac{\partial u}{\partial r} - \dot{\sigma} \frac{\partial u}{\partial \sigma} + fv + \frac{v^2}{r} + \\ & \frac{R\theta\sigma(p^*\sigma + p_{top})^{\kappa-1}}{p_0^\kappa} \frac{\partial p^*}{\partial r} - \frac{\partial \phi}{\partial r} + D_u, \end{aligned} \quad (2.2)$$

$$\frac{\partial v}{\partial t} = -u \frac{\partial v}{\partial r} - \dot{\sigma} \frac{\partial v}{\partial \sigma} - fu - \frac{uv}{r} + D_v, \quad (2.3)$$

$$\frac{\partial \phi}{\partial \sigma} = -\frac{Rp^*(p^*\sigma + p_{top})^\kappa}{p_0^\kappa} \theta, \quad (2.4)$$

where  $u$  and  $v$  are velocity components in the radial and tangential directions,  $R$  is the specific gas constant for dry air,  $\kappa = R/c_p$ ,  $c_p$  is the specific heat of dry air,  $\theta$  is the potential temperature,  $\phi$  is the geopotential, and  $D_u$  and  $D_v$  represent terms associated with turbulence in the  $r$ - and  $\lambda$ -directions, respectively, and  $p_0 = 1000$  mb. The surface

pressure tendency equation, derived from the continuity equation and boundary conditions is

$$\frac{\partial p^*}{\partial t} = - \int_0^1 \frac{1}{r} \frac{\partial}{\partial r} (p^* r u) d\sigma, \quad (2.5)$$

and  $\dot{\sigma}$  is given by

$$\dot{\sigma} = - \frac{1}{p^*} \int_0^\sigma \frac{1}{r} \frac{\partial}{\partial r} (p^* r u) d\sigma + \frac{\sigma}{p^*} \int_0^1 \frac{1}{r} \frac{\partial}{\partial r} (p^* r u) d\sigma. \quad (2.6)$$

The thermodynamic and moisture equations are

$$\frac{\partial \theta}{\partial t} = -u \frac{\partial \theta}{\partial r} - \dot{\sigma} \frac{\partial \theta}{\partial \sigma} + Q_\theta + D_\theta + R \quad (2.7)$$

and

$$\frac{\partial q}{\partial t} = -u \frac{\partial q}{\partial r} - \dot{\sigma} \frac{\partial q}{\partial \sigma} + Q_q + D_q, \quad (2.8)$$

where  $\theta$  is the potential temperature,  $q$  is the specific humidity,  $Q_\theta$  and  $Q_q$  represent the diabatic heat and moisture sources associated with deep cumulus convection, and  $D_\theta$  and  $D_q$  denote contributions from turbulence. The term  $R$  represents radiative cooling. The temperature  $T$  is related to  $\theta$  by

$$T = \left( \frac{p}{p_0} \right)^\kappa \theta = \frac{(p^* \sigma + p_{top})^\kappa}{p_0^\kappa} \theta. \quad (2.9)$$

## 2.2 Parameterization of turbulence

### 2.2.1 Surface turbulent fluxes

The turbulent flux of momentum to the sea surface and the surface fluxes of sensible and latent heat are represented by bulk aerodynamic formulae in the form

$$\begin{aligned} (F_u, F_v) &= -\rho C_D |\mathbf{u}_b| (u_b, v_b) \\ F_{sh} &= \rho c_p C_K |\mathbf{u}_b| (T_s - T_{air}) \\ F_q &= \rho C_K |\mathbf{u}_b| (q_s^* - q_b), \end{aligned} \quad (2.10)$$

where the subscript ‘b’ denotes the value at the middle of the boundary layer,  $|\mathbf{u}_b|$  is the horizontal wind speed,  $T_s$  and  $q_s^*$  are the sea surface temperature and the saturated specific humidity at this temperature (and at sea surface pressure), respectively. Furthermore,  $\rho$  denotes the near-surface air density,  $C_D$  is the surface drag coefficient, and  $C_K$  is the exchange coefficient for enthalpy. For the calculations of the surface latent heat flux, it is assumed that the specific humidity is well mixed and hence constant throughout



the boundary layer. The value for the temperature near the surface,  $T_{air}$ , is obtained by extrapolating  $T_b$  along a dry adiabat to the 2-m level above the sea surface. This extrapolation has not been done in the calculations by Zhu *et al.* (2001), Zhu and Smith (2002), and Nguyen *et al.* (2002) using the present model (or the three-dimensional version of it). These authors used  $T_b$  instead. Except in the calculations presented in sections 6.3 and 6.4,  $C_K$  is assumed to be equal to  $C_D$ , which is calculated from the formula used by Shapiro (1992):

$$C_D = (1.024 + 0.05366R_F |\mathbf{u}_b|) \times 10^{-3}, \quad (2.11)$$

where  $R_F = 0.8$  reduces the boundary layer wind speed,  $|\mathbf{u}_b|$ , to the 10-m level.

When the equations are finally discretized in the vertical, the surface fluxes of heat and momentum enter the equations for the boundary layer through the  $D$ -terms as follows. The contributions of the frictional drag terms to  $D_u$  and  $D_v$  in Eqs. 2.2 and 2.3 are obtained by dividing the corresponding terms  $F_u$  and  $F_v$  in Eq. 2.10 by the depth  $z_b$  and the density  $\rho_b$  of the lower layer. Dividing  $F_{sh}$  by  $(\rho_b c_p \pi_s z_b)$  and  $F_q$  by  $(\rho_b z_b)$  gives the contributions of the surface fluxes of sensible and latent heat to  $D_\theta$  and  $D_q$ , respectively.

### 2.2.2 Subgrid-scale diffusion

To suppress small-scale noise and numerical instability in the calculations, it is necessary to filter out energy in high-frequency waves. In an axisymmetric model, the parameterization of subgrid-scale diffusion does not only represent unresolved subgrid-scale motions. Any non-axisymmetric motion such as mesovortices in the eye/eyewall, boundary layer roll vortices, upper-level asymmetric outflow jets, or vortex Rossby waves must be viewed as turbulence in an axisymmetric model, and hence, must be incorporated through parameterization (Bryan and Rotunno 2009).

As in the asymmetric version of the model, a biharmonic damping term is appended to all prognostic equations except the pressure tendency equation. This term has the form

$$-k_4 \nabla^4 \chi, \quad (2.12)$$

where  $\chi$  is any of the variables  $u, v, \theta, q$ , and  $k_4$  is a diffusion coefficient with  $k_4 = \Delta^4 / \tau_4$ , where  $\Delta$  is the horizontal grid spacing, and  $\tau_4$  is a time scale, set to 0.375 hours (except stated otherwise).

This model allows for the explicit condensation on the grid scale. According to Nguyen *et al.* (2002), the biharmonic damping term is not sufficient to smear out large amplitude shocks that occur at grid points where there is a sudden release of latent heat. Hence, an additional diffusion term is added to the right-hand-side of all prognostic equations excluding again the pressure tendency equation. This second-order diffusion term has the following form:

$$K \left( \nabla^2 \chi - \delta_{[u,v],\chi} \frac{\chi}{r^2} \right), \quad (2.13)$$

where  $\delta_{[u,v],\chi} = 1$  for either  $\chi = u$  or  $\chi = v$ , and  $\delta_{[u,v],\chi} = 0$  otherwise. The factor  $K$  is set proportional to the divergence, a procedure implemented by Ooyama (1984), *i.e.*

$$K = \left| \frac{1}{r} \frac{\partial(ru)}{\partial r} \right| \frac{\Delta^3}{l}, \quad (2.14)$$

where  $\Delta$  is the horizontal grid spacing and  $l$  is a length scale set to 10800 m. Formally, this damping term is equivalent to the representation of Reynolds stresses in terms of an eddy diffusivity. According to Shapiro (1992), a divergence-dependent coefficient has the advantage that it prevents a purely tangential axisymmetric spinning vortex from appreciable decay.

In addition, Newtonian damping terms of the form  $-\nu u$  and  $-\nu v$  are added to the momentum equations for  $u$  and  $v$  in the outermost quarter of the domain in order to diminish the amplitude of disturbances that may reach the outer boundary. The damping coefficient increases with radius according to

$$\nu = \frac{1}{2\tau_1} \left( 1 - \cos\left(\frac{(r - r_d)\pi}{R - r_d}\right) \right), \quad (2.15)$$

where  $r_d$  is the radius at which the Newtonian damping term is first applied,  $R$  is the domain size in the radial direction, and  $\tau_1$  is a timescale set to 360 s.

### 2.3 Parameterization of convection

This model has three options to represent subgrid-scale convection. These are modified versions of cumulus parameterization schemes proposed by Arakawa (1969), Ooyama (1969), and Emanuel (1995a). They differ by their closure assumption that determines the cloud-base mass flux. In all calculations presented in this study, the parameterization scheme proposed by Arakawa (1969) is used with a slight modification to represent the effects of precipitation-induced downdraughts. This scheme is a type of mass flux scheme in which the subgrid-scale mass flux is determined by assuming that deep convection tends to remove any conditional instability on a prescribed time scale. This time scale is typically on the order of an hour. The removal of instability is accomplished by relaxing the moist static energy of the upper layer towards that of the boundary layer on the assumed time scale. For further details see Zhu *et al.* (2001).

### 2.4 Explicit moist processes

The convection parameterization scheme is complemented by a simple explicit scheme that is implemented where there is condensation on the grid scale. The two schemes are complementary in the sense that once a grid column saturates, the convection parameterization scheme turns off in that grid column.

The simple explicit scheme is applied before the subgrid-scale convection scheme and is implemented as follows. If at any time the air becomes supersaturated at a grid point,

the specific humidity is set equal to the saturation specific humidity. The excess water vapour is condensed to liquid water and is assumed to fall out as precipitation. However, the associated latent heat release is added to the air at that grid point. A small number of iterations is necessary as the release of latent heat raises the specific humidity which, in turn, requires a further adjustment of the amount of condensed water.

## 2.5 Parameterization of radiative cooling

The effect of radiative cooling is crudely represented by adding a newtonian cooling term of the form  $-(\theta - \theta_{ref})/\tau_R$  to the right-hand-side of the thermodynamic equation (Eq. 2.7). Here,  $\theta_{ref}$  denotes the potential temperature profile of the basic state and  $\tau_R$  is a radiative timescale. Following Rotunno and Emanuel (1987, p546), this timescale is set to 12 hours.

## 2.6 Boundary and initial conditions

The calculations are carried out in a cylindrical domain ( $0 \leq r \leq R, 0 \leq \sigma \leq 1$ ), with  $R = 1000$  km. The boundary conditions are:

$$u = 0, v = 0, \frac{\partial A}{\partial r} = 0, \text{ at } r = 0 \text{ and } r = R, \quad (2.16)$$

where  $A$  can be any of the quantities  $u, v, \theta, q$ . The initial tangential wind profile in the lower layer is that used by Smith (2003) and given by

$$v(r) = v_1 s \exp(-\alpha_1 s) + v_2 s \exp(-\alpha_2 s), \quad (2.17)$$

where  $s = r/r_m$  and  $r_m, v_1, v_2, \alpha_1$  and  $\alpha_2$  are constants chosen to make  $v = v_m = 15$  m s<sup>-1</sup> at  $r = r_m = 120$  km. The values of  $v_1$  and  $\alpha_1$  are calculated by

$$\begin{aligned} \alpha_1 &= (1 - \mu \alpha_2 \exp(-\alpha_2)) / (1 - \mu \exp(-\alpha_2)), \\ v_1 &= v_m \exp(\alpha_1) (1 - \mu \exp(\alpha_2)), \end{aligned} \quad (2.18)$$

where  $\mu = v_2/v_m$ . The calculations are initialized with  $\mu = 0.3$  and  $\alpha_2 = 0.5$ . The profiles in the middle and upper layers are the same, but their amplitudes are multiplied by factors of 0.9 and 0.3, respectively.

The surface pressure and geopotential are obtained by integrating the gradient wind equation in  $\sigma$ -coordinates radially inwards, *i.e.*

$$RT_s [\ln(p_s(R)) - \ln(p_s(r))] = \int_r^R \left( fV_s + \frac{V_s^2}{r} \right) dr, \quad (2.19)$$

$$\phi(R) - \phi(r) = \int_r^R \left( fV + \frac{V^2}{r} - \frac{RT}{p} \sigma \frac{\partial p^*}{\partial r} \right) dr. \quad (2.20)$$

The surface temperature,  $T_s$ , required in Eq. 2.19, is set equal to the sea surface temperature, taken here to be  $28^\circ\text{C}$ . The temperature in each layer is obtained from the potential temperature by solving Eq. (2.9).

The far-field temperature and humidity structure are based on the mean West Indies sounding for the ‘hurricane season’ (Jordan 1957), but the near-surface mixing ratio has been reduced slightly so that the sounding is initially stable to deep convection. The initial surface pressure is 1015 mb. In the presence of the initial vortex, the minimum surface pressure (at the vortex centre) is 1008 mb. Horizontal variations of mixing ratio in the presence of the initial vortex are neglected.

## 2.7 Numerical methods

The model has three layers of unequal depth with boundaries at  $\sigma = 1, \sigma_4, \sigma_2$  and 0 as depicted in Fig. 2.1. All dependent variables, such as horizontal velocity, potential temperature, specific humidity and geopotential, are defined in the middle of each layer ( $\sigma = \sigma_b, \sigma_3$ , and  $\sigma_1$ ) and the vertical velocity is staggered, *i.e.* it is defined at the boundaries between the layers ( $\sigma = \sigma_4$  and  $\sigma_2$ ). In the radial direction, the horizontal velocity components,  $u$  and  $v$ , are staggered also as indicated in Fig. 2.1. This is the so-called Lorenz-grid (L-grid). The advantage with the L-grid model is that total energy is conserved. In addition, the mean potential temperature and the variance of the potential temperature are conserved under adiabatic and frictionless processes (Arakawa and Suarez 1983). The equations are expressed in finite difference form in both the radial and vertical and integrated using the Adams-Bashforth third-order method with an integration timestep of 6 s. The initial pressure, temperature, specific humidity and geopotential height in the middle of each layer and at the boundaries between the layers are listed in Appendix A.

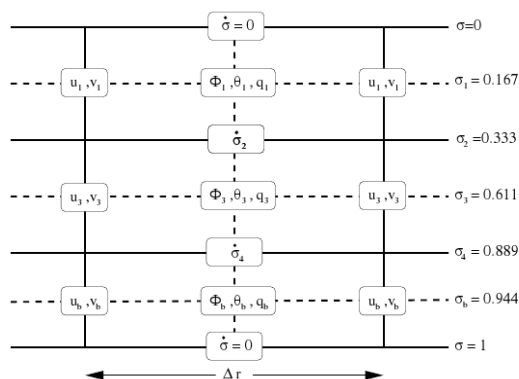


Figure 2.1: Configuration of  $\sigma$ -levels in the model showing locations where the dependent variables are stored. The horizontal velocity components, geopotential, temperature, specific humidity are calculated in the middle of each layer. These are the layers 1, 3 and b. The vertical velocity  $\dot{\sigma}$  and the convective mass fluxes are stored at the two interface levels 2 and 4. From Nguyen *et al.* (2002).

# Chapter 3

## Control experiment

A control experiment is carried out on an  $f$ -plane to investigate the evolution of a weak baroclinic initial vortex to a mature tropical cyclone. The Coriolis parameter,  $f$ , is set to a constant value that corresponds to a reference latitude of  $20^\circ\text{N}$  and is denoted as  $f_0$ . The model has a 10 km radial grid spacing and the radial domain size extends to 1000 km. Deep cumulus convection is parameterized by a scheme proposed by Arakawa (1969). This scheme is complemented by a simple explicit scheme that is implemented at grid points where supersaturation occurs. The initial and boundary conditions are given in section 2.6. The results of this control experiment serve as a reference with which to compare the results presented in Chapter 6 that examines the sensitivity of the model to certain parameters and physical processes.

The initial radial profile of tangential wind in the lower layer is shown in Fig. 3.1. The profiles in the middle and upper layers are the same, but their amplitudes are multiplied by factors of 0.9 and 0.3, respectively.

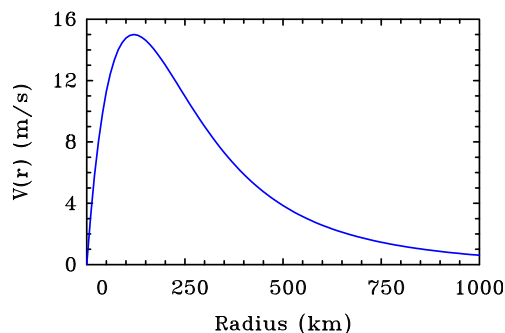


Figure 3.1: Radial profile of tangential wind in the lower layer for the initial vortex.

### 3.1 Overview of vortex evolution

Figure 3.2 shows time series of the minimum surface pressure and the maximum tangential wind speed in the lower layer. It shows also the radius,  $r_{gales}$ , at which the tangential wind speed in the lower layer reaches gale force ( $17 \text{ m s}^{-1}$ ). The vortex evolution can be divided into three successive stages:

- a gestation period during which the vortex first decays and then gradually intensifies and the minimum surface pressure slowly falls,
- a short period that lasts for only ten hours, where the vortex undergoes rapid intensification and deepening, and
- a mature stage during which the maximum tangential wind speed increases only slightly and eventually reaches an approximate steady state.

During the first four hours of the gestation period, the vortex slows down due to surface friction before it gradually intensifies. It was shown in section 1.4, that significant vortex spin-up can occur within the boundary layer due to the frictionally-induced convergence of absolute angular momentum. However, a closer inspection of the magnitude of the terms of the tangential momentum equation reveals that the frictional drag is the dominant term during the first four hours of development. Above the boundary layer, the vortex spins down due to frictionally-induced divergence. The onset of rapid intensification can best be discerned from the maximum tangential wind speed and occurs after approximately one and a half days. The physical reason for the intensification is the release of latent heat in the inner-core region. The associated radial gradient of diabatic heating leads to convergence in the lower troposphere that more than offsets the frictionally-induced divergence (see Eq. (1.5) in section 1.2). This offset is a necessary requirement for the intensification of the vortex (e.g. Ooyama 1969, 1982, Smith 2000). As will be shown in section 3.2, the onset of rapid intensification occurs when there is saturation on the grid-scale in the middle layer. However, the inclusion of a parameterization scheme for convection also leads to latent heat release that gives rise to the gradual increase in intensity just before the vortex ultimately spins up rapidly. After the period of rapid intensification, the vortex reaches an approximate steady-state. The maximum tangential wind speed at twelve days is  $56.8 \text{ m s}^{-1}$ .

The occurrence of rapid intensification is a typical feature during the development of tropical storms to a mature hurricane. According to Willoughby *et al.* (2007), rapid intensification may increase the maximum winds by more than  $20 \text{ m s}^{-1}$  in twelve to 24 hours. In the control calculation described here, the maximum tangential wind speed increases from  $29.4 \text{ m s}^{-1}$  at 39 hours to  $48.7 \text{ m s}^{-1}$  only 10 hours later. Willoughby *et al.* (2007) state that nearly all major hurricanes, *i.e.* those that reach Category 3, 4 or 5 on the Saffir-Simpson scale, become major through rapid intensification. Still, rapid intensity changes remain almost unpredictable (NOAA 2006).

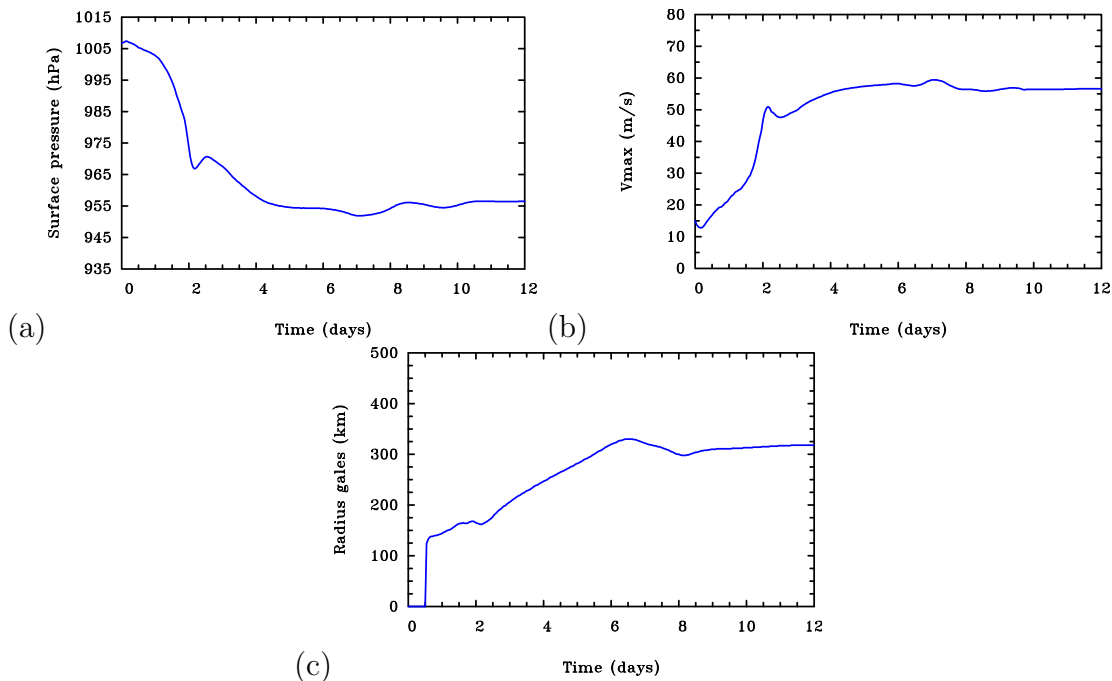


Figure 3.2: Time-series of (a) the minimum surface pressure, (b) the maximum tangential wind speed in the lower layer, and (c) the radius of gale-force tangential winds in the lower layer.

Interestingly, the evolution of the vortex size, as characterized by the radius of gale-force tangential winds, is not obviously related to the evolution of the intensity. The vortex reaches gale-force wind speed for the first time after half a day at  $r = 120$  km and subsequently increases only slightly in size until two and a half days, whereas it intensifies rapidly during the same period. After the period of rapid intensification, the intensity increases only slightly, whereas the vortex size increases steadily from 160 km to 320 km over a time period of four days. A shorter period follows, where the vortex becomes smaller in size, before the radius of gales increases again a little bit and eventually reaches a steady state of about 310 km. This behaviour matches the observations of typhoons described by Weatherford and Gray (1988), mentioned in section 1.4, that inner-core changes in the azimuthal-mean tangential wind speed often occur independently from those in the outer core. A physical explanation for this behaviour has been provided recently by Smith *et al.* (2009). As described in section 1.4, these authors described two (sic) independent mechanisms that account for the spin-up of the inner core and outer core, respectively. However, the statement made by Smith *et al.* that the two mechanisms are independent is too strong. There must be a degree of coupling between them through boundary layer dynamics as discussed by Montgomery and Smith (2011). Even though the vortex size and the intensity develop largely independently, as noted above, both the maximum tangential wind speed and the radius of gales in the lower layer reveal a slight decrease between six and eight days before they eventually level out. A physical reason, why the vortex size

starts to decrease after reaching its maximum is given in section 3.4. More insight on the two mechanisms that govern the intensification of the inner and outer core, respectively, is offered in section 3.3.

## 3.2 Some details on vortex evolution

Time-radius plots of a variety of quantities are presented now to help elucidate further aspects of the vortex evolution.

Figure 3.3 shows time-radius plots of the tangential and radial wind speed components in each of the three layers. Similar plots of vertical velocity at the two interface levels and relative humidity in the middle and lower layers are presented in Fig. 3.4. During the first 39 hours, the vortex intensity increases gradually in all three layers, while the radius of maximum tangential wind speed decreases, e.g. from 120 km to about 50 km in the boundary layer. The strong moisture fluxes at the sea surface, that increase with wind speed and decreasing pressure, lead to rapid saturation in the lower layer after only three hours (see Fig. 3.4c). The moistening of the inner core in the middle layer occurs by vertical advection from below. However, even prior to the occurrence of grid-scale saturation in the middle layer after 39 hours, subgrid-scale convection leads to slight warming of the inner core. This warming generates a moderate secondary circulation with low- and middle-level convergence, ascent near the radius of maximum tangential wind speed and divergence aloft (see right panels of Figures 3.3 and 3.4). The frictionally-induced convergence in the boundary layer leads initially to divergence immediately above it, which would spin down the vortex there due to conservation of absolute angular momentum. The warming of the inner core, that occurs even prior to rapid intensification, however, generates convergence in the middle layer, that more than offsets the frictionally-induced divergence. It is well known, that this convergence in the lower free troposphere is a prerequisite for vortex intensification (e.g. Ooyama 1969, 1982, Smith 2000).

The onset of rapid intensification, however, occurs when there is grid-scale saturation in the inner core of the middle layer (Fig. 3.4a) after 39 hours. Subsequently, latent heat is released, which leads to a sudden increase in the radial gradient of diabatic heating with a pulse of an intensified secondary circulation, *i.e.* strong convergence in the lower and middle layers, strong ascent at both interface levels and divergence aloft. The radius of maximum vertical velocity at the upper interface level (Fig. 3.4b) is slightly larger than that at the lower interface level (Fig. 3.4d), which reflects the slope of the eyewall. This slope can also be discerned from the radii of maximum tangential wind speed after the onset of rapid intensification in the lower and middle layers. In the upper layer, however, the maximum tangential wind speed is located closer to the vortex axis as compared to the middle layer. The reason is that, as air parcels are advected into the upper layer, they move outwards and, by conserving their absolute angular momentum, spin more slowly. The annular region of strong ascent depicted in the right panels of Fig. 3.4 is accompanied by subsidence near the centre, indicative of an eye. Another prominent feature is the development of an upper-level anticyclone at outer radii after about half a day.



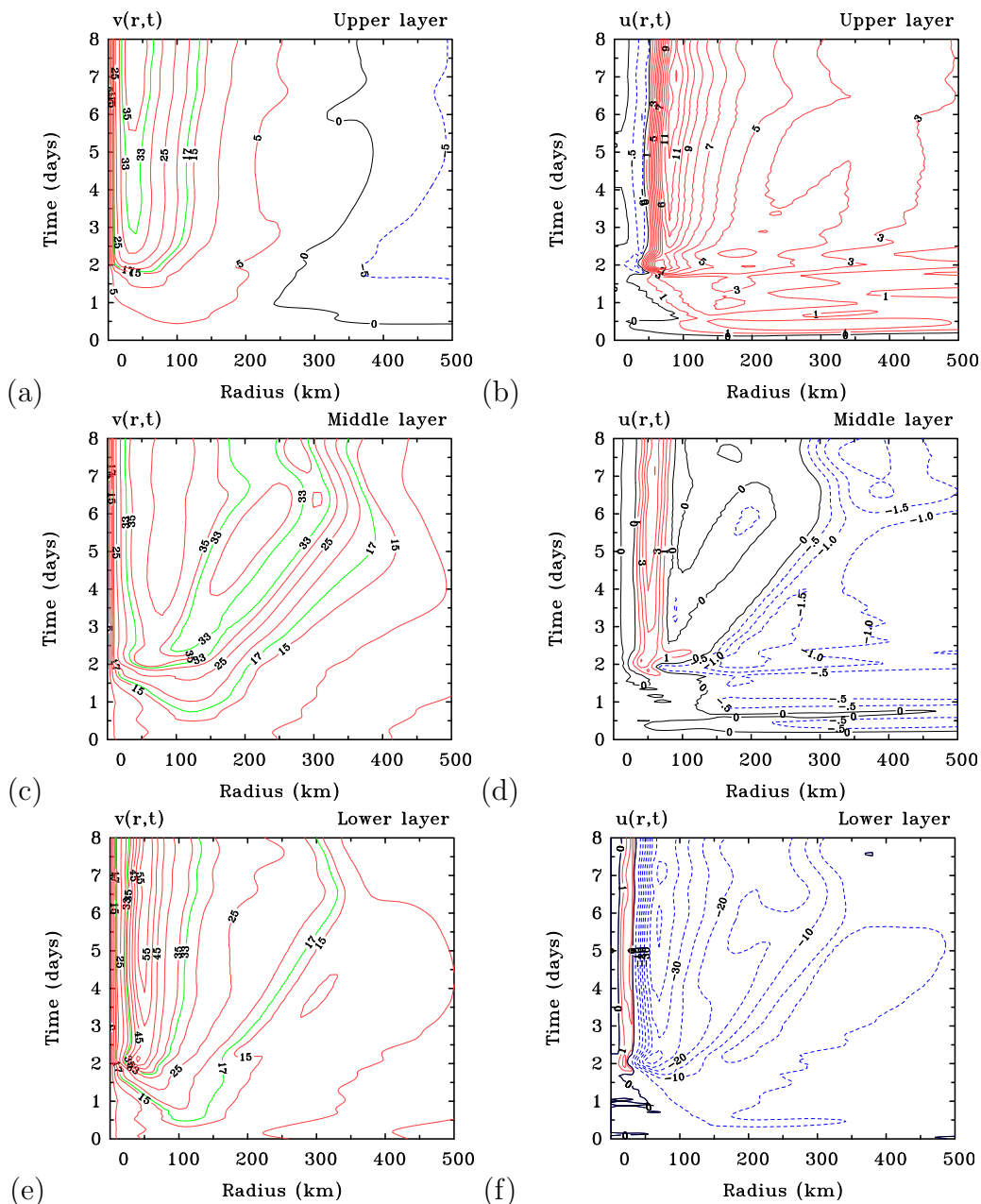


Figure 3.3: Time-radius plots of the tangential,  $v$ , and radial wind speed components,  $u$ . Positive values red/solid, negative values blue/dashed. (a)  $v$  in the upper layer (contour interval is  $5 \text{ m s}^{-1}$ ), (b)  $u$  in the upper layer (contour interval is  $0.5 \text{ m s}^{-1}$  (negative values) and  $1 \text{ m s}^{-1}$  (positive values)), (c)  $v$  in the middle layer (contour interval as in panel a), (d)  $u$  in the middle layer (contour interval as in panel b), (e)  $v$  in the lower layer (contour interval as in panel a), (f)  $u$  in the lower layer (contour interval is  $5 \text{ m s}^{-1}$  (negative values) and  $1 \text{ m s}^{-1}$  (positive values)). The green contours in panels (a), (c) and (e) show the location of gale-force ( $17 \text{ m s}^{-1}$ ) and hurricane-force ( $33 \text{ m s}^{-1}$ ) winds.

With the onset of rapid intensification, the vertical velocity fields show also regions of strong subsidence outside the inner-core region, which account for adiabatic warming and drying in the middle and lower layers. The amount of drying (cf. the relative humidity plots in Figures 3.4a,c) is not realistic and can be attributed to the coarse vertical resolution.

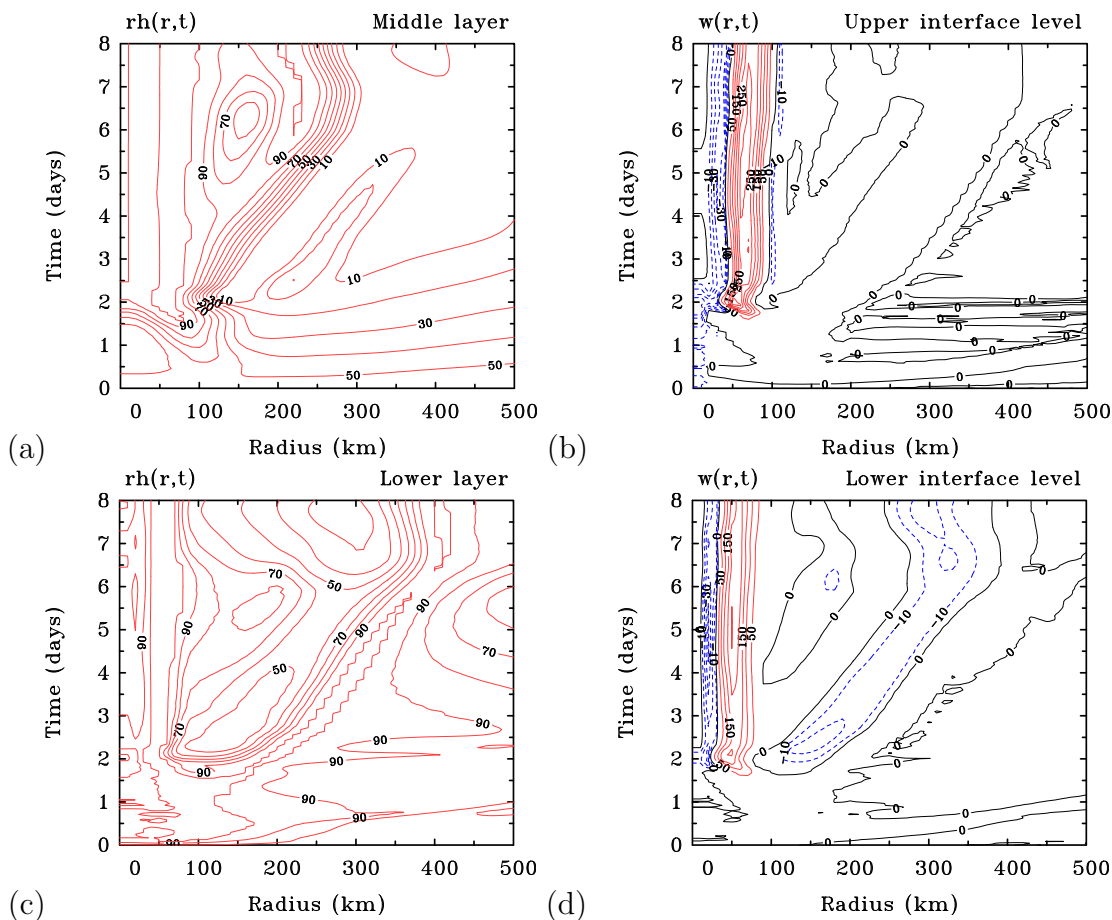


Figure 3.4: Time-radius plots of relative humidity,  $rh$ , and vertical velocity,  $w$ . (a)  $rh$  in the middle layer, (b)  $w$  at the upper interface level, (c)  $rh$  in the lower layer, (d)  $w$  at the lower interface level. Contour interval in panel (a) and (c) is 10% and in panel (b) and (d)  $50 \text{ cm s}^{-1}$  (positive values, red/solid) and  $10 \text{ cm s}^{-1}$  (negative values, blue/dashed).

Figure 3.5 shows time-radius plots of convective and explicit precipitation. The parameterization scheme for convection and the explicit scheme for condensation are complementary in the sense that once a grid column saturates, the convection parameterization scheme turns off in that column. As shown above, grid-scale saturation first occurs in the boundary layer, before vertical moisture advection leads to saturation on the grid-scale in the middle and upper layers after 39 hours. At the same time, the convection scheme in the inner-core region shuts down, and precipitation occurs exclusively on the grid-scale, at least in the inner-core region (Fig. 3.5b). All precipitation that occurs prior to the period of rapid intensification is associated with the cumulus parameterization scheme (Fig. 3.5a).

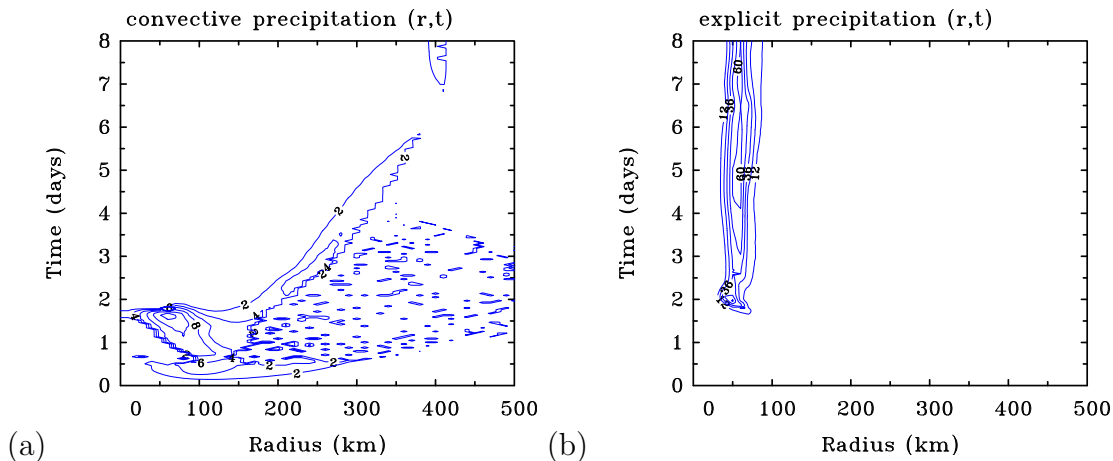


Figure 3.5: Time-radius plots of (a) convective precipitation (contour interval  $2 \text{ mm h}^{-1}$ ), and (b) explicit precipitation (contour interval  $12 \text{ mm h}^{-1}$ ).

Time-radius plots of the surface sensible and latent heat fluxes are shown in Fig. 3.6. They increase strongly with wind speed in the inner core and reach maximum values of about  $900 \text{ W m}^{-2}$  and  $4900 \text{ W m}^{-2}$  during the mature stage, respectively. Albeit being somewhat larger, the magnitude of the latent heat flux compares well with those in a numerical study by Chen and Yao (2003, their Fig. 3). According to the WISHE-mechanism detailed in subsection 1.3.3, the wind-speed dependence of these fluxes is essential for the intensification of tropical cyclones. Recently, Montgomery *et al.* (2009) showed that, if the surface wind-speed dependence in the formulae for the sea-to-air vapour fluxes is capped at a nominal (trade-wind) value, vortex intensification still occurs by a pathway which involves the locally buoyant VHTs and by the near-surface convergence that is induced by these convective structures (see subsection 1.3.4). These results led the authors to a challenging question. Is the WISHE-mechanism actually *necessary* for tropical-cyclone spin-up to occur? In section 6.4, similar sensitivity experiments will be presented that investigate to what extent the vortex in an axisymmetric model can intensify when the WISHE-mechanism is suppressed.

### 3.3 Spin-up in the model

Figure 3.7 shows time-radius plots of a passive tracer in the middle and lower layers. The evolution of the passive tracer,  $X$ , is calculated by solving the radial advection equation (3.1) in each layer with the initial value of the tracer equal to the initial radius.

$$\frac{\partial X}{\partial t} = -u \frac{\partial X}{\partial r} \quad (3.1)$$

This equation was solved using the Adams-Bashforth third-order scheme, with a time step of 6 s as for all other prognostic variables. The tracer contours correspond approximately

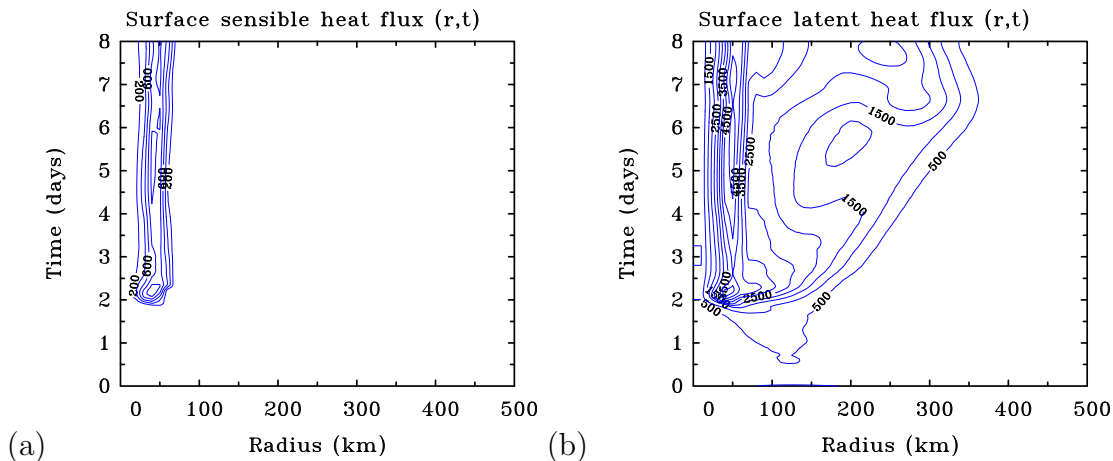


Figure 3.6: Time-radius plots of (a) surface sensible heat flux (contour interval  $200 \text{ W m}^{-2}$ ), and (b) surface latent heat flux (contour interval  $500 \text{ W m}^{-2}$ ).

with the trajectories of air columns in a layer except in regions where there is appreciable vertical exchange of mass. Therefore, contours in the inner regions are not shown, where there is a substantial flow of air entering from the boundary layer or exiting into the upper layer. It is evident that the radial displacements are very much larger in the boundary layer, where friction is important, than in the middle layer. As discussed in section 1.4, Smith *et al.* (2009) showed that significant tangential wind speed can be achieved within the boundary layer if the radial inflow is sufficiently large to bring the air parcels to small radii with minimal loss of angular momentum. In fact, Fig. 3.7 suggests that this mechanism might be important to spin up the inner core of the model vortex. The subsequent discussion addresses the question how the spin-up occurs in the present model.

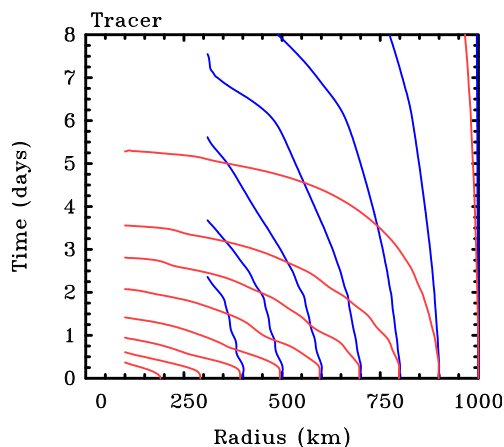


Figure 3.7: Time-radius plots of trajectories in the middle layer (blue lines) and boundary layer (red lines).

A scale analysis by Vogl and Smith (2009) is consistent with classical boundary-layer theory (e.g. Jones and Watson 1963), that states that the radial pressure gradient within the boundary layer is the same as that at the top of the boundary layer. However, surface friction acts to reduce the tangential wind speed outside some radius of maximum gradient wind in the boundary layer and thus, the centrifugal and Coriolis forces in this layer are reduced also. Consequently, gradient wind balance, that exists to a good approximation in the interior vortex, is disrupted within the boundary layer. Instead, an inward-directed agradiant force prevails and it is this force imbalance, that leads to strong inflow near the surface. The agradiant force (per unit mass),  $F_a$ , is defined as the difference between the local pressure gradient force and the sum of the centrifugal and Coriolis forces (per unit mass), *i.e.*  $F_a = -(1/\rho)(\partial p/\partial r) + (v^2/r + fv)$ . The tangential flow is in exact gradient-wind balance if  $F_a = 0$ . If  $F_a < 0$ , the flow is *subgradient* and if  $F_a > 0$ , it is *supergradient*. Given the fact that surface friction acts to reduce the tangential wind speed in the boundary layer, it is surprising that the maximum tangential wind speed actually occurs in this layer. The latter fact is evident in the time-radius plot of the difference,  $dv$ , between the tangential wind speed component in the boundary layer and the middle layer depicted in Fig. 3.8. However, as mentioned above and supported by Fig. 3.7, from a purely dynamical point of view the role of surface friction in the boundary layer has a dual character with two competing effects (Anthes 1971). On the one hand, it acts to reduce the tangential wind speed component in the boundary layer. On the other hand, however, this leads to strong inflow, so that air parcel trajectories undergo only few revolutions per unit radial displacement and are therefore shorter in length so that friction has less distance over which to slow the parcels down. Consequently, the stronger the inflow in the boundary layer, the less is the reduction of absolute angular momentum,  $M$ , due to surface friction. If air parcels can be brought in to relatively small radii, both terms on the right-hand side of Eq. (1.8) introduced in section 1.4 ( $v = M/r - fr/2$ ) may then lead to an increase in  $v$  as  $r$  decreases, even in the boundary layer (Smith *et al.* 2009).

Figure 3.9 shows time-radius plots of the agradiant force in the boundary layer and the middle layer, respectively. After the onset of rapid intensification, the flow in the boundary layer becomes strongly subgradient beyond a radius of about 50 to 70 km due to surface friction. The agradiant force drives the air parcels rapidly inwards with some loss of absolute angular momentum. Consequently, the tangential wind speed component eventually becomes so large at inner radii, that the flow becomes supergradient, rapidly decelerates and turns upwards and outwards into the eyewall. Figure 3.9a shows that the region of supergradient winds coincides with the region of strong ascent from the boundary layer into the interior vortex. The region of ascent is indicated by the thick black line that depicts the  $20 \text{ cm s}^{-1}$  contour of vertical velocity at the top of the boundary layer. Figure 3.9b shows that the values for the agradiant force per unit mass in the middle layer are about one order of magnitude smaller as compared to the boundary layer, so that especially outside the inner-core region, gradient wind balance serves as a good approximation. The positive agradiant force in the inner-core region of the middle layer drives an outflow (see Fig. 3.3d), that leads to a readjustment back to gradient wind balance. It is due to the coarse vertical resolution of this model with only one layer for the boundary layer that

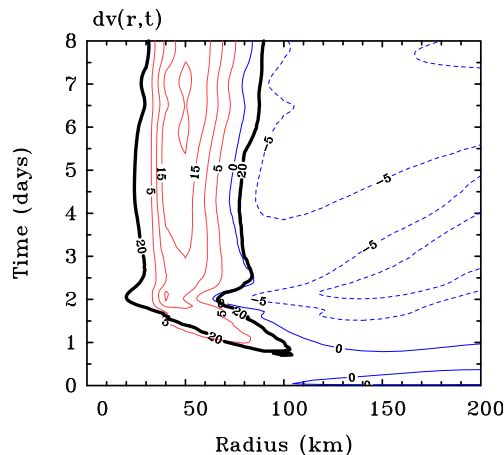


Figure 3.8: Time-radius plot of the difference between the tangential wind speed in the boundary layer and the middle layer (contour interval  $5 \text{ m s}^{-1}$ , positive contours red/solid, negative contours blue/dashed). The thick black curve is the  $20 \text{ cm s}^{-1}$  contour of vertical velocity from the boundary layer to the middle layer.

accounts for the fact that a big part of this readjustment process occurs in the middle layer. Smith *et al.* (2008) presented a modified conceptual model (their Fig. 6) that shows that after the supergradient flow rapidly decelerates, it turns upwards and outwards in a shallow layer above the inflow, thereby adjusting back to the radial pressure gradient, *before* it leaves the boundary layer to turn upwards into the eyewall. Precisely, the latter statement depends on the definition of the boundary layer. The shallow outflow layer would not be part of the boundary layer when the latter is dynamically defined as advocated recently by Smith and Montgomery (2010). The dynamical definition declares the boundary layer as the shallow layer near the surface, where the inward-directed gradient force exceeds a certain threshold value. Smith and Montgomery (2010) emphasize that this definition is uncontroversial in the outer regions of a tropical cyclone, but that it has limitations in the inner-core region, where the flow is upwards out of the boundary layer. They note also that the applicability of conventional boundary-layer theory is questionable at these inner radii, where the flow is akin to that of separation in aerodynamic boundary layers.

The conceptual model presented in Smith *et al.* (2008) matches the radial wind fields shown in Smith *et al.* (2009) who investigated the azimuthally-averaged aspects of calculations performed by Nguyen *et al.* (2008) with a three-dimensional, nonhydrostatic tropical-cyclone model. In particular, the azimuthally-averaged radial wind fields (their Figures 5c and d) reveal a localized region of strong outflow just above the strong inflow at the radius of maximum tangential wind speed. Bui *et al.* (2009) investigated the balanced and unbalanced aspects of tropical-cyclone intensification using the same azimuthally-averaged data used by Smith *et al.* (2009). They showed that, while a major fraction of the secondary circulation can be captured by axisymmetric balanced theory, the latter greatly underestimates the strong radial inflow within the boundary layer as well as the localized outflow region immediately above it. Consequently, Bui *et al.* argue that ax-

isymmetric balanced theory “significantly underestimates the maximum azimuthal-mean tangential wind tendency.”

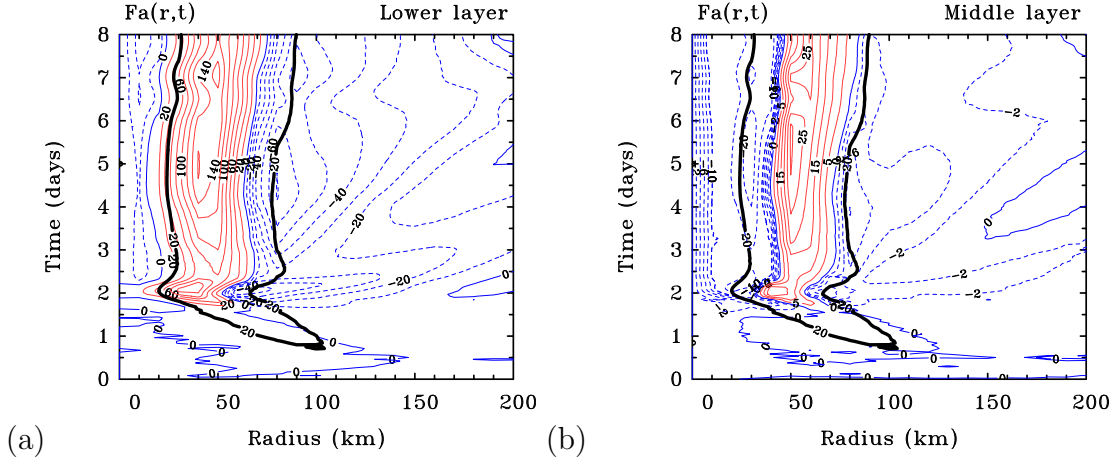


Figure 3.9: Time-radius plots of the gradient force in (a) the boundary layer (contour interval  $20 \text{ m s}^{-1} \text{ h}^{-1}$  (positive values),  $10 \text{ m s}^{-1} \text{ h}^{-1}$  (negative values)) and (b) the middle layer (contour interval  $5 \text{ m s}^{-1} \text{ h}^{-1}$  (positive values),  $2 \text{ m s}^{-1} \text{ h}^{-1}$  (negative values)). Positive contours red/solid, negative contours blue/dashed. The thick black curve in each panel is the  $20 \text{ cm s}^{-1}$  contour of vertical velocity from the boundary layer to the middle layer.

At this stage, it is pertinent to investigate the magnitude of each of the terms in the tangential momentum equation (Eq. 2.3) in order to understand the spin-up process in the axisymmetric tropical-cyclone model. Before presenting the corresponding figures, it is helpful to recall different forms of the tangential momentum equation. With a few lines of algebra, it can be shown, that these three equations are equivalent:

$$\frac{\partial v}{\partial t} = -u \frac{\partial v}{\partial r} - \dot{\sigma} \frac{\partial v}{\partial \sigma} - fu - \frac{uv}{r} + D_v, \quad (3.2)$$

$$\frac{\partial v}{\partial t} = -u(\zeta + f) - \dot{\sigma} \frac{\partial v}{\partial \sigma} + D_v, \quad (3.3)$$

$$\frac{1}{r} \frac{\partial M}{\partial t} = -\frac{u}{r} \frac{\partial M}{\partial r} - \frac{\dot{\sigma}}{r} \frac{\partial M}{\partial \sigma} + \frac{D_v}{r}, \quad (3.4)$$

where  $\zeta = (1/r)\partial(rv)/\partial r$  is the vertical component of relative vorticity in the model coordinates. All other variables have been defined earlier. These equations show that the sum of terms representing the horizontal advection of  $v$ , the centrifugal force and Coriolis force is equivalent to the radial flux of absolute vorticity and is equivalent also to the radial advection of absolute angular momentum. Equation (3.4) shows that, above the boundary layer, absolute angular momentum is conserved, *i.e.*  $DM/Dt = 0$ , in regions where diffusion is negligible. It will be shown in due course that diffusion becomes important in the inner-core region.



The time-radius plots shown in Figures 3.10 and 3.11 show the contribution by the horizontal flux of absolute vorticity,  $-u(\zeta + f)$ , and the vertical advection,  $-\sigma\partial v/\partial\sigma$ , to the tendency,  $\partial v/\partial t$ , of the tangential wind speed component in the lower and middle layers, respectively. All panels show also where there is vertical motion and, in particular, strong upward motion. The contribution by surface friction and radial diffusion will be discussed in due course. In the same annular region, where there is strong ascent, there is a strong inward flux of absolute vorticity in the boundary layer, equivalent to a positive advection of absolute angular momentum. Also the vertical advection of  $v$  contributes positively to  $\partial v/\partial t$  in the inner-core region of the boundary layer. The latter fact is not intuitive, but becomes clear by recalling the vertical differencing scheme for the vertical advection of the prognostic variables in the model and recalling that  $v_b$ , that is stored in the middle of the boundary layer, represents a vertically-averaged value over the depth of the boundary layer. Accordingly, in regions where  $vb > v_3$  (see Fig. 3.8),  $-\sigma\partial v_b/\partial\sigma$  is positive also.

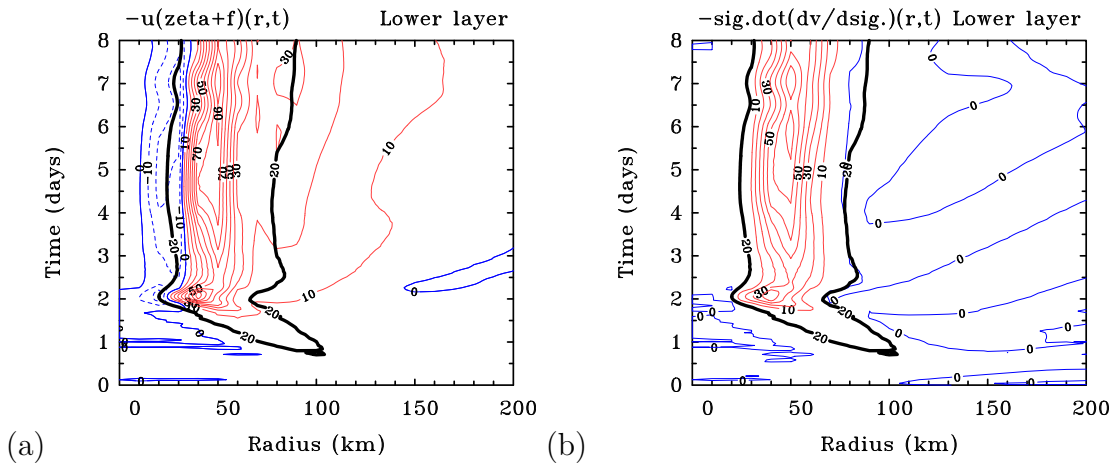


Figure 3.10: Time-radius plots of (a) the radial flux of absolute vorticity in the boundary layer, and (b) the vertical advection of the tangential wind speed component in the boundary layer. The contour interval is  $10 \text{ m s}^{-1} \text{ h}^{-1}$ , positive contours red/solid, negative contours blue/dashed. The thick black curve in each panel is the  $20 \text{ cm s}^{-1}$  contour of vertical velocity from the boundary layer to the middle layer.

It is significant that the strong upward motion from the boundary layer to the middle layer coincides with the region where the tangential wind speed is larger in the boundary layer (see Fig. 3.8). Thus, in this region, the middle layer is being fed by angular-momentum enriched air, as can be seen in the time-radius plots of  $-\sigma\partial v_b/\partial\sigma$  for the middle layer, depicted in Fig. 3.11b. However, Fig. 3.11a shows that, in the same annular region, there is a strong outward flux of absolute vorticity in the middle layer, equivalent to a negative advection of absolute angular momentum, which, by itself would rapidly spin down the flow. Clearly, the spin-up of the middle layer in this annular region is a result of the upward transfer of higher values of absolute angular momentum from the boundary layer and not from the radial convergence of absolute angular momentum in the middle



layer, supporting the ideas articulated by Nguyen *et al.* (2002), Smith *et al.* (2009) and Smith and Montgomery (2010). It is worth pointing out that this process of spin-up cannot occur in time-dependent models that directly or tacitly assume gradient wind balance in the boundary layer such as those of Ooyama (1969), Emanuel (1997), Frisius (2006) and Wirth and Dunkerton (2006).

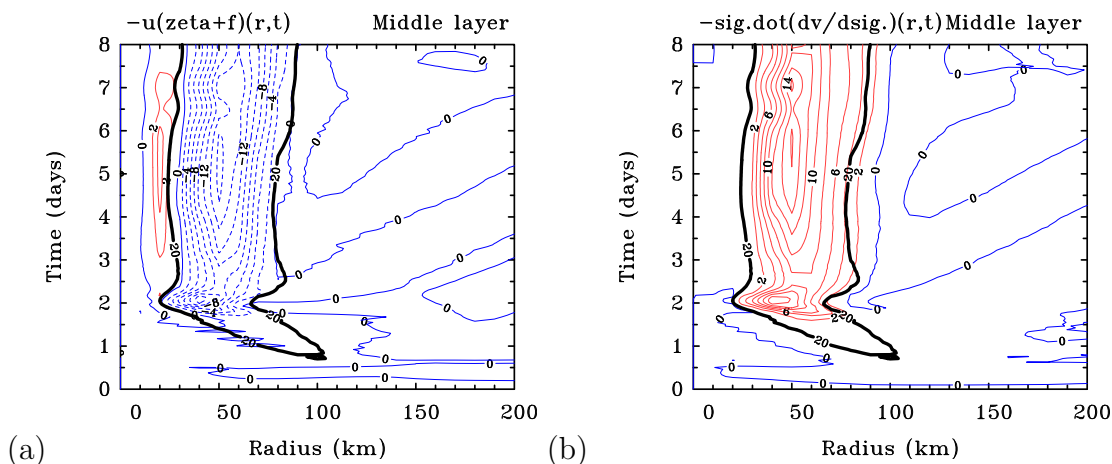


Figure 3.11: Legend as in Fig. 3.10, but for the middle layer. The contour interval is  $2 \text{ m s}^{-1} \text{ h}^{-1}$ , positive contours red/solid, negative contours blue/dashed.

Figure 3.12 shows radial profiles of all the contributions to the tangential momentum equation in the lower and middle layers at 46 hours, *i.e.* during the period of rapid intensification. The inner-core region and the outer region are depicted separately. These contributions include also surface friction (in the boundary layer) and radial diffusion (in both layers) in addition to the terms already presented in the previous two figures. The radial profiles of the sum of all contributions, *i.e.* the tendency of  $v$ ,  $\partial v/\partial t$ , are depicted also. The sign for the values of the horizontal flux of absolute vorticity and the vertical advection of  $v$  are as expected from Figures 3.10 and 3.11. However, Fig. 3.12a shows even better that, during rapid intensification, the magnitude of  $-\sigma \partial v/\partial \sigma$  in the middle layer is larger than the magnitude of  $-u(\zeta+f)$ . This result shows that the spin-up mechanism that occurs in the boundary layer articulated above is responsible for the spin-up of the interior vortex here. However, it is significant that the radial diffusion term becomes of similar magnitude in the inner core. Nevertheless, at this stage of development, the upward transfer of higher values of  $v$  from the boundary layer is dominant and more than offsets the other two terms that contribute negatively to  $\partial v/\partial t$  in the middle layer.

Figure 3.12c shows that the vortex spin-up in the inner core of the boundary layer occurs predominantly by the inward flux of absolute vorticity (equivalent to the inward advection of absolute angular momentum). Another positive contribution to  $\partial v/\partial t$  is the vertical advection term with a magnitude that is half of that of  $-u(\zeta+f)$ . Significantly, the radial diffusion term becomes strongly negative in the inner core with absolute values that are similar to the values of  $-u(\zeta+f)$ . Surface friction, a dominant term in the boundary layer, becomes very large also in the inner core on account of the high wind speed near the

eyewall. However, the positive terms prevail during rapid intensification. It is noticeable that the radius of largest  $\partial v/\partial t$  is closer to the axis in the boundary layer as compared to the middle layer. The left panels of Fig. 3.12 highlight the important role of radial diffusion and surface friction in the spin-up mechanism of the inner core. Bryan and Rotunno (2009) found that the maximum tangential wind speed in their model calculations is most sensitive to the turbulence in the radial direction. In Chapter 6, numerical experiments are presented that explore the model sensitivities to the representation of both the radial diffusion and surface friction.

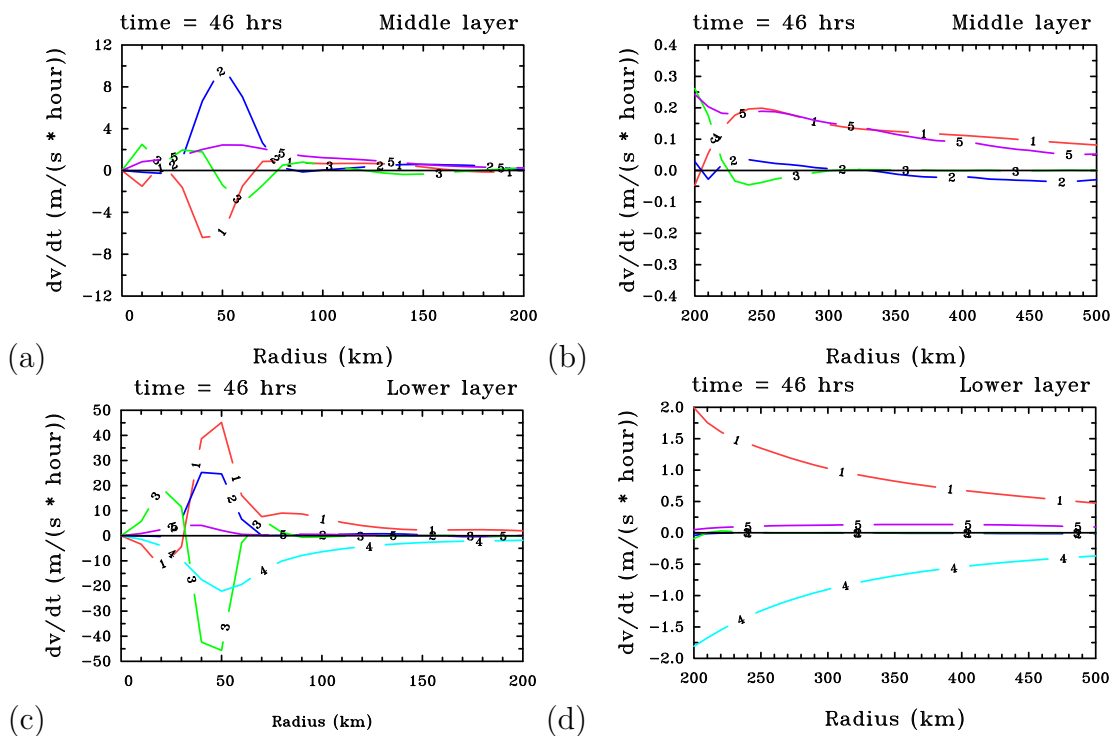


Figure 3.12: Radial profiles of the contributions to the tangential momentum equation during rapid intensification at 46 hours in the middle layer in (a) the inner-core region and (b) the outer-core region. Panels (c) and (d) show the corresponding profiles in the boundary layer. Curves 1 - 4 denote the contributions from the radial flux of absolute vorticity ( $-u(\zeta + f)$ , curve 1), vertical advection ( $-\dot{\sigma}\partial v/\partial\sigma$ , curve 2), radial diffusion (curve 3), and surface friction (curve 4). Curve 5 denotes the sum of these terms, *i.e.* the tendency of  $v$ ,  $\partial v/\partial t$ . Note the different scales in each panel.

The right panels of Fig. 3.12 show the radial profiles of the contributions to the tangential momentum equation at outer radii. In both layers, radial diffusion is of negligible importance. The absolute vorticity flux in both layers is inwards, which means that the spin-up at outer radii is associated with radial convergence of absolute angular momentum. This situation in the middle layer mirrors that which has been described as the conventional view of vortex intensification in subsection 1.3.2. In the middle layer, the rate at which the vortex size increases is somewhat reduced by the import of lower values of abso-

lute angular momentum from the upper layer. In the lower layer, the inward vorticity flux is very much larger than above. However, surface friction with absolute values of similar magnitude to those of  $-u(\zeta + f)$  acts to reduce the tangential wind speed. Nevertheless, even at these radii, the vortex size increases on account of some import of absolute angular momentum.

Figure 3.13 shows similar radial profiles at twelve days. In the inner core of the middle layer, the magnitudes of  $-u(\zeta + f)$  and  $-\dot{\sigma} \frac{\partial v}{\partial \sigma}$  have both increased over time. Depending on the radius, either of these quantities outweighs the other. However, the contribution of the radial diffusion makes the vortex steady, which, according to Shapiro (1992) is an advantage of a divergence-proportional horizontal eddy diffusivity as used in the present model. Similarly, in the lower layer, the magnitudes of  $-u(\zeta + f)$  and  $-\dot{\sigma} \partial v / \partial \sigma$  have increased and are almost equal near the radius of maximum tangential wind speed. It is noticeable that the radial diffusion has become the most dominant term. Surface friction has increased also on account of the higher wind speed during the mature stage. In the outer-core region, it is most interesting that the vorticity flux,  $-u(\zeta + f)$ , in both layers takes on negative values, and in particular beyond 300 km where there is inflow (see Figures 3.3d and f). Recalling that  $-u(\zeta + f)$  is equivalent to  $-(u/r)\partial M/\partial r$ , this means that, if there is inflow, the negative values of  $-u(\zeta + f)$  correspond to a reversal in the radial gradient of absolute angular momentum, or equivalently, to the development of negative absolute vorticity. In the following section, it will be shown, that the sign of  $\partial M/\partial r$  reverses in local regions beyond certain radii after the period of rapid intensification. An explanation for this behaviour using two different approaches will also be given.

### 3.4 Inertial instability

Another aspect of tropical-cyclone dynamics is the development of regions where a necessary criterion for inertial instability is satisfied. In an axisymmetric model, this criterion is that the quantity  $I^2 = (\zeta_{abs})(f + 2v/r) < 0$ , where  $\zeta_{abs} = \zeta + f$  is the vertical component of the absolute vorticity, and the second factor is twice the absolute angular velocity (Rayleigh 1917). Unless  $v(r) < -\frac{1}{2}rf$ , regions of negative  $I^2$  coincide with regions of negative  $\zeta_{abs}$ . It turns out that the second factor is only negative in a small region in the upper layer at radii beyond 500 km. Thus, the signs of  $I^2$  and  $\zeta_{abs}$  are the same in the region that is investigated here. Regions where  $I^2 < 0$  are potentially important for two reasons: firstly, inertial instability may occur there and secondly, a balanced solution cannot exist in these regions. Whether or not inertial instability operates in the boundary layer is controversial. A reason why it might not is that there is an actual force imbalance that drives air parcels inwards, irrespective of the degree of inertial stability. Thus, because of friction, there is no inertial resistance to radial displacements in this layer<sup>1</sup>. A scale analysis of the full boundary-layer equations by Smith and Montgomery (2008), however, indicates that the boundary-layer depth is inversely proportional to the square root of the inertial stability

<sup>1</sup>The concept of inertial stability is normally presented for a situation in which a swirling flow in gradient wind balance with no radial motion is symmetrically perturbed (Rayleigh 1917, Charney 1973).

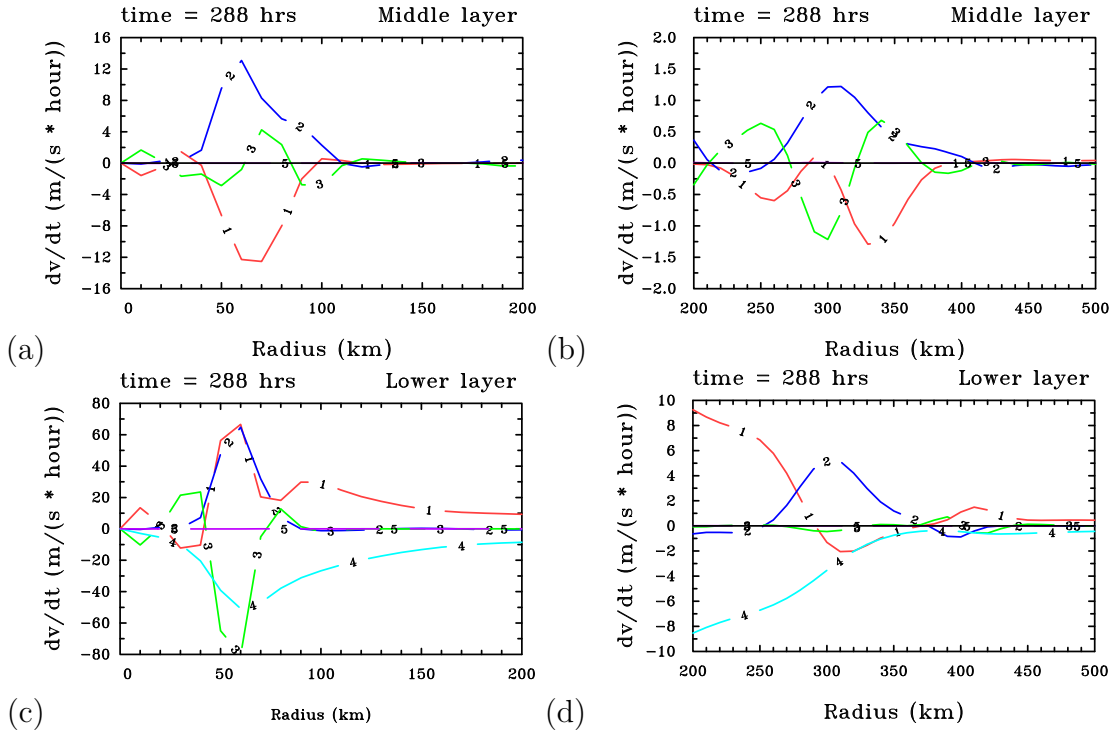


Figure 3.13: Legend as in Fig. 3.12, but in the mature stage at twelve days. Note the different scales in each panel.

parameter,  $I^2$ , at the top of the boundary layer. In view of this aspect, the gradient force in the boundary layer may be related to the inertial stability. Whether or not inertial instability operates in the free troposphere is controversial also. Anthes (1972) merely notes that this instability “does not appear to play an important role” in hurricane dynamics. A reason why it does not occur in models with a very coarse vertical resolution is given by Ooyama (1969). Although regions with  $I^2 < 0$  develop in his calculations, he notes that inertial instability might not occur there as inertial unstable displacements would lead to compensating displacements in other regions that would have to occur against inertial and static stability.

Figure 3.14 shows time-radius plots of  $I^2$  in the middle and upper layers, respectively. In the upper layer, a region of negative  $I^2$  develops after 19 hours at about 150 km. In the course of time this region moves gradually outwards. With the onset of rapid intensification at 39 hours a region of negative  $I^2$  develops in the middle layer initially at radii between 180 and 200 km, but this region moves also gradually outwards in the course of time. A second region of negative  $I^2$  in the upper layer appears a few hours later.

The production of negative  $\zeta_{abs}$  (negative  $I^2$ ) is identical to the production of a negative radial gradient of absolute angular momentum,  $\partial M/\partial r$  (compare Eq. (3.3) with Eq. (3.4)). Therefore, the physical process that leads to this development can be interpreted both from the vorticity equation as well as from absolute angular momentum considerations. It can be interpreted also in terms of the vertical transfer of potential vorticity (Flatau and Stevens,

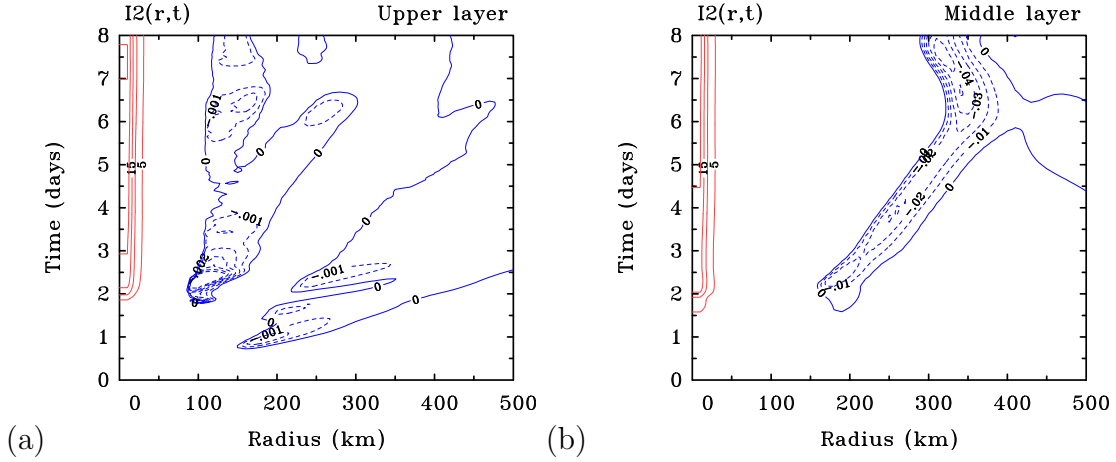


Figure 3.14: Time-radius plots of the inertial stability parameter in (a) the upper layer and (b) the middle layer. For positive values (red/solid), the contour intervals are  $5 \times 10^{-6} \text{ s}^{-2}$ . For negative values (blue/dashed) the contour intervals are  $0.001 \times 10^{-6} \text{ s}^{-2}$  (panel a) and  $0.01 \times 10^{-6} \text{ s}^{-2}$  (panel b), respectively.

1989), but this approach will not be demonstrated here. The vorticity equation may be written in  $\sigma$ -coordinates as:

$$\frac{\partial \zeta}{\partial t} = -u \frac{\partial}{\partial r} (\zeta + f) - \dot{\sigma} \frac{\partial \zeta}{\partial \sigma} - \frac{\zeta + f}{r} \frac{\partial (ru)}{\partial r} - \xi \frac{\partial \dot{\sigma}}{\partial r} + \frac{1}{r} \frac{\partial (rD_v)}{\partial r}, \quad (3.5)$$

where  $\xi = \partial v / \partial \sigma$  is the horizontal component of relative vorticity. All other variables have been defined earlier. The first two terms on the right-hand-side represent contributions from horizontal and vertical advection. The remainder are the divergence, twisting (or tilting), and diffusion terms, respectively. Given an initial distribution of positive absolute vorticity, the divergence term itself cannot produce negative  $\zeta_{abs}$ . In regions of divergence, it could only reduce the magnitude of existing positive absolute vorticity. In that case, negative values of  $\zeta_{abs}$  are produced by the tilting of the horizontal component of relative vorticity. This mechanism is illustrated schematically in Fig. 3.15. In a region, where the tangential wind speed component is decreasing with height (as it is typical for a hurricane), there is a component of shear vorticity, that is oriented in the positive  $r$ -direction. If at the same time the vertical velocity decreases with radius, differential advection by the vertical motion will tilt the existing shear vorticity into the vertical and thereby generate negative vertical vorticity (Holton 2004, p102).

Figure 3.16 shows radial profiles of all terms on both sides of Eq. (3.5) at three selected times: 38 hours (upper panels), 72 hours and 96 hours. At 38 hours, just one hour prior to rapid intensification and the development of negative  $I^2$  in the middle layer, the divergence term (curve 3) is strongly negative at radii between 40 and 90 km (panel a). At these radii, the flow is divergent, and hence existing positive vorticity is diluted. Another major negative contribution stems from the tilting term (curve 4). The minimum of this term is little further outward, beyond the radius of maximum vertical velocity. A third major

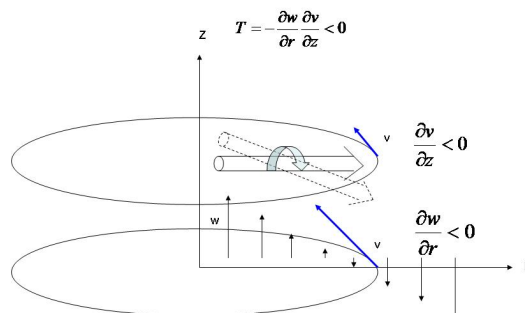


Figure 3.15: Schematic illustrating the vorticity generation by the tilting of the horizontal vorticity vector indicated by the double arrows. The tilting term,  $T$ , in  $(r, \lambda, z)$ -coordinates is  $T = -(\partial w / \partial r)(\partial v / \partial z)$ .

term contributing to a negative vorticity tendency (curve 6) is the diffusion term (curve 5). At these inner radii, the vertical advection term is strongly positive as expected from the discussion in section 3.3: the middle layer is being fed by absolute angular momentum-rich air from the boundary layer. Figure 3.16b shows similar profiles at the same time, but at larger radii. Between 190 and 230 km from the axis, slightly further outwards where  $I^2$  first becomes negative,  $\partial\zeta/\partial t$  is negative predominantly on account of the diffusion term. This is contrary to the finding of Anthes (1972), who notes that this term is much smaller in magnitude than the divergence and tilting terms. It is likely that this difference can be accounted for by the different parameterization of radial diffusion. At 38 hours, the tilting term has another minimum at a radius of 170 km. The lower panels of Fig. 3.16 show radial profiles of these terms during the mature stage at 72 hours and 96 hours, respectively. The tendency of  $\zeta$  (curve 6) becomes negative at radii between 250 and 280 km (at 72 hours) and between 290 and 320 km (at 96 hours) mainly on account of the tilting and the diffusion term, both being similar in magnitude. These radii are again a little further outwards than the corresponding radii where  $I^2 < 0$  at these times. The latter fact explains why the region of negative  $I^2$  (negative  $\zeta_{abs}$ ) moves outwards with time.

As mentioned earlier, in an axisymmetric model, the region where  $\zeta_{abs} < 0$  is identical to the region where the radial gradient of absolute angular momentum is negative, *i.e.*  $\partial M / \partial r < 0$ . Figure 3.17 shows a time-radius plot of the absolute angular momentum in the middle layer. During the early stage of vortex development, absolute angular momentum increases radially outwards, a fact noted also by Anthes (1972). However, with the onset of rapid intensification, a region with a negative radial gradient,  $\partial M / \partial r$ , develops at radii between 180 and 200 km. In the course of time, the region of negative  $\partial M / \partial r$  moves radially outwards.

Absolute angular momentum considerations help to physically interpret the development of regions of negative  $\partial M / \partial r$ . Air at large radii (with large values of  $M$ ) is advected

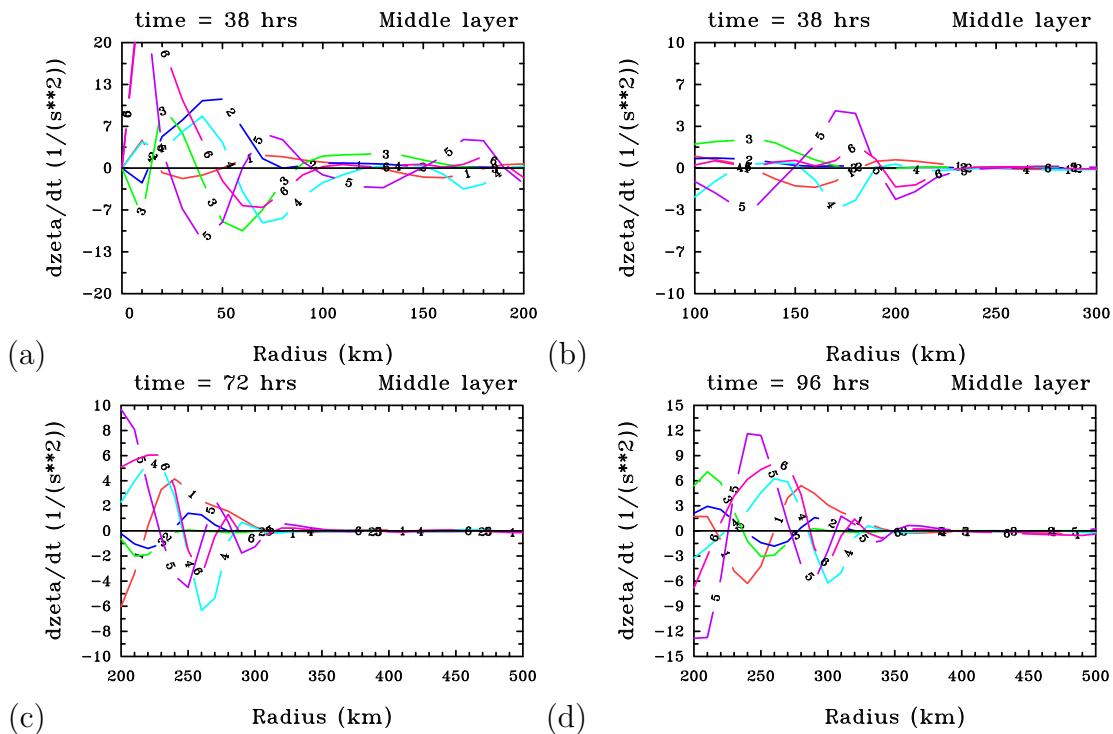


Figure 3.16: Radial profiles of the contributions to the vorticity equation in the middle layer at (a) 38 hours at inner radii, (b) 38 hours between 100 and 300 km, (c) 72 hours between 200 and 500 km, and (d) 96 hours between 200 and 500 km. Curves 1 - 5 denote the contributions from the radial advection of absolute vorticity ( $-u \frac{\partial(\zeta+f)}{\partial r}$ , curve 1), vertical advection ( $-\dot{\sigma} \frac{\partial \zeta}{\partial \sigma}$ , curve 2), divergence term ( $-\frac{\zeta+f}{r} \frac{\partial(ru)}{\partial r}$ , curve 3), tilting (twisting) term ( $-\xi \frac{\partial \dot{\sigma}}{\partial r}$ , curve 4), and diffusion term ( $\frac{1}{r} \frac{\partial r D_v}{\partial r}$ , curve 5). Curve 6 denotes the sum of these terms, *i.e.* the tendency of  $\zeta$ ,  $\partial \zeta / \partial t$ . Note the different scales in each panel.

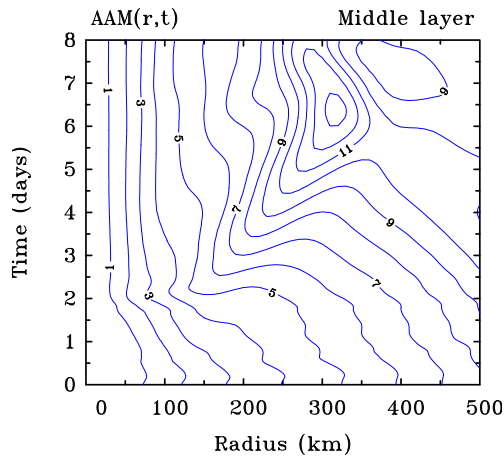


Figure 3.17: Time-radius plot of absolute angular momentum in the middle layer. Contour interval is  $1 \times 10^6 \text{ m}^2 \text{ s}^{-1}$ .



inwards in the boundary layer. It is ultimately carried upwards in the eyewall and flows outwards in the upper troposphere while conserving its absolute angular momentum. However, during their way inwards within the boundary layer, the air parcels lose some angular momentum to the sea surface. For this reason the flow becomes anticyclonic in the upper troposphere as it moves outwards at some radius from the vortex axis. The development of an upper-level anticyclone can be seen in Fig. 3.3a after already twelve hours. Anthes (1972) explains that the reversal of  $\partial M/\partial r$  occurs because the air that is transported upwards near the centre of the vortex may, “in spite of some frictional loss to the sea surface, retain a higher value of  $M$  than air at the same level but at a larger radial distance.” Unpublished radius-height cross-sections of isopleths of absolute angular momentum from a calculation using a modified version of the Penn State/NCAR fifth-generation Mesoscale Model (MM5, version 3.6) depicted in Fig. 3.18 reveal however, that absolute angular momentum surfaces bend over in the middle to upper troposphere leading to a reversed  $\partial M/\partial r$  (Smith 2011, personal communication). It is the downward advection of air with lower values of  $M$  that accounts for this behaviour. In this calculation, a reversed  $\partial M/\partial r$  develops already after twelve hours (left panel). Multiple regions of negative  $\partial M/\partial r$  are evident in the right panel of Fig. 3.18 that depicts the situation after 53 hours.

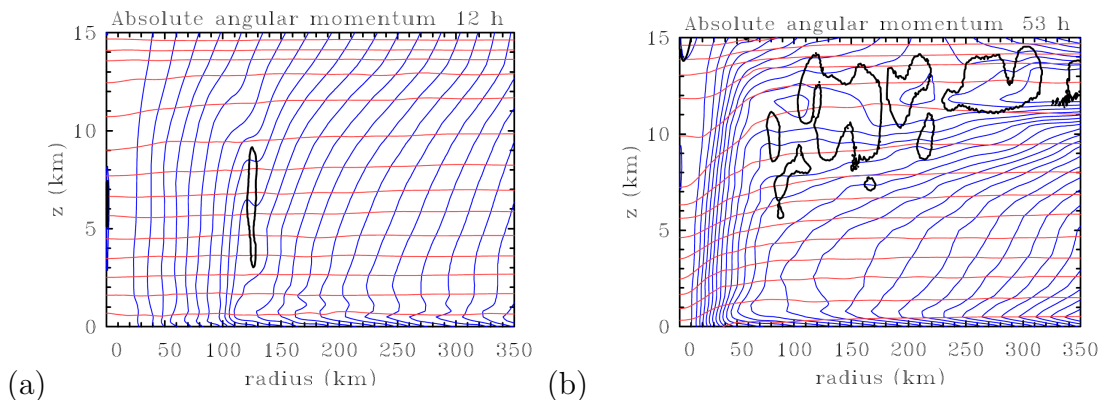


Figure 3.18: Height-radius plots of azimuthally-averaged absolute angular momentum (blue contours) from a calculation using a modified version of the Penn State/NCAR fifth-generation Mesoscale Model (MM5, version 3.6). The red contours depict potential temperature. Regions of a reversed  $\partial M/\partial r$  are encircled with a thick black curve. Plots by courtesy of Roger Smith.

Even though inertial instability might not occur in the axisymmetric model on account of the low vertical resolution, the question still remains, whether the development of a reversed radial gradient of absolute angular momentum has some impact on the dynamics of the tropical cyclone. One consequence of a reversed  $\partial M/\partial r$  is obvious in Fig. 3.3c of section 3.2. After about 5 days, the size of the vortex, as defined by the radius of gale-force wind, decreases in the middle layer even though the radial flow depicted in Fig. 3.3d is inwards. At these radii and times,  $\partial M/\partial r$  is negative, and consequently, lower values of  $M$  are advected inwards leading to a smaller-sized storm. In this section the focus has been



on the middle layer. However, the tangential wind field in the boundary layer depicted in Fig. 3.3e suggests that the impact of a reversed  $\partial M/\partial r$  in limiting or even reducing the size of the vortex is relevant in this layer also.

## 3.5 Summary

The control calculation with the axisymmetric version of a three-layer hurricane model reveals several aspects of vortex evolution that appear also in the three-dimensional version of the same model as described by Zhu *et al.* (2001). In broad terms, the vortex evolution can be divided into a gestation period, with only a gradual increase in vortex intensity, followed by a short period of rapid intensification and eventually a mature stage, where the vortex is in an approximate steady-state. Consistent with conclusions made by Zhu *et al.* (2001), rapid intensification coincides with grid-scale saturation in the middle layer. It was shown, however, that the inner core saturates much earlier in the boundary layer, *i.e.* after only three hours. Nevertheless, close to the surface the air is never saturated, which means that the surface latent heat fluxes do not cease. Two other typical features of tropical-cyclones, that have been described by Zhu *et al.* (2001), are present also in a calculation with the axisymmetric model: an upper-level anticyclone and subsidence near the axis indicative of an eye.

Interestingly, the vortex intensity, as defined by the maximum tangential wind speed in the boundary layer, develops largely independently from the evolution of the vortex size, as defined by the radius of gale-force tangential wind. This result is consistent with the observed behaviour of typhoons described by Weatherford and Gray (1988). An explanation for this behaviour was given by Smith *et al.* (2009), who proposed that there exist two (sic) independent mechanisms to spin up the inner and the outer core, respectively. Montgomery and Smith (2010) noted that this statement is too strong: there must be a degree of coupling between these two mechanisms through boundary-layer dynamics. However, the findings of Smith *et al.* (2009) are confirmed by the results presented in this chapter: the spin-up of the inner-core region occurs in the boundary layer and is associated with the development of supergradient winds. The other mechanism described by Smith *et al.* (2009), that also forms part of the conventional view of vortex spin-up, intensifies the tangential wind speed at outer radii, thereby increasing the vortex size. The former mechanism is associated with gradient wind imbalance that is a prominent feature of the hurricane boundary layer. It implies a net agradient force that drives a strong near-surface inflow. The absolute angular momentum in the boundary is not conserved as the air flows inwards, however, it has been shown, that air parcels converge much more quickly and also towards lower radii as air parcels above the boundary layer. The flow ultimately becomes supergradient, rapidly decelerates and turns upwards to enter the middle layer. The spin-up of the interior vortex occurs by vertical advection of angular momentum-rich air from the boundary layer. These results match the conceptual model of the steady, inner-core region of a tropical cyclone proposed by Smith *et al.* (2008). An important difference here is that the outflow region above the inflow jet within the boundary layer, that generates

the supergradient winds, is not confined to a shallow region, as in the conceptual model, but occurs over a deeper layer representing the lower free troposphere, *i.e.* the middle layer. However, this is only a consequence of the low vertical resolution of the model that has only three layers.

The development of supergradient winds has been shown to be a ubiquitous feature in the hurricane boundary layer by e.g. Zhang *et al.* (2001), Kepert and Wang (2001), Nguyen *et al.* (2002), and Smith and Vogl (2008). In particular, numerical simulations of Hurricane Andrew (1992) by Zhang *et al.* (2001) provided evidence for the important role of the boundary layer in spinning up the vortex. The results presented in this chapter confirm the finding by Bui *et al.* (2009) that the unbalanced dynamics in the boundary layer is an important ingredient in the spin-up mechanism of the inner-core region. Accordingly, this process is not represented in time-dependent models that directly or tacitly assume gradient wind balance in the boundary layer such as those of Ooyama (1969), Emanuel (1997), Frisius (2006) and Wirth and Dunkerton (2006).

Radial profiles of terms in the tangential momentum equation revealed that radial diffusion in the inner core becomes one of the dominant terms. This finding was highlighted by Anthes (1974, p505), who notes that in the vicinity of the eye and eywall, "... the horizontal and cumulus diffusion terms and the inertial terms contribute substantially in the tangential wind equation." However, in an investigation of the importance of the vertical momentum transfer by cumulus convection with the three-dimensional version of this model, Zhu and Smith (2002) did not find it to significantly alter the maximum intensity attained. Recently, Bryan and Rotunno (2009) found that the maximum tangential wind speed in an axisymmetric numerical model was most sensitive to the intensity of turbulence in the radial direction. This finding, together with the results presented in this chapter, motivate sensitivity studies to investigate the model behaviour on the magnitude of the horizontal eddy diffusivity. The results of these experiments will be presented in Chapter 6.

Another interesting aspect presented in this chapter, is the development of regions where a necessary criterion for the occurrence of inertial instability is fulfilled. It turned out that these regions coincide with regions of negative absolute vorticity, or equivalently, with regions of negative radial gradient of absolute angular momentum. For reasons described by Ooyama (1969), inertial unstable motions are highly unlikely to occur in models with very low vertical resolution. However, it has been shown here that the development of an inverse radial gradient of absolute angular momentum does influence the vortex evolution. For example, in regions where  $\partial M/\partial r < 0$  and where there is inflow, the size of the vortex is found to decrease.

# Chapter 4

## Rotational influences on the intensity and size of tropical cyclones

This chapter addresses two questions, *i.e.* how does the ambient rotation rate characterized by the Coriolis parameter influence the intensity and size of a tropical cyclone, and can this influence be interpreted in terms of the Turner-Lilly-Morton ideas? These ideas may serve as a possible conceptual framework for these issues and are discussed in the following section. An assessment of the applicability of these ideas to tropical cyclones is also given.

### 4.1 The Turner-Lilly-Morton ideas

In general, *there are two fundamental requirements for vortex amplification: a source of rotation and some forcing mechanism to concentrate the rotation.* An example is one of the laboratory experiments described by Turner and Lilly (1963), in which a vortex was produced in water contained in a rotating cylinder by releasing bubbles from a thin tube along the upper part of the rotation axis. A sketch of the flow configuration is shown in Fig. 4.1. The drag on the fluid exerted by the ascending bubbles generates a secondary circulation in the water, producing convergence in the region below the source of bubbles. Except in a shallow boundary layer near the lower boundary, converging rings of fluid conserve their angular momentum and spin faster. The ultimate degree of amplification of the angular velocity depends on how far rings of fluid can be drawn inwards and on the background rotation rate, factors that are not independent.

How far rings of fluid can be drawn inwards depends, *inter alia*, on the forcing strength, *i.e.* on the bubbling rate. If the forcing ( $F$ ) is sufficiently large for a given rotation rate ( $\Omega$ ), rings of fluid may be drawn in to relatively small radii before the centrifugal force ( $v^2/r$ ) and Coriolis force ( $2\Omega v$ ) opposing the inward motion balance the radial pressure gradient induced by the bubbles that drives the rings of fluid inwards (see inset to Fig. 4.1). If the forcing is comparatively weak, or if the rotation rate is sufficiently strong, this balance may be achieved before the radial displacement is very large so that a significant amplification of the background rotation will not be achieved. Of course, if there is no

background rotation, there will be no amplification, and if the background rotation is very weak, the centrifugal and/or Coriolis forces never become large enough to balance the radial pressure gradient, except possibly at large radii from the source of bubbles. It is important to note that these arguments emphasize the unbalanced wind adjustment from the instant that the bubbling is turned on.

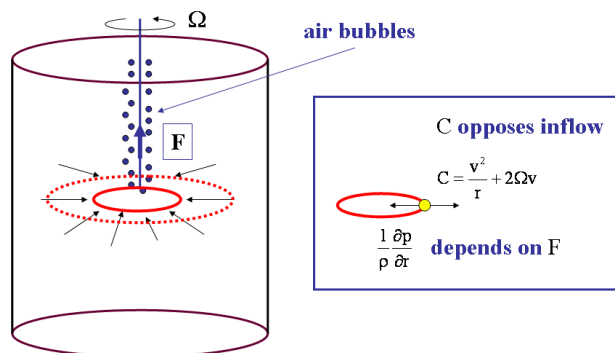


Figure 4.1: Schematic of flow configuration in the Turner and Lilly experiment. The inset indicates the principal forces per unit mass acting on an air parcel in the radial direction: an inward-directed pressure gradient force  $-(1/\rho)(\partial p/\partial r)$  and an outward force  $C$ , the sum of the centrifugal force ( $v^2/r$ ) and Coriolis force ( $2\Omega v$ ).

Clearly, one would expect the existence of an optimum forcing strength to produce the maximum amplification of the angular velocity for a given strength of background rotation, or an optimum background rotation rate for a given forcing strength. These ideas were explained eloquently by Morton (1966) and demonstrated in related numerical experiments by Smith and Leslie (1976, 1978). The dust-devil-like vortices investigated in Smith and Leslie (1976) are driven by the buoyancy arising from thermal heating of the surface, but it turns out that the high rotation rate regime produces warm-cored, two-cell vortices reminiscent of tropical cyclones. A question arises: to what extent do the above ideas apply to tropical cyclones?

One difference between the foregoing laboratory and numerical experiments and a tropical-cyclone model is that, in the latter, one does not have the flexibility to independently vary the rotation rate and the strength of the forcing. Indeed, it will be shown in section 4.4 that the “effective forcing strength” varies with the intensity. However, one *can* control the effective background rotation by varying the Coriolis parameter,  $f$ . Another potential difference is the role of the boundary layer in tropical-cyclone spin-up, which has been discussed in section 3.3 (Chapter 3). Whether the boundary layer is of comparable importance in the spin-up of tall narrow vortices of the type discussed above is not clear, although Turner’s (1966) approximate theoretical description of his laboratory vortex recognised the strong constraint imposed by the boundary layer in the steady problem. A third difference is the fact that the azimuthally-averaged component of flow in a tropical cyclone is close to gradient wind balance except in the boundary layer and the outflow layer in the upper troposphere (Willoughby 1979). In contrast, as noted above, the

Turner-Lilly-Morton ideas highlight the temporal adjustment to gradient wind balance.

## 4.2 The calculations

A set of calculations is carried out in order to investigate the evolution of a vortex growing from the same initial baroclinic vortex in an otherwise quiescent environment with different levels of background rotation characterized by the Coriolis parameter,  $f$ . In particular, the aim is to give more insight on the dependence of the vortex intensity, characterized by the maximum tangential wind speed, and the vortex size, characterized by the radius of gale-force winds, on the background rotation strength, measured by the Coriolis parameter. Taking a reference latitude of  $20^\circ\text{N}$  and denoting the corresponding Coriolis parameter as  $f_o$ , calculations for ten values of  $f$  are carried out:  $f = 0, 0.1f_o, 0.25f_o, 0.5f_o, 0.75f_o, f_o, 1.25f_o, 1.5f_o, 1.75f_o,$  and  $1.9f_o$ , corresponding to the Equator and latitudes  $2.4^\circ\text{N}, 4.9^\circ\text{N}, 9.8^\circ\text{N}, 14.9^\circ\text{N}, 20.0^\circ\text{N}, 25.3^\circ\text{N}, 30.9^\circ\text{N}, 36.8^\circ\text{N}$  and  $40.5^\circ\text{N}$ .

## 4.3 Dependence on the Coriolis parameter

Figure 4.2 shows time-series of maximum tangential wind speed,  $v_{max}$ , in the middle and lower layers in the set of ten calculations with different values of  $f$  and with the initial vortex profile in Fig. 3.1. It shows also the radius,  $r_{gales}$ , at which the tangential wind speed reaches gale force ( $17 \text{ m s}^{-1}$ ) in each layer. The dependence of  $v_{max}$  and  $r_{gales}$  on  $f$  are discussed in the next two subsections.

### 4.3.1 Vortex intensity

There is a clear dependence of  $v_{max}$  on  $f$ , with both the onset time of rapid intensification increasing and the intensification rate decreasing slightly as the rotational constraint (*i.e.*  $f$ ) increases. The low-latitude vortices ( $f \leq 0.25f_o$ ) show the earliest and most rapid intensification, but their intensity after a few days is less than those at higher latitudes. The intensity of the two lowest-latitude vortices shows considerable oscillatory behaviour during the decay phase. Significantly, the largest values of  $v_{max}$  occur in the lowest layer, which is the layer influenced by surface friction. The reason for this behaviour has been discussed in section 3.3 (Chapter 3).

The intensity after twelve days, characterized by  $v_{max}$  in either the boundary layer or middle layer, is summarized in Fig. 4.3a, which shows  $v_{max}$  as a function of  $f$  in both layers. The most intense vortex is that which develops in an environment with background rotation  $f = 1.5f_o$ , *i.e.* there exists an optimum background rotation for maximum intensity. At first sight, this result would seem to be consistent with those of the Turner-Lilly laboratory experiments, but as will be shown in section 4.5, care is required in making a direct analogy with the experiments. It is consistent also with the results of DeMaria and Pickle (1988, p1552), who found that the intensity at  $20^\circ$  latitude ( $57 \text{ m s}^{-1}$ ) was marginally stronger

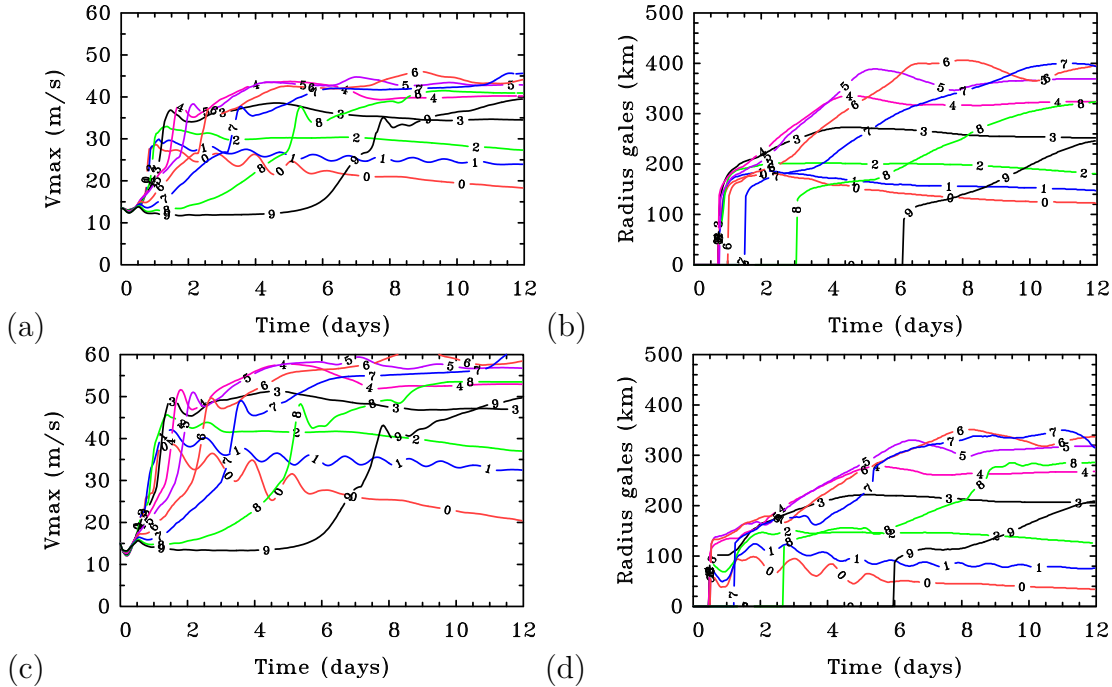


Figure 4.2: Time-series of maximum tangential wind speed (left panels) and radius of gale-force winds (right panels) in the middle layer (upper panels) and in the lower layer (lower panels), in the set of calculations with different values of  $f$  as indicated. Curves 0-9 correspond with the sequence of  $f$  values: 0 (curve 0),  $0.1f_o$  (curve 1),  $0.25f_o$  (curve 2),  $0.5f_o$  (curve 3),  $0.75f_o$  (curve 4),  $1.0f_o$  (curve 5),  $1.25f_o$  (curve 6),  $1.5f_o$  (curve 7),  $1.75f_o$  (curve 8) and  $1.9f_o$  (curve 9).

(by  $2 \text{ m s}^{-1}$ ) than that at  $10^\circ$  latitude and decreased to  $51 \text{ m s}^{-1}$  at  $30^\circ$  and  $46 \text{ m s}^{-1}$  at  $40^\circ$  latitude.

### 4.3.2 Vortex size

Referring to the Fig. 4.2b, it is seen that, in the middle layer, for the smallest values of  $f$  ( $0 \leq 0.5f_o$ : curves 0-3),  $r_{gales}$  increases rapidly to a maximum and thereafter slowly declines. For larger values of  $f$  (curves 4-9),  $r_{gales}$  increases steadily with time and finally levels out, or it reaches a peak and then declines a little, in some cases fluctuating (e.g. curves 5 and 6), before levelling out. In the lower layer, the behaviour is broadly similar (Fig. 4.2d). Note that, in this layer,  $r_{gales}$  is generally smaller than in the middle layer because the winds at large radii are subgradient on account of friction.

Figure 4.3b shows  $r_{gales}$  as a function of  $f$  in the middle and lower layers after twelve days. The results indicate the existence of an optimum background rotation strength to obtain the largest vortex as characterized by  $r_{gales}$ . This finding is contrary to that of DeMaria and Pickle (1988), who found that the vortex size increases monotonically with latitude. Nevertheless, it is pertinent to ask also whether the result obtained in this study

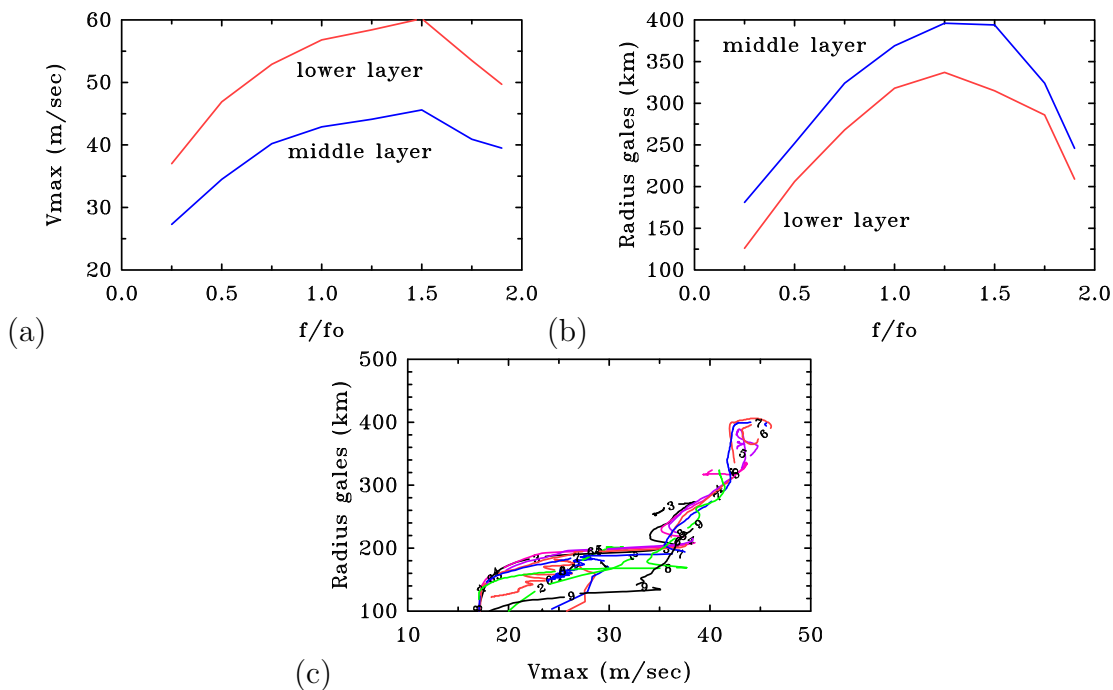


Figure 4.3: Variation of (a) the maximum tangential wind, and (b) radius of gales (based on this wind component) with the Coriolis parameter in the lower and middle layers at twelve days in the calculations described in section 4.3. Panel (c) shows the radius of gales in the middle layer as a function of intensity, measured by the instantaneous value of  $v_{max}$  during the twelve-day life cycle of the ten variable  $f$  calculations.

can be interpreted in terms of those from the Turner-Lilly laboratory experiments. In fact, it will be shown in section 4.5 that this is not the case, but in doing so a number of issues are raised that might be important in tropical-cyclone dynamics.

DeMaria and Pickle noted that their finding concerning vortex size “... appears to be related to the radial positioning of the diabatic heating”. They argued (p1551) that the boundary-layer convergence and thus the diabatic heating are closer to the centre as the storm latitude is decreased. Since the diabatic heating does not vary rapidly as a function of latitude, “the same diabatic heating occurs at smaller radii at low latitudes resulting in smaller storms”. A difficulty with this interpretation is that the diabatically-induced secondary circulation is related to the radial gradient of diabatic heating rate rather than the heating rate alone (see section 4.4).

### 4.3.3 Intensity versus size

Figure 4.3c shows  $r_{gales}$  as a function of  $v_{max}$  at all times during the foregoing calculations. Note that there is not a one-to-one correspondence between the intensity of a vortex and its size (as measured by  $r_{gales}$ ) during the entire period of development. This lack of a relationship is in line with the observational study of Weatherford and Gray (1988) and a

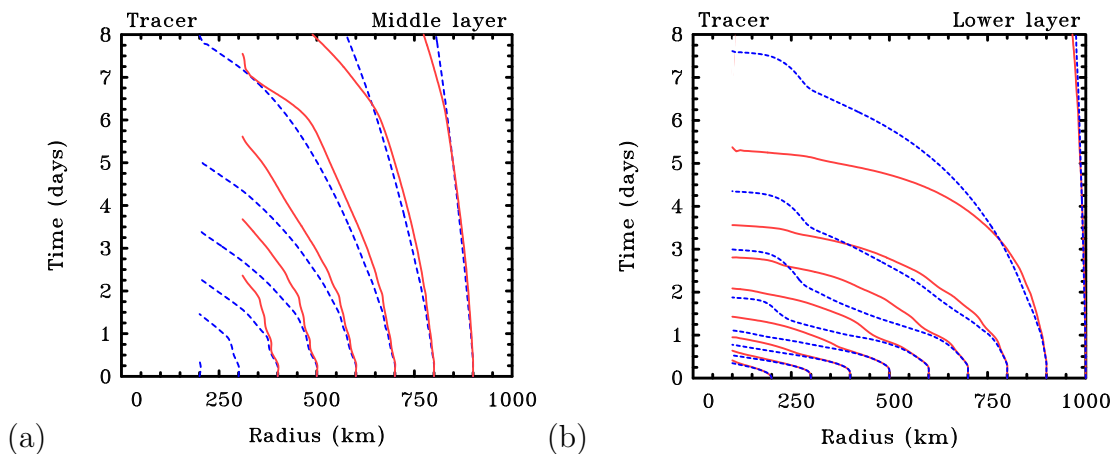


Figure 4.4: Time-radius plots of the trajectories in (a) the middle layer and (b) the boundary layer in the calculations with  $f = 0.25f_o$  (blue/dashed lines) and  $f = f_o$  (red/solid lines).

possible reason for it is discussed by Smith *et al.* (2009). However, it is evident from the figure that, for the vortices studied here, which all start with the same modest-sized initial vortex, there *is* an approximate linear increase in  $r_{gales}$  with  $v_{max}$  for  $v_{max} > 35 \text{ m s}^{-1}$ .

### 4.3.4 Trajectories

The Turner-Lilly-Morton ideas invoke the ability of a given forcing strength to produce radial displacements of rings of air. Thus it is pertinent to examine the air-parcel trajectories. Figure 4.4 shows time-radius plots of a passive tracer in the lower and middle layers in the calculations with  $f = 0.25f_o$  and  $f = f_o$ . The evolution of the passive tracer has been calculated as described in section 3.3 (Chapter 3). For the same reasons as described there, contours in the inner region are not shown.

The patterns of tracer movement *in the middle layer* are consistent with the idea discussed in section 4.1 that the inward radial displacements of air columns should be larger in the case with smaller  $f$ , although this argument assumes that the forcing strength does not change appreciably between these calculations. In fact, it will be shown in section 4.4 that the forcing strength is mostly larger in the case with  $f = f_o$ , so that there are two competing effects.

It is clear from Fig. 4.4 that the radial displacements in each experiment are very much larger in the lower layer, where friction is important, than in the middle layer. As discussed in section 3.3 (Chapter 3), it is for this reason that the largest tangential wind component occurs in the boundary layer (cf. left panels of Fig. 4.2).



## 4.4 Effective forcing

At this point it is appropriate to examine the nature of the “effective forcing” in the experiments in the previous section and how this forcing might be quantified. In balance models in which gradient and hydrostatic balance is assumed, the forcing of the secondary circulation is related, *inter alia*, to the radial gradient,  $\partial\dot{\theta}/\partial r$ , of the diabatic heating rate,  $\dot{\theta}$  (see Shapiro and Willoughby 1982, Bui *et al.* 2009). The overturning circulation *outside the eye* is characterized by the maximum magnitude of the *negative* radial gradient of diabatic heating that lies radially outside the heating maximum. Since balance dynamics is found to be a good first approximation above the friction layer (e.g. Willoughby 1990, Bui *et al.* 2009), it would seem reasonable to take the maximum of  $-\partial\dot{\theta}/\partial r$  as a suitable measure for the effective forcing, at least to a first approximation. To this end the heating rate and its radial gradient have been diagnosed from the model output (see Appendix B).

Figure 4.5 shows the time evolution of this maximum for eight of the ten calculations described above (the curves for  $f = 0$  and  $f = 0.1f_o$  are omitted as they have significant oscillations that clutter the diagram). Comparing Figures 4.2 and 4.5 it is seen that the maximum of  $-\partial\dot{\theta}/\partial r$  increases sharply at the time of onset of rapid intensification. As shown in section 3.2, the onset of rapid intensification is accompanied by saturation on the grid-scale in the inner-core region. At grid points where saturation occurs, the parameterized convection scheme switches off and the explicit scheme for latent heat release takes over. For each value of  $f$ , the maximum gradient of the heating rate increases sharply at first and then declines, but with significant oscillations. As in calculations with more complex models (e.g. Rotunno and Emanuel 1987, Persing and Montgomery 2003, Nguyen *et al.* 2008), these oscillations are associated with pulsations in the explicit convection, which, in turn, are accompanied by inertia-gravity waves that the convection induces. After about day 10, the “effective forcing” is larger in the calculations at the higher latitudes ( $f \geq 1.25f_o$ , curves 6-9) than those at latitudes with  $f \leq f_o$ .

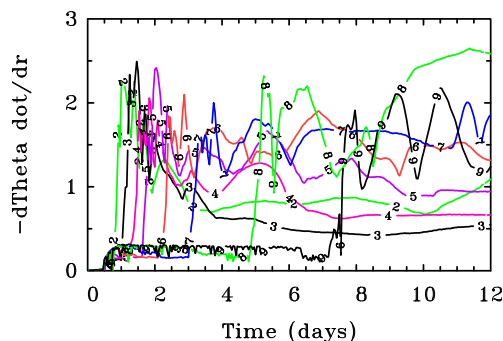


Figure 4.5: Time-series of the maximum magnitude of the negative radial gradient of the diabatic heating rate ( $\text{K hour}^{-1} \text{ km}^{-1}$ ) in the middle layer in the set of calculations with different values of  $f \geq 0.25f_o$ . Curve numbering as in the legend to Fig. 4.2.

Following DeMaria and Pickle’s (1988) finding that the boundary-layer convergence and thus the diabatic heating occur much closer to the storm centre as the latitude is

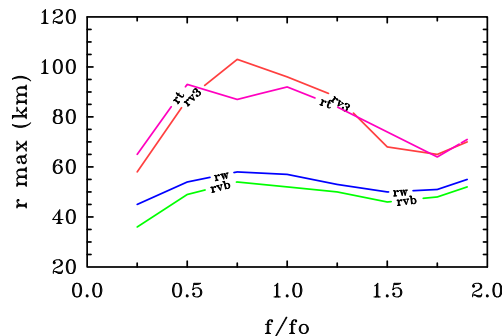


Figure 4.6: Variation of the radii of maximum radial gradient of diabatic heating rate (curve  $rt$ ), maximum vertical velocity (curve  $rw$ ) from the boundary layer to the middle layer, and maximum tangential wind speed in the middle layer (curve  $rv3$ ) and boundary layer (curve  $rvb$ ), with the Coriolis parameter at twelve days in the calculations described in section 4.3.

decreased, it is pertinent to investigate the dependence of the radius of the maximum magnitude of the *negative radial gradient* of diabatic heating rate,  $rmax(-\partial\dot{\theta}/\partial r)$ , in the middle layer and to compare this with the radius of maximum vertical velocity,  $rmax(w)$ , from the lower layer to the middle layer and the radii of maximum tangential wind speed in the lower and middle layers,  $rmax(v_b)$  and  $rmax(v_3)$ , respectively. These radii are shown in Fig. 4.6 after twelve days of integration. It is seen that there is a reasonable correlation between  $rmax(-\partial\dot{\theta}/\partial r)$  and  $rmax(w)$  with the former lying between 10 and 40 km outside the latter, which is one to four times the horizontal grid spacing in the model<sup>1</sup>. Consistent with the absolute angular momentum surfaces sloping outwards above the boundary layer,  $rmax(v_3)$  is significantly larger than  $rmax(v_b)$ , but note that  $rmax(v_b)$  and  $rmax(w)$  follow each other, with  $rmax(w)$  lying outside of  $rmax(v_b)$ , but within 10 km (*i.e.* one grid interval) of it. The broadest vortex, based on either  $rmax(v_b)$  or  $rmax(v_3)$ , occurs for  $f = 0.75f_o$ , but this is not the most intense vortex. Indeed, comparison of the left panels of Fig. 4.2 with Fig. 4.6 shows that there is not an obvious relationship between the maximum tangential wind speed and the radius at which it occurs in either layer.

## 4.5 An appraisal of the TLM ideas

The second question posed in the introduction of this chapter is examined now: can the foregoing results be interpreted in terms of the TLM ideas discussed in section 4.1?

<sup>1</sup>To produce smoother fields, the radius of the maxima of particular quantities were obtained to within a kilometre by spline interpolation.

### 4.5.1 Relevance to intensity

At first sight, the dependence of  $v_{max}$  on  $f$  discussed in section 4.3.1 is suggestive that the TLM-ideas might apply in a broad sense. Moreover, as shown in section 4.3.4, the patterns of tracer movement in the middle layer would be consistent with the expectation based on inertial stability considerations that the inward radial displacements of air columns should be larger in the case with smaller  $f$ , at least as long as the forcing strength does not change appreciably between these calculations. However, it has been shown in section 4.4 that the forcing strength is mostly larger in the case with the larger rotation rate, at least for the two values of  $f$  shown in Fig. 4.4. Thus there are two competing effects: while the forcing tries to draw air columns inwards in the middle layer, the inertial stability resists these displacements. It does not appear possible to foresee the outcome of these competing effects in a simple way and one needs to do an explicit calculation.

A further issue is that, as noted in section 4.1, the optimum amplification in the Turner-Lilly experiment refers to the fractional increase in angular velocity and not directly to intensity, which is the quantity of interest here, and indeed to tropical-cyclone forecasters.

Another important limitation is the fact that in a tropical cyclone, the spin-up of the inner-core winds occurs in the boundary layer (Emanuel 1997, Zhang *et al.* 2001, Smith *et al.* 2009, Sanger 2011). The results in the previous chapter (section 3.3) show the same feature in that the intensity in the middle layer is determined by the vertical advection of air from the boundary layer and is not a result of the convergence of absolute angular momentum in the middle layer as envisaged by the conventional view of tropical-cyclone intensification (Ooyama 1969, 1982 (see p374), Shapiro and Willoughby 1982, Smith *et al.* 2009, Montgomery and Smith 2011).

In the light of these findings, a curve showing maximum angular velocity in the middle layer as a function of  $f$  has not been plotted because the TLM ideas apply only to radial advection above the boundary layer.

The breakdown of the TLM ideas in the boundary layer are illustrated by the patterns of tracer movement in the lower layer shown in Fig. 4.4b. In this layer, the degree of inertial stability is overshadowed by the effects of friction, which, beyond a certain radius ensure that the net radial force is inward, irrespective of the degree of inertial stability as normally calculated. Thus, because of friction, there is no inertial resistance to radial displacements in this layer.

### 4.5.2 Relevance to size

However, the question remains whether the TLM ideas provide an interpretation of the optimum value of background rotation to produce the largest vortex as found in section 4.3.2. One could argue that, at zero ambient rotation, the only source of angular momentum is that of the initial vortex and this angular momentum is progressively removed by surface friction. As long as deep convection is maintained, there has to be a period of intensification and broadening in this case. Ultimately, however, the angular momentum in the lower and middle troposphere will steadily diminish and the vortex will weaken. Thus the radius of

gales will contract with time.

As the background rotation rate is increased, there will be an increasing reservoir of planetary angular momentum for the vortex to draw upon, allowing it to sustain itself. However, inertial stability considerations dictate that, at least for a fixed forcing strength, the stronger the ambient rotation in the middle layer, the harder it is for air parcels in the outer region to be drawn inwards (see section 4.1). Certainly, smaller radial displacements will lead to smaller increases in the maximum amplification of the angular velocity, but not necessarily to a smaller increase in the tangential wind speed. The reason is that the degree of amplification of the tangential wind speed depends both on the magnitude of the inward parcel displacement and the background rotation rate<sup>2</sup>. Thus smaller inward displacements do not necessarily lead to smaller-sized storms.

## 4.6 Summary

This chapter has sought to develop a basic framework for understanding the rotational influences on the intensity and size of tropical cyclones, as characterized by the maximum tangential wind speed and the radius of gales, respectively.

Using a suite of idealized calculations with the minimal axisymmetric tropical-cyclone model, it has been shown that there is an optimum ambient rotation, characterized by the Coriolis parameter, for the largest vortex intensity and for the largest vortex size. The former finding is consistent with earlier results of DeMaria and Pickle (1988), but the latter is not. At first sight these findings appear to be broadly consistent with expectations from the Turner-Lilly-Morton ideas. However, a number of reasons have been identified why these ideas are of limited applicability to tropical cyclones. For one thing, the interpretations in the calculations described herein are complicated by the fact that the effective forcing is found to change with latitude, making it difficult to anticipate the outcome in a simple way. Due to this additional tier of complexity that results from the additional coupling between the forcing associated with the diabatic heating and the wind distribution in the boundary layer, a second set of similar calculations is carried out, where the forcing is held fixed. The results of these experiments are presented in the next chapter.

A more serious limitation of the Turner-Lilly-Morton ideas has already been shown in Chapter 3, *i.e.* the fact that the spin-up of the maximum tangential winds in the tropical-cyclone inner core occurs in the boundary layer, where, because of friction, there is a net inward force, irrespective of the perceived inertial resistant radial motion. In this layer, absolute angular momentum is not conserved so that the Turner-Lilly-Morton ideas do not strictly apply. In consequence of this spin-up mechanism, a *simple* interpretation for the dependence of intensity and size of tropical cyclones remains elusive. However, based on the findings herein an articulation of the key components of the dynamics has been offered

---

<sup>2</sup>If a ring of air initially at radius  $R$  in uniformly-rotating fluid with angular velocity  $\frac{1}{2}f$  is displaced to radius  $r$  while conserving its absolute angular momentum,  $rv + \frac{1}{2}fr^2$ , the tangential velocity at the new radius will be  $v = \frac{1}{2r}f(R^2 - r^2)$ , which depends on  $f$ . However, the relative amplification of the angular velocity is  $v/(rf) = \frac{1}{2}(R^2/r^2 - 1)$ , which is independent of  $f$ .

which help to interpret the foregoing dependence. Because of several competing effects, one has to do the relevant calculation to determine which effects outweigh the others for a particular level of ambient rotation.

Furthermore, it has been shown that in the calculations presented in this chapter, there is not a one-to-one correspondence between the vortex intensity and size during the entire period of development. This lack of a relationship is in line with the observational study by Weatherford and Gray (1988). However, it was found that for more intense storms ( $v_{max} > 35 \text{ m s}^{-1}$ ), there is an approximate linear increase in the radius of gales with intensity. Due to the occurrence of intense midget storms, one has to be cautious about the generality of this relationship.



# Chapter 5

## Rotational influences on the intensity and size - fixed forcing

It is evident from a comparison of Figures 4.2 and 4.5 of Chapter 4 that there is not a simple one-to-one correspondence between the intensity and size of the vortex at a particular latitude and time and the “effective forcing” at that time. The additional tier of complexity that results from the additional coupling between the forcing associated with the diabatic heating and the wind distribution in the boundary layer motivates a second set of calculations similar to those presented in the previous chapter. They differ from the foregoing calculations in that the vortex is forced by a prescribed radial profile of diabatic heating typical of that in the control experiment and other moist processes excluded. These calculations will be discussed now.

### 5.1 The calculations

For the reason above, a set of simplified experiments with a modified version of the minimal axisymmetric model is examined in which the radial and vertical structure of the diabatic heating rate are specified. By design, the effects of moisture are not considered explicitly. A heating distribution is prescribed in all the three layers, the specification of which is guided by the radial and vertical structure of the diagnosed heating rates in the mature stage in the foregoing moist calculation with  $f = f_o$ . The formula for the diabatic heating rate is given in Appendix C. The heating rate, which is the same in all experiments here, is multiplied by a simple function of time that allows the heating to build up exponentially from zero to a constant level on a time scale of the order of 24 hours. This procedure minimizes the spurious generation of inertia-gravity waves.

The experiments start from the initial vortex profile in Fig. 3.1 and are distinguished by their latitude. The corresponding values of  $f$  are:  $f = 0, 0.1f_o, 0.25f_o, 0.5f_o, 0.75f_o, 1.0f_o, 1.5f_o, 2.0f_o, 3.0f_o, 5.0f_o, 7.0f_o,$  and  $10.0f_o$ . The larger values of  $f$  are clearly unrealistic for the Earth, but are used to provide an adequate survey of the vortex behaviour.

## 5.2 Results

Figure 5.1 shows time series of  $v_{max}$  in the middle layer for this set of calculations. It shows also time series of  $r_{gales}$  in the middle layer. Again there is a clear dependence of the evolution of these quantities on  $f$ . Except in the calculations for  $f \leq 0.25f_o$ , the intensity becomes approximately steady after about four days. In the case of zero background rotation,  $f = 0$ , the intensity reaches a maximum after about two and a half days and then steadily declines as the initial absolute angular momentum is progressively removed by surface friction.

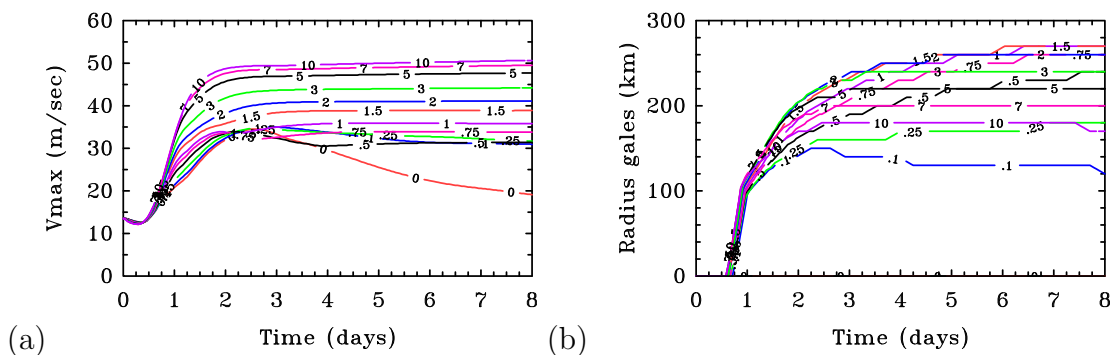


Figure 5.1: Time-series of (a) the maximum tangential wind and (b) the radius of gale-force winds in the middle layer in the set of calculations with fixed forcing and different values of  $f$ :  $0, 0.1f_o, 0.25f_o, 0.5f_o, 0.75f_o, f_o, 1.5f_o, 2f_o, 3f_o, 5f_o, 7f_o$  and  $10f_o$ . Curves are labelled with the corresponding multiple of  $f_o$ .

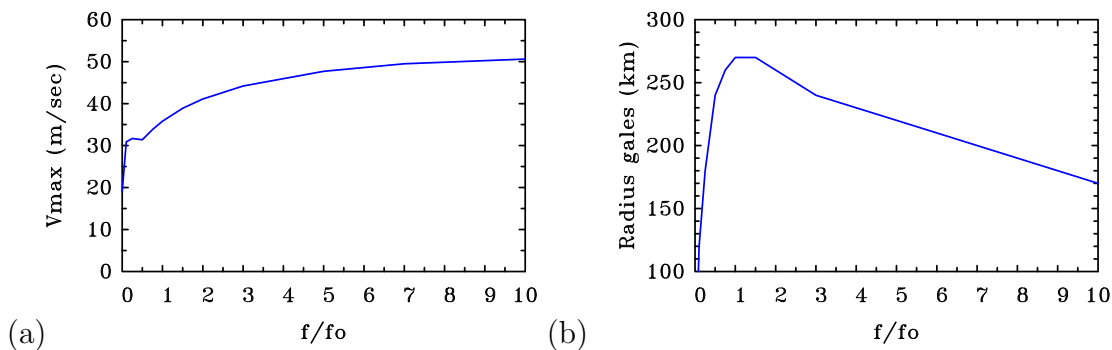


Figure 5.2: Variation with the background rotation of (a) the maximum tangential wind and (b) the radius of gale-force winds in the middle layer at 8 days in the set of calculations with fixed forcing.

Figure 5.2 shows  $v_{max}$  and  $r_{gales}$  after eight days of integration as a function of  $f$ . The maximum tangential wind speed increases with increasing  $f$ . However, unlike the moist case described in section 4.3 (Chapter 4), there is no optimum background rotation rate for intensity, neither within the range of realistic values of  $f$ , nor beyond. This finding



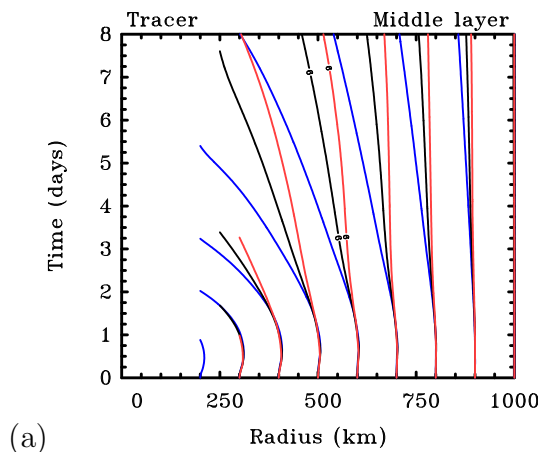


Figure 5.3: Time-radius plots of the trajectories in the middle layer in the calculations with  $f = 0.5f_o$  (blue lines),  $f = f_o$  (black lines), and  $f = 1.5f_o$  (red lines).

implies that the dependence of the effective forcing strength on the rotation rate found in the moist calculations is an important additional consideration for tropical cyclones.

Unlike intensity, there *is* an optimum background rotation rate for maximum vortex size (see Fig. 5.2b). For  $f < 0.75f_o$  (*i.e.* to about  $15^\circ\text{N}$ ),  $r_{gales}$  in the middle layer increases strongly with  $f$ . For  $f$  between  $f_o$  and  $1.5f_o$  (about  $30^\circ\text{N}$ ), its rate of increase slows and its value levels out at 270 km. For larger values of  $f$ ,  $r_{gales}$  decreases.

Figure 5.3 shows time-radius plots of a passive tracer in the middle layer in the calculations with  $f = 0.5f_o$ ,  $f = f_o$  and  $f = 1.5f_o$ . As in Fig. 4.4, the patterns of tracer movement are consistent with the idea discussed in section 4.1 (Chapter 4) that the inward radial displacements of air columns should decrease as the rotational constraint increases. In this case the forcing strength does not change between these calculations. Moreover, the trajectories do not cross as they do in Fig. 4.4, where the forcing strength does change.

## 5.3 Interpretation

An interpretation of the foregoing results is provided by an examination of the steady-state radial profiles of various quantities after 8 days of integration for different values of  $f$ . These quantities include: the radial, tangential and vertical velocity components; the absolute angular momentum; the tangential wind tendency due to the radial advection<sup>1</sup> of absolute vorticity<sup>2</sup>; and the gradient force defined in section 3.3 (Chapter 3). The profiles are shown in Figures 5.4-5.6 for a subset of the values for  $f$  in Fig. 5.1.

<sup>1</sup>The complete radial and tangential momentum equations are given in Chapter 2.

<sup>2</sup>The absolute vorticity is equal to the radial gradient of absolute angular momentum divided by radius (see section 3.3).

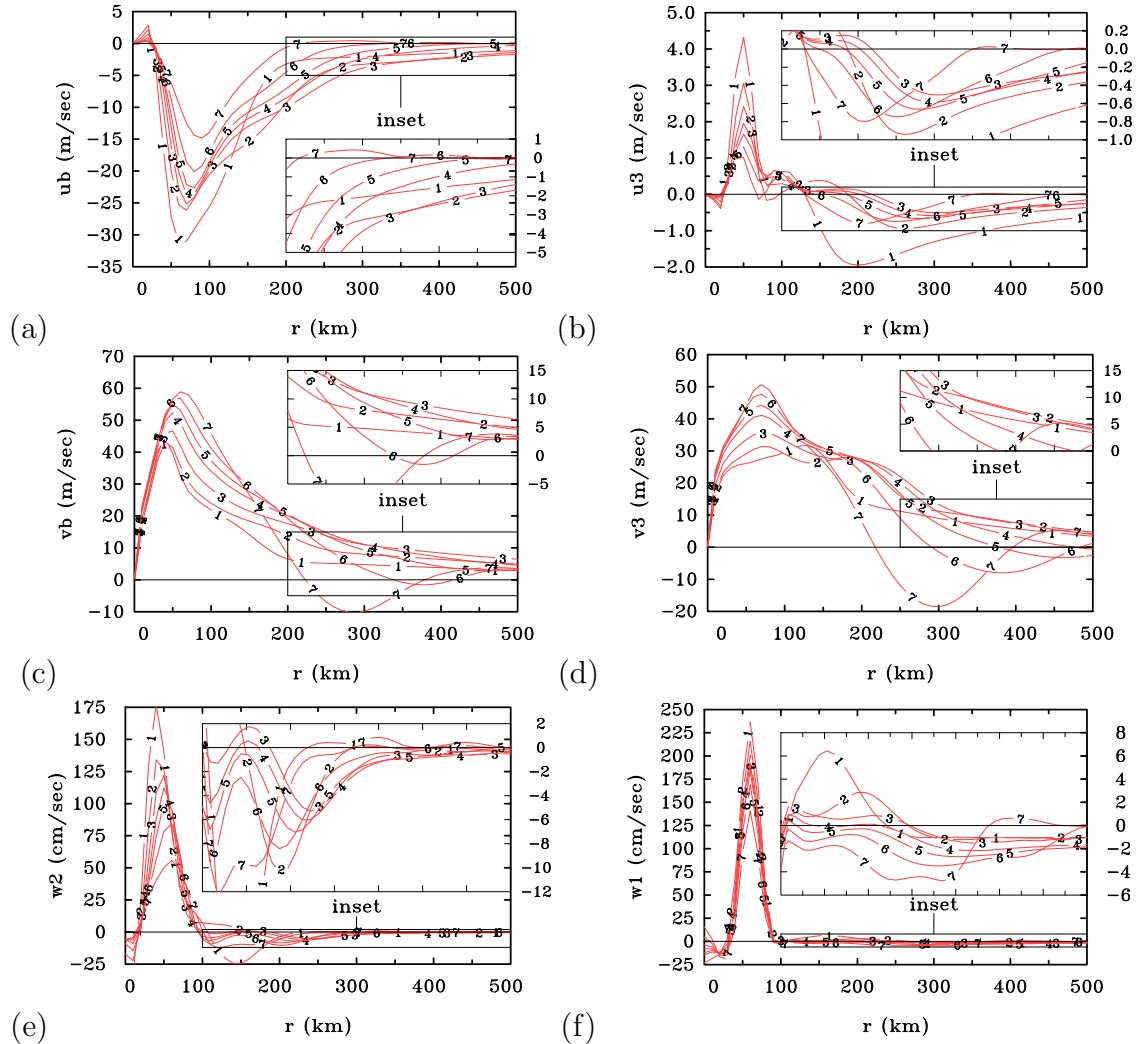


Figure 5.4: Steady-state radial profiles of radial wind speed in (a) the boundary layer ( $u_b$ ) and (b) the middle layer ( $u_3$ ) for selected values of  $f$  (curve 1 for  $f = 0.25f_o$ , curve 2 for  $f = 0.5f_o$ , curve 3 for  $f = f_o$ , curve 4 for  $f = 2f_o$ , curve 5 for  $f = 3f_o$ , curve 6 for  $f = 5f_o$ , curve 7 for  $f = 10f_o$ ) after 8 days. Panels (c) and (d) show the corresponding profiles for tangential wind speed ( $v_b$  and  $v_3$ , respectively), and panels (e) and (f) those of vertical velocity between the boundary layer and middle layer ( $w_2$ ) and middle layer and upper layer ( $w_1$ ), respectively. The inset regions show an amplified view of the rectangular region outlined beyond a certain radius.

### 5.3.1 Constraints on the secondary circulation

The imposed forcing function leads to inflow in the middle layer beyond a certain radius (130 km for  $f = 0.25f_o$ , 180 km for  $f = 0.5f_o$ , 220 km for  $f = f_o$ , then decreasing to 130 km as  $f$  increases: see Fig. 5.4b). The maximum inflow decreases in strength as  $f$  increases to  $f_o$  and the radius of the maximum increases. As  $f$  increases beyond  $f_o$ , the inflow increases

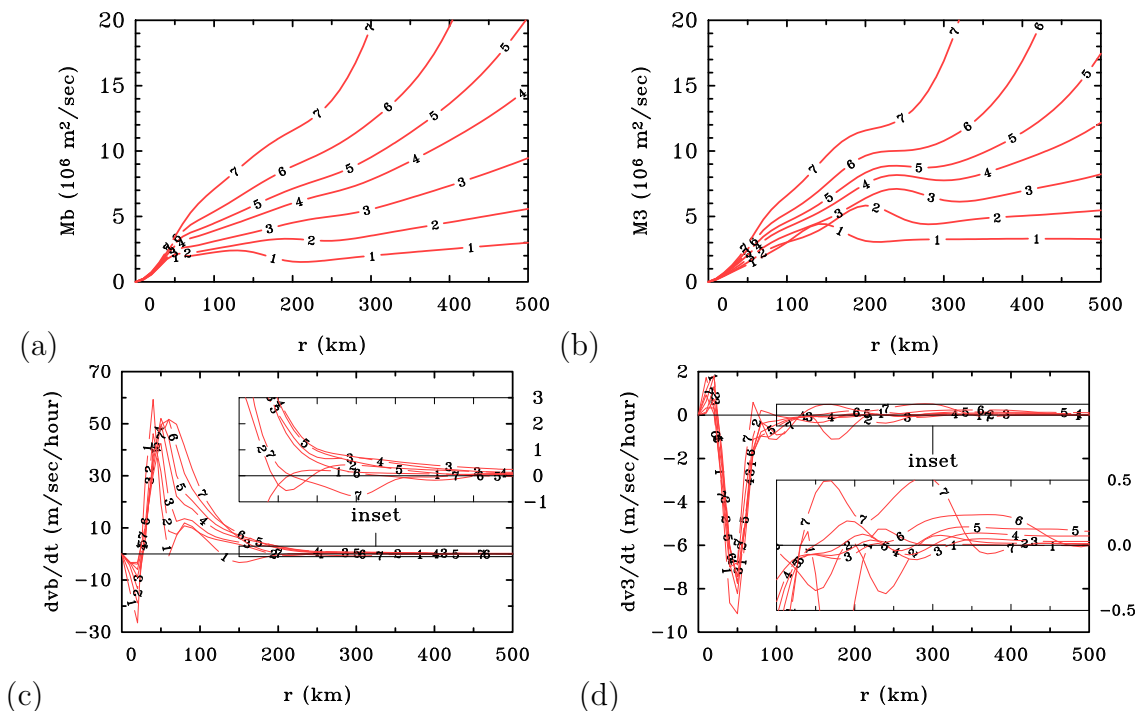


Figure 5.5: Steady-state radial profiles of the absolute angular momentum in (a) the boundary layer and (b) the middle layer after 8 days for the values of  $f$  in Fig. 5.4. Panels (c) and (d) show the corresponding profiles of the time tendency of the tangential wind associated with the radial flux of absolute vorticity. The inset region in each panel shows an amplified view of the rectangular region outlined beyond a certain radius.

again in magnitude and the radius of the maximum inflow decreases. It is plausible that the initial decrease in strength and increase in the radius of maximum inflow are associated with the increase in the inertial stability, which makes it harder for the fixed forcing to draw air parcels inwards. However, as  $f$  increases further, the increasing stability to radial motion confines the subsidence closer and closer to the forcing region (Figures 5.4e,f) so that, to the extent that the mass flux carried by the secondary circulation is not appreciably reduced in strength, the return radial inflow must increase in strength and its maximum must move inwards. Figures 5.4e,f show that the maximum vertical velocity at the model interface levels, and hence the mass flux of the secondary circulation, is actually reduced in strength as  $f$  increases, but clearly not sufficiently to reverse the increase in maximum radial inflow discussed above. As  $f$  increases beyond  $f_o$ , the geometric effect takes over, *i.e.* the subsidence occurs over an area that decreases in proportion to the radius squared whereas the inflow increases inversely with radius. As a result, the maximum subsidence increases and the radius of the maximum inflow decreases.

### 5.3.2 Factors controlling size

Figure 5.4d shows the tangential wind profiles after 8 days in the middle layer for selected values of  $f$ . As a preliminary to understanding the behaviour of these profiles as  $f$  increases, it is important to recall from Chapter 3 that, beyond a certain radius, the spin-up of the tangential wind in the middle layer occurs solely because of inflow in regions where the radial gradient of absolute angular momentum,  $M$ , is positive, *i.e.* by the radial advection of  $M$  divided by radius. The spin-up is moderated by the downward advection of  $M$  by subsidence from the upper layer, where values of  $M$  at any radius are typically less than in the middle layer because of prior frictional loss in the boundary layer. As  $f$  increases, the maximum subsidence increases in strength because, as shown above, the secondary circulation becomes more confined radially. The effect of this subsidence on the tangential wind profile is most evident at background rotation rates exceeding  $2f_o$  (curves 5-7 in Fig. 5.4d), where it leads to anticyclonic flow inside a radius of 500 km.

At a given radius beyond about 150 km, the tangential wind speed increases with increasing  $f$  up to a certain value ( $f \leq f_o$  for  $r < 400$  km,  $f \leq 0.5f_o$  for  $r > 400$  km) and then decreases as  $f$  increases further. The increase has to be associated with the radial advection of  $M$ ,  $-u(\partial M/\partial r)$  by the inflow in regions where<sup>3</sup>  $\partial M/\partial r > 0$ . While at most values of  $r$ ,  $\partial M/\partial r$  is mostly positive and increases with  $f$ , the behaviour of  $u$  as  $f$  increases is more complicated (Fig. 5.4b) and it is not possible to simply infer the change in  $-u(\partial M/\partial r)$  as  $f$  increases: one must do the calculation. For this reason, it is pertinent to show in Fig. 5.5d the radial profiles of the tangential wind tendency associated with the radial advection of absolute vorticity,  $-(u/r)(\partial M/\partial r)$ , in the middle layer for various values of  $f$ . It turns out that the variation of  $-(u/r)(\partial M/\partial r)$  with  $f$  is a strong function of radius, which is complicated by the fact that the range of radii for which  $\partial M/\partial r < 0$  varies with  $f$  also. For example, in the radial range from 360 km to 400 km,  $-(u/r)(\partial M/\partial r)$  increases with  $f$  for values less than  $5f_o$  and then decreases, but at other radii the behaviour is different.

For small values of  $f$ , the radial advection of  $M$  accounts for the largest contribution to the increase in the tangential wind speed with increasing  $f$  outside the core region. For these values the subsidence is relatively weak in this region (Fig. 5.4d) and the reduction of  $M$  by the vertical advection of lower values of  $M$  from the upper layer is correspondingly weak. However, as  $f$  increases, this reduction of  $M$  in the middle layer by downward advection becomes increasingly important. It is primarily these two competing effects that provide an explanation for the existence of an optimum size as shown in Fig. 5.4b.

---

<sup>3</sup>Similar to the results of section 3.4, Fig. 5.5b shows that there is a small range of radii in which  $\partial M/\partial r < 0$ . This relatively weak negative gradient arises because of the downward advection of  $M$  from the upper layer, where values of  $M$  are typically smaller than those in the middle layer. In these regions, of course, the local tendency of the tangential wind,  $\partial v/\partial t$ , is negative.

### 5.3.3 The role of the boundary layer

In the boundary layer, the agradiant force per unit mass,  $F_{agrad}$ , is negative beyond a radius of 70 km and has a minimum value just inside a radius of 100 km, except for  $f = 0.25f_o$  where this minimum occurs at a radius of about 120 km (Fig. 5.6). The minimum force decreases in value at first as  $f$  increases, but it increases again as  $f$  increases beyond  $0.5f_o$ . In contrast, changes in the breadth of the agradiant force profile as  $f$  increases are complicated and depend on the range of radii one considers. A cursory examination of Fig. 5.6, for example suggests that the broadest profile is that for  $f = 0.25f_o$ , but a closer inspection of the inset region would suggest that the profile for  $f = 0.5f_o$  is the broadest. What matters most is the maximum inward displacement of  $M$ -surfaces, taking account of the loss of  $M$  en route (Smith *et al.* 2009). This displacement is determined by an inward radial integral of the sum of the agradiant force and the frictional force, while the loss of  $M$  is determined by a radial integral of the tangential momentum equation (e.g Smith and Vogl 2008). According to boundary-layer theory, the radial pressure gradient in the boundary layer is equal to that in the middle layer, which is directed inwards. The centrifugal, Coriolis and the radial frictional forces, which for cyclonic flow are all directed outwards, depend on the tangential wind speed in the boundary layer. Thus the radial and tangential velocity components in the boundary layer are determined by solving these two coupled equations that, in turn, depend on the radial pressure gradient in the middle layer.

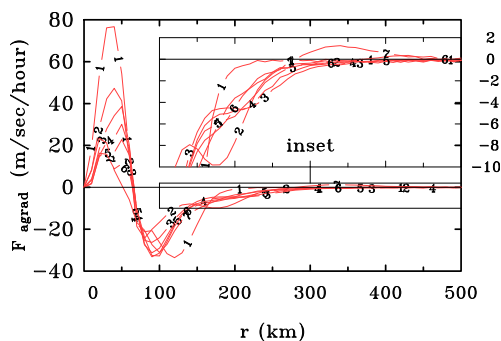


Figure 5.6: Steady-state radial profiles of the agradiant force in the boundary layer after 8 days in the calculations with fixed forcing for the same values of  $f$  as in Fig. 5.4. The inset region shows an amplified view of the rectangular region outlined beyond a radius of 100 km.

### 5.3.4 Factors controlling intensity

Inside a radius of about 70 km, the agradiant force becomes positive (*i.e.* the tangential flow becomes supergradient) and the boundary-layer inflow rapidly decelerates and turns upwards to enter the middle layer. It is the vertical advection of absolute angular momentum out of the boundary layer that determines the maximum tangential wind speed in the

middle layer as described in Chapter 3.

It is evident from the foregoing discussion that the boundary layer and interior flow are tightly coupled and for this reason, attempts to construct simple cause and effect arguments to explain the behaviour of the vortex as  $f$  varies are fraught with danger! However, an attempt to describe the nature of the coupling allows one to understand the behaviour of the fields in Fig. 5.4 as  $f$  varies.

In the boundary layer, the maximum radial inflow decreases and the radius at which it occurs increases as  $f$  increases (Fig. 5.4a). In addition, its radial profile broadens with increasing  $f$  for values less than  $f_o$  and decreases for larger values of  $f$ . This behaviour influences the radial profile of  $-(u/r)(\partial M/\partial r)$  and thereby the profile of tangential wind. There are two main opposing effects that determine the radial profile of  $v$ : one is the radial advection of absolute vorticity and the other is the surface friction. Figure 5.5a shows that as  $f$  increases, so does  $\partial M/\partial r$ , but the maximum radial velocity decreases (Fig. 5.4a). Moreover, the loss of  $M$  due to surface friction increases as  $M$ , itself, increases, but it decreases as the radial wind speed increases. The last result is essentially because with higher inflow, air parcel trajectories undergo fewer revolutions per unit radial displacement and are therefore shorter in length so that friction has less distance over which to slow the parcels down. The calculations discussed in this chapter show that as  $f$  increases, the larger gradient of  $M$  outweighs the reduced radial inflow and larger loss of  $M$  to the surface so that the largest tangential wind in the boundary layer occurs for the largest values of  $f$ . Thus, the fact that the spin-up of the tangential wind speed at inner radii in the middle layer occurs by vertical advection of  $M$  (or tangential momentum) from the boundary layer explains why the maximum tangential wind speed in the middle layer (Fig. 5.1a) increases as  $f$  increases.

## 5.4 Summary

As an aid to understanding the results of Chapter 4, a set of calculations has been carried out with the vortex forced by a prescribed radial profile of diabatic heating typical of that in the control experiment and other moist processes excluded. The set comprised twelve calculations that are distinguished by their value of  $f$ , including also larger values that are unrealistic for the Earth, but helped to provide an adequate survey of the vortex behaviour.

When the forcing is held fixed, it was found that the maximum intensity increases monotonically with increasing rotation rate, even for unrealistically large rotation rates. However, there *is* an optimum rotation rate to produce the vortex with the largest size. It has been possible to provide an understanding of this behaviour, based on diagnostics of competing processes involved.

There are primarily two competing effects that provide an explanation for the existence of an optimum ambient rotation for the largest vortex size. For small values of the Coriolis parameter,  $f$ , the radial advection of absolute angular momentum,  $M$ , accounts for the largest contribution to the increase in the tangential wind speed with increasing  $f$ . For these values, the reduction of  $M$  by the vertical advection of lower values of  $M$  from the

upper layer is correspondingly weak. However, as  $f$  increases, this reduction of  $M$  in the middle layer by downward advection becomes increasingly important. Thus, the radial advection of  $M$  is reduced also resulting in smaller-sized storms. There are two main opposing effects that determine the radial profile of the tangential wind speed: one is the radial advection of absolute angular momentum and the other is the surface friction. It was shown that as  $f$  increases, so does the radial gradient of  $M$ , but the radial velocity decreases, thereby increasing the loss of  $M$  to the surface. However, the increased radial gradient of  $M$  dominates, so that the largest values of the maximum tangential wind speed occurs for the largest value of  $f$ .

The results of this Chapter (and also of Chapter 4) point to the existence of dynamical constraints that are not explicitly included in existing theories for the maximum possible intensity of hurricanes. This study is a first step to try to understand hitherto unexplored aspects of the rotational constraints on tropical-cyclone intensification and final intensity.





# Chapter 6

## Sensitivity studies on model parameters and physical processes

In this chapter, four sensitivity studies on model parameters and important physical processes are carried out as listed in Table 6.1. Special emphasis is placed on the parameterization of turbulence, *i.e.* the radial diffusion, the turbulent flux of momentum to the sea surface and the surface fluxes of sensible and latent heat. More introductory words and descriptions of the experiments are given in the particular sections.

Table 6.1: List of sensitivity experiments.

Experiment	Name
A	Radial resolution
B	Radial diffusion
C	Surface drag coefficient
D	Capped surface enthalpy flux

### 6.1 Radial resolution

#### 6.1.1 Introduction

Previous numerical studies have shown that the simulated vortex intensity increases as the horizontal resolution is increased (e.g. Baik *et al.* 1990, Braun and Tao 2000, Hausman, 2001, Persing and Montgomery 2003, Yau *et al.* 2004, Davis *et al.* 2008, Hill and Lackmann 2009, Nguyen *et al.* 2008, Bryan and Rotunno 2009), at least for grid spacings exceeding 1 km. A comparison of the results of Hill and Lackmann (their Fig. 1) with those of Bryan and Rotunno (their Table 1) indicates that the degree of this sensitivity is model-dependent suggesting that this issue should be investigated for the present model.

### 6.1.2 The calculations

In this section, four calculations are compared using horizontal grid spacings of 5 km, 10 km (control case), 15 km and 20 km, respectively. In the formulation of these calculations it is necessary to consider a particular aspect of the scheme for representing horizontal diffusion (see section 6.2). In this scheme, the eddy diffusivity is set proportional to the horizontal divergence with a proportionality factor equal to  $\Delta^3/l$ , where  $\Delta$  is the horizontal grid spacing and  $l$  denotes a length scale that is prescribed. Without any compensating change in  $l$ , the turbulent tendencies would be decreased as the horizontal resolution is increased. Following Bryan and Rotunno (2009), the factor  $\Delta^3/l$  is kept constant for the resolution sensitivity tests presented herein.

### 6.1.3 Results and interpretation

Figure 6.1 shows time-series of the maximum tangential wind speed,  $v_{max}$ , in the lower layer and the radius,  $r_{max}(v_b)$ , of this maximum in the four calculations. It shows also time-series of the radius,  $r_{gales}$ , at which the tangential wind speed in the lower layer reaches gale force. To produce smoother fields, the values for  $v_{max}$ ,  $r_{max}(v_b)$ , and  $r_{gales}$  were obtained to within a kilometre by spline interpolation. During the gestation period, the maximum tangential wind speeds do not differ in the four calculations. However, after the period of rapid intensification, the intensity becomes larger and  $r_{max}(v_b)$  becomes smaller as the horizontal grid size is reduced, consistent with results in previous studies mentioned above. At twelve days, the maximum tangential wind speed ranges from 53.6  $\text{m s}^{-1}$  ( $\Delta = 20$  km) to 59.0  $\text{m s}^{-1}$  ( $\Delta = 5$  km), and the values for  $r_{max}(v_b)$  decrease from 63 km to 53 km. The sensitivity of both  $v_{max}$  and  $r_{max}(v_b)$  to the horizontal resolution is strongest after the period of rapid intensification. After about six days of integration, however, the values for both  $v_{max}$  and  $r_{max}(v_b)$  in the four calculations are close (within a grid distance) to each other. In particular,  $v_{max}$  in the calculation using a horizontal grid resolution of 15 km is almost identical to that in the control run ( $\Delta = 10$  km). Panel c reveals that the radius of gales is little affected by the horizontal resolution. A slight exception is the vortex size in the calculation using a horizontal grid spacing of 5 km. In this simulation the storm size is somewhat larger than the storms in the simulations with coarser horizontal resolutions between about two and half days and five and a half days. However, after about eight days of integration, the vortex size is approximately the same in all four calculations. Consequently, the sensitivity of the vortex size on the ambient rotation rate examined in Chapters 4 and 5 is independent of the horizontal resolution.

Hausman (2001) suggested that, by increasing the horizontal resolution, the radius of maximum tangential wind speed decreases “because the model resolves a smaller eye.” Furthermore, he notes that  $v_{max}$  increases “because the inflow, which is limited by  $r_{max}$ , advects angular momentum closer to the center.” However, Hausman does not say at what levels this inflow occurs.

As opposed to Hausman, Bryan and Rotunno (2009) state that the intensity increases as the eyewall becomes smaller and better resolved. However, they do not give any further

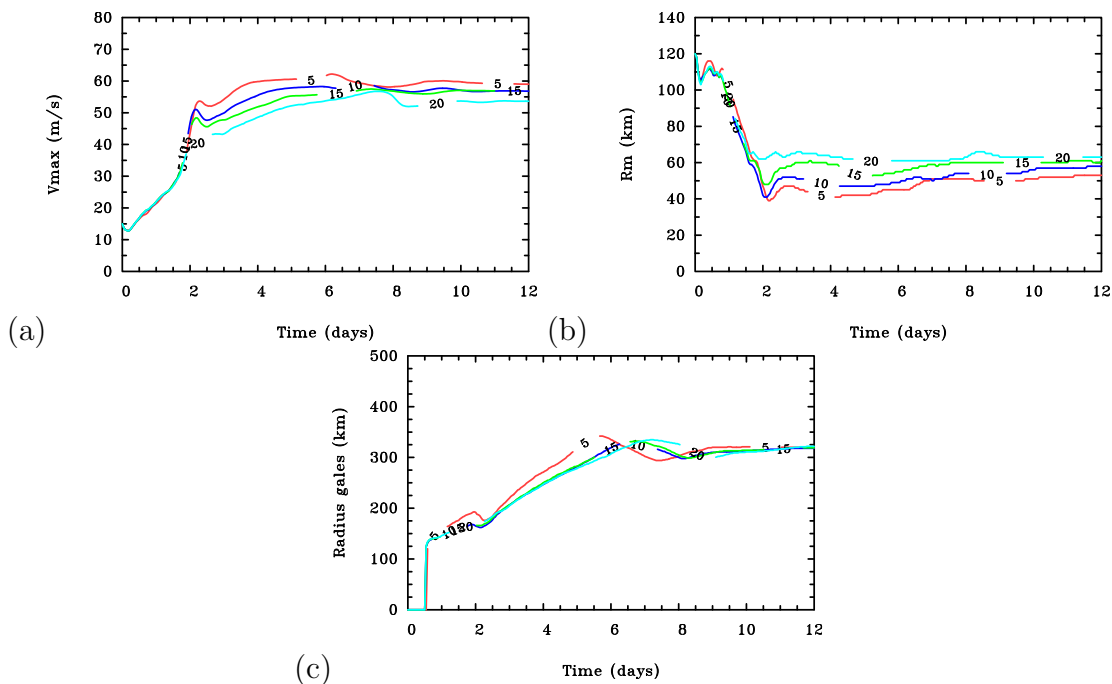


Figure 6.1: Time-series of (a) the maximum tangential wind speed in the lower layer, (b) the corresponding radius of maximum tangential wind speed, and (c) the radius of gale-force tangential winds in the lower layer in the four calculations using grid spacings of 5 km, 10 km, 15 km and 20 km.

reasons for this sensitivity. According to Anthes (1971), the use of a staggered grid in the radial direction, as used in the present model, leads to a higher effective resolution of the strong radial pressure gradient near the centre of the storm. On basis of these arguments, one may surmise, that increasing the horizontal resolution leads to an increase of the radial inflow in the boundary layer on account of an increased gradient forcing that drives the air parcels inwards. To test this supposition, plots of the radial profiles of the gradient force,  $F_a$ , in the boundary layer are made at individual times. This force (per unit mass) is defined in Chapter 3 as the difference between the local pressure gradient force and the sum of the centrifugal and Coriolis forces (each per unit mass). Figure 6.2 shows radial profiles of  $F_a$  shortly after rapid intensification (at 60 hours) and at twelve days. At 60 hours, the radius beyond which the flow in the boundary layer becomes subgradient decreases from 80 km ( $\Delta = 20$  km) to 75 km ( $\Delta = 15$  km), 70 km ( $\Delta = 10$  km), and 65 km ( $\Delta = 5$  km), respectively. Consequently, using a smaller grid spacing yields an increased forcing in the boundary layer. The flow is accelerated towards smaller radii, where it eventually becomes supergradient, decelerates and turns upwards to enter the middle layer. After twelve days, the differences in  $F_a$  between the calculations become less. In particular, the radius at which  $F_a$  changes sign outside  $r_{max}(v_b)$  is 90 km for the calculations using horizontal grid spacings of 10 km and 15 km. At this time,  $v_{max}$  in these two calculations is almost identical. Again, this fact has implications for the results of Chapters 4 and 5 concerning

the influence of the Coriolis parameter on the intensity. Using a horizontal resolution of 15 km would not have modified the results presented in these chapters.

The radial profiles of  $F_a$  show that increasing the horizontal resolution has a larger impact on the profiles at inner radii (inside 100 km), where radial gradients of  $F_a$  are larger. At outer radii, the radial gradient of  $F_a$  is much weaker and thus, decreasing the horizontal grid size does not alter the radial profile of  $F_a$  very much. This explains why the radius of gale-force winds are only slightly affected as the horizontal resolution is increased.

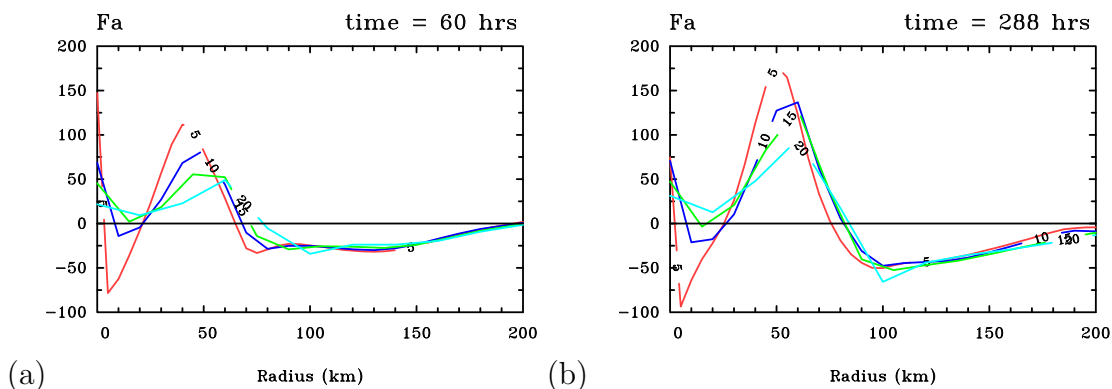


Figure 6.2: Radial profiles of the gradient force (units in  $\text{m s}^{-1} \text{h}^{-1}$ ) in the boundary layer in the four calculations using grid spacings of 5 km, 10 km, 15 km and 20 km at (a) 60 hours and at (b) twelve days.

## 6.2 Radial diffusion

### 6.2.1 Introduction

An important result of Chapter 3 is that the radial diffusion becomes one of the dominant terms in the tangential momentum equation in the inner-core region. Using an axisymmetric numerical model, Bryan and Rotunno (2009) showed that the maximum tangential wind speed is most sensitive to the intensity of turbulence in the radial direction. Motivated by their finding, together with the results of Chapter 3, this section examines the sensitivity of the present model to the magnitude of the radial diffusion.

The diffusive terms,  $D_\chi$ , where  $\chi$  is any of the prognostic variables  $u$ ,  $v$ ,  $\theta$ ,  $q$ , are tendencies that are parameterized in order to represent unresolved motions, *i.e.* turbulence. Bryan and Rotunno (2009) emphasize that this parameterization is one of the most uncertain aspects of axisymmetric numerical models. Furthermore, these authors note that, in such models, parameterization of turbulence does not represent only unresolved subgrid-scale motions, but also any three-dimensional motions including e.g. vortex Rossby waves, eyewall mesovortices, upper-level asymmetric outflow jets, etc. Turbulence in the axisymmetric tropical-cyclone model used herein is parameterized not only by a biharmonic damping term, as in the three-dimensional version of this model, but includes also a

procedure that is equivalent to the representation of Reynolds stress terms in terms of an eddy diffusivity. This procedure is similar to the parameterization scheme for turbulence in the axisymmetric models by Rotunno and Emanuel (1987) and Bryan and Rotunno (2009). However, the radial eddy viscosity,  $\nu_h$ , in their models is set proportional to the magnitude of deformation of the horizontal motion. Using the notation of these authors, the diagnostic equation for the eddy viscosity,  $\nu_h$ , in the radial direction is

$$\nu_h = l_h^2 S_h,$$

where  $l_h$  is the horizontal turbulence (mixing) length scale that has to be prescribed, and  $S_h$  denotes the horizontal deformation. Similar representations of diffusion were used also by Smagorinsky *et al.* (1965) and Anthes (1972). A consequence of the formulation is that diffusion becomes very much larger in magnitude in frontogenetic regions such as the eyewall.

In the present model, the eddy viscosity,  $K$ , given in Eq. (2.14) of Chapter 2, is not proportional to the deformation, but to the divergence, *i.e.*

$$K = \frac{\Delta^3}{l} \left| \frac{1}{r} \frac{\partial(ru)}{\partial r} \right|,$$

where  $l$  is a length scale that has to be prescribed and  $\Delta$  denotes the horizontal grid spacing. A divergence-dependent coefficient not only damps the generation of very small scales by convectively-induced convergence, but has the additional advantage that it prevents a purely tangential axisymmetric spinning vortex from appreciable decay (Shapiro 1992). In this formulation, the constant  $\Delta^3/l$  is the analogue to the square of the horizontal turbulence length scale,  $l_h$ , in the formulation by Bryan and Rotunno (2009). However, the magnitude is different as the factor  $\Delta^3/l$  is multiplied by the absolute value of horizontal divergence, whereas the factor  $l_h$  in Bryan and Rotunno's model is multiplied by the absolute value of deformation. Nguyen *et al.* (2002) used the same numerical model as used here, but they erroneously referred to the length scale  $l$  as a timescale, denoted as  $\tau_2$  (see their appendix). Another error in the appendix of their paper is the omission of the power of 3 in the nominator of the corresponding formula. The code, however, did not include this error. Nguyen *et al.* (2002) chose a horizontal resolution of 20 km and set the (sic) timescale  $\tau_2$  to 24 hours implying a true length scale of  $24 \times 3600 \text{ m} = 86400 \text{ m}$ . Throughout this thesis, the horizontal resolution in the experiments was 10 km (except in section 6.1). Following Bryan and Rotunno (2009), who state that  $l_h$  should be kept constant when changing the horizontal resolution, the parameter  $l$  in the calculation of  $K$  was set to 10800 m.

### 6.2.2 The calculations

In order to investigate the sensitivity of the vortex evolution to the magnitude of the eddy viscosity, nine calculations are carried out in which the parameter  $l$  is varied according to Table 6.2. In one calculation (experiment B9), the second-order diffusion scheme is

switched off. However, this case should not be regarded as the ‘inviscid case’ as there is still inherent diffusion associated with the biharmonic damping term.

Table 6.2: Sensitivity experiments on the eddy diffusivity.

Experiment number	$l$ [m]	$(\Delta^3/l)^{1/2}$ [m]
B1	675	38490
B2	1350	27217
B3	2700	19245
B4	5400	13608
B5	10800	9623
B6	21600	6804
B7	43200	4811
B8	86400	3402
B9	-	0

### 6.2.3 Results and interpretation

Figure 6.3 shows the time-series as Fig. 6.1, but for the nine calculations using different values of  $l$ . There is a strong sensitivity of  $v_{max}$  to the magnitude of radial diffusivity. Larger values of  $l$  decrease the intensity of turbulent diffusion, which leads to larger intensification rates and larger final maximum intensities. An increased level of turbulent diffusivity leads also to smaller values of  $rmax(v_b)$ . The final maximum intensity at twelve days ranges between  $31.0 \text{ m s}^{-1}$  in the most diffusive simulation presented herein ( $l = 675\text{m}$ ) and  $68.6 \text{ m s}^{-1}$  in the calculation, where the second-order diffusion has not been included. The corresponding values for  $rmax(v_b)$  at twelve days decrease from 87 km to 48 km, respectively. The size of the vortices in terms of the radius of gale-force (tangential) winds increases with the parameter  $l$  until it attains its value in the control calculation ( $l = 10800 \text{ m}$ , curve 5). Increasing  $l$  beyond this value (*i.e.* decreasing the level of turbulent diffusivity), does not lead to an increase of the size of the vortices any further.

Using the same model as that here, Nguyen *et al.* (2002) describe a simulation with a radial grid size of 20 km. They argue that the diffusion associated with the biharmonic damping term “is not sufficient to smear out the large amplitude shocks that arise at grid points where there is a sudden release of latent heat associated with explicit precipitation.” It is highly likely that this is due to the coarser horizontal resolution in their study. It would appear that when using a horizontal grid spacing of 10 km as in this study, one may argue that parameterizing turbulence by the biharmonic damping term only (experiment B9) *is* enough to represent turbulence.

Emanuel (1997) describes the eyewall as a frontogenetic zone. The diffusion terms, however, are frontolytic leading to weaker radial gradients of the diffused quantities. Figure 6.4 shows radial profiles of the absolute angular momentum,  $M$ , for three of the nine calculations at twelve days. These are the experiments B2, B5 (control calculation), and

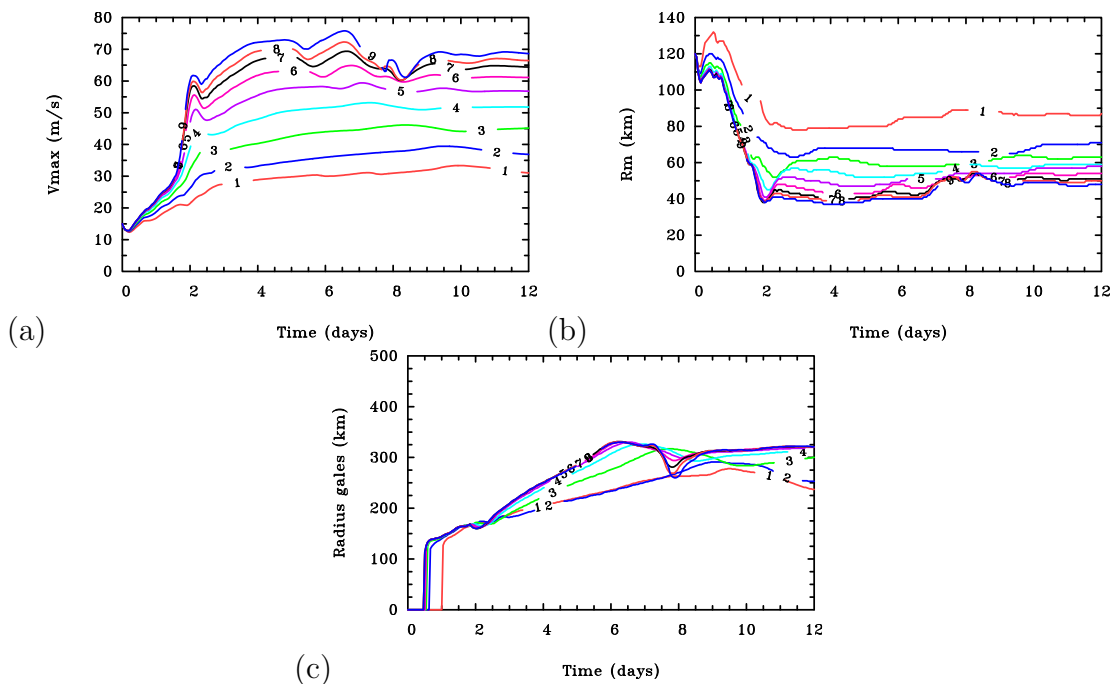


Figure 6.3: Legend as in Fig. 6.1, but in the nine experiments using different values for  $l$ . The curves 1-9 correspond to experiments B1 to B9 as listed in Table 6.2.

B8, respectively (see Table 6.2). The radial gradient of  $M$ ,  $\partial M/\partial r$ , becomes larger as the turbulent diffusion becomes weaker, with the maximum gradient located at smaller radii. The radius of maximum tangential wind speed coincides approximately with the location of the maximum in  $\partial M/\partial r$  as highlighted by the black circles. These results are consistent with those of Bryan and Rotunno (2009), who show that the intensity decreases as the diffusivity is increased. The reason is that absolute angular momentum is not advected as far towards the centre as it can be in less diffusive simulations. However, Bryan and Rotunno did not comment on where the radial advection of  $M$  occurs.

It has been shown in Chapter 3 that the spin-up of the inner core occurs in the boundary layer and is intrinsically associated with unbalanced dynamics. More precisely, despite some loss of  $M$  due to surface friction, significant vortex spin-up can occur due to the radial advection of absolute angular momentum, if the radial inflow is sufficiently large. Figure 6.5 shows radial profiles of the gradient force,  $F_a$ , in the boundary layer from the same three simulations in Fig. 6.4 after 48 hours. The minimum (negative) value of  $F_a$  becomes lower (*i.e.* the flow becomes more subgradient) as  $l$  increases at radii beyond the region, where the flow is supergradient. Figure 6.6 shows radial profiles of all the contributions to the tangential momentum equation in the lower layer at 48 hours in the three simulations as in Fig. 6.4. In the less diffusive simulations, where the flow becomes more subgradient in the boundary layer, the inflow, and thereby the horizontal flux of absolute vorticity,  $-u(\zeta + f)$ , becomes larger in magnitude. The vertical advection term,  $-\dot{\sigma}\partial v/\partial\sigma$ , in experiment B8 becomes almost as large in magnitude in the inner-core region

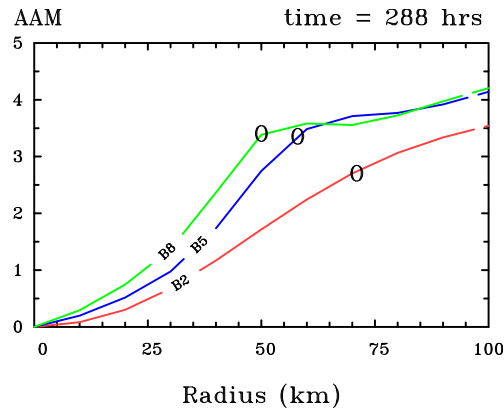


Figure 6.4: Radial profiles of the absolute angular momentum (unit  $10^6 \text{ m}^2 \text{ s}^{-1}$ ) in the boundary layer at twelve days in the experiments B2 ( $l = 1350 \text{ m}$ ), B5 ( $l = 10800 \text{ m}$ ), and B8 ( $l = 86400 \text{ m}$ ).

as  $-u(\zeta + f)$ . In the control calculation, the magnitude of the contribution to the tendency of  $v$ ,  $\partial v / \partial t$ , by  $-\dot{\sigma} \partial v / \partial \sigma$  is only about half of that of  $-u(\zeta + f)$ , and it is almost negligible in B2. The increasing importance of  $-\dot{\sigma} \partial v / \partial \sigma$  in the tangential momentum equation as the level of turbulent diffusivity is decreased can be explained by the fact that the flow becomes more supergradient (see Fig. 6.5), with larger values in  $v_{max}$ . Subsequently, the inflowing air rapidly decelerates and turns upwards into the eyewall.

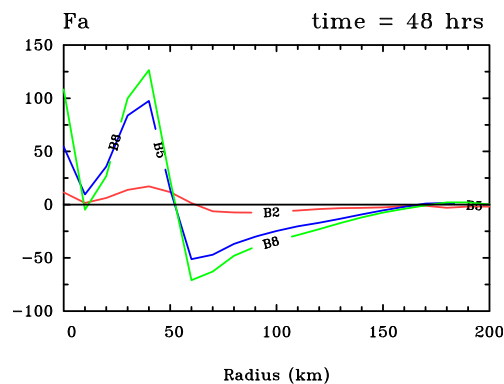


Figure 6.5: Radial profiles of the gradient force (units in  $\text{m s}^{-1} \text{ h}^{-1}$ ) in the lower layer at 48 hours in the experiments B2 ( $l = 1350 \text{ m}$ ), B5 ( $l = 10800 \text{ m}$ ), and B8 ( $l = 86400 \text{ m}$ ).

Rotunno *et al.* (2009) investigated the effect of turbulence in tropical cyclones using the Advanced Research Weather research and forecast (ARW) model (version 2.2). By decreasing the horizontal grid size from 1.67 km to 185 m, the simulated tropical cyclone became more intense, consistent with the results presented in section 6.1. However, as the horizontal resolution was increased further with a grid spacing below 100 m, Rotunno *et al.* claimed that turbulence could be resolved in terms of simulated large-scale eddies that led to somewhat weaker tropical cyclones in their simulations. This weakening is analogous to the finding that axisymmetric tropical-cyclone simulations produce weaker



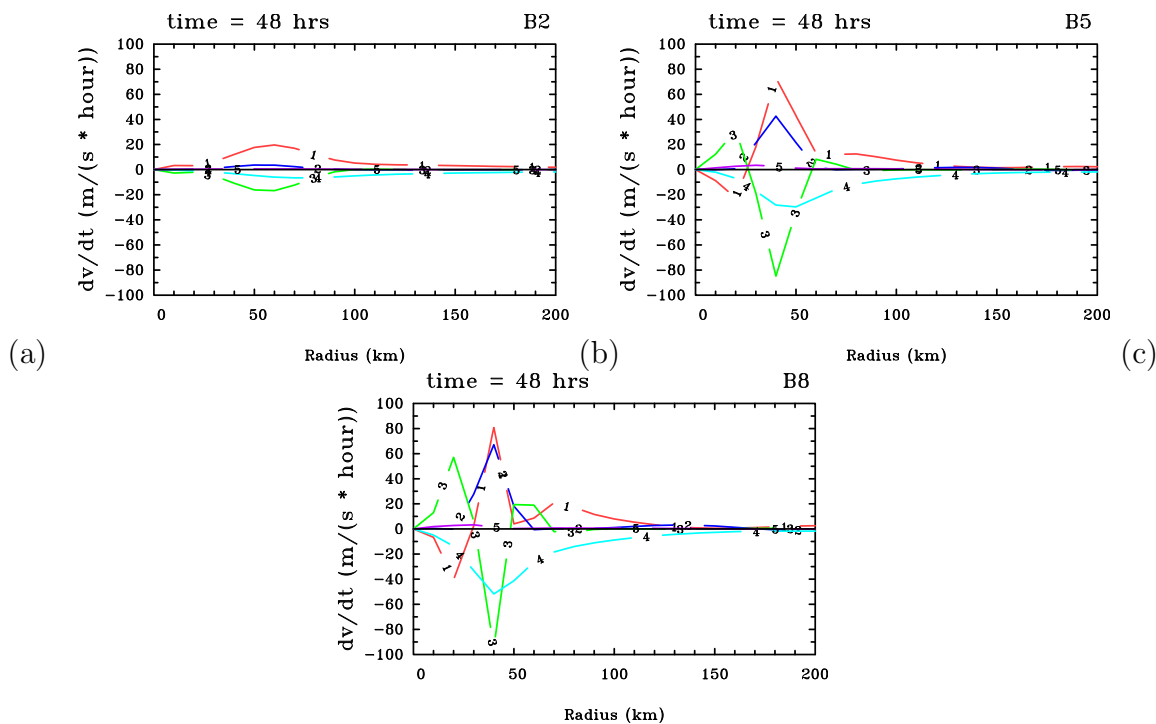


Figure 6.6: Radial profiles of the contributions to the tangential momentum equation during rapid intensification at 48 hours in the lower layer in (a) experiment B2, (b) experiment B5 (control), and (c) experiment B8. Curves 1 - 4 denote the contributions from the radial flux of absolute vorticity ( $-u(\zeta + f)$ , curve 1), vertical advection ( $-\sigma\partial v/\partial\sigma$ , curve 2), radial diffusion (curve 3), and surface friction (curve 4). Curve 5 denotes the sum of these terms, *i.e.* the tendency of  $v$ ,  $\partial v/\partial t$ .

intensities as the parameterized turbulence is increased. One may question whether the simulations carried out by Rotunno *et al.* did resolve turbulence, because the authors did not simultaneously increase the vertical resolution. Bryan and Rotunno (2009) conclude that “large uncertainty is an inherent characteristic of axisymmetric numerical model simulations, considering that there is currently no quantitative theoretical guidance with which to specify turbulence effects (particularly in the radial direction).”

## 6.3 Surface drag coefficient

### 6.3.1 Introduction

In a seminal paper, Malkus and Riehl (1960) showed that the maximum swirling wind in a steady-state tropical cyclone is proportional to the square root of the ratio of the surface exchange coefficients for sensible heat and momentum,  $C_T$  and  $C_D$ , respectively. The importance of the oceanic heat source, or more precisely, the sea-to-air vapour fluxes, characterized by an exchange coefficient,  $C_q$ , was recognized by Ooyama (1969). Building

on these pioneering works, Emanuel (1986) developed an analytic steady-state axisymmetric tropical-cyclone model that forms the basis for his theory for potential intensity (PI) (Emanuel 1986, 1988, 1995b, 2004, Bister and Emanuel 1998). This theory suggests that the maximum swirling wind is proportional to the square root of the ratio of surface exchange coefficients for enthalpy<sup>1</sup>,  $C_K$ , and momentum,  $C_D$ . Consistent with the findings of Malkus and Riehl (1960), Ooyama (1969) and Rosenthal (1971), the maximum winds in Emanuel’s model, as well as in his PI-theory, increase with  $C_K$  and decrease with  $C_D$ .

Based on these findings, much effort has been put into acquiring measurements of the exchange coefficients at very high wind speeds of hurricane-strength (Black *et al.* 2007, Drennan *et al.* 2007, French *et al.* 2007, Zhang *et al.* 2008). The field observations by Black *et al.* (2007) and Zhang *et al.* (2008) suggest the ratio  $C_K/C_D$  lies in the range of 0.6 to 0.7, whereas recent laboratory work by Haus *et al.* (2010) suggests it to be lower ( $\approx 0.5$ ) for wind speeds in the range between  $30 \text{ m s}^{-1}$  and  $40 \text{ m s}^{-1}$ . The value of  $C_K/C_D$  beyond wind speeds of  $40 \text{ m s}^{-1}$  remains controversial.

Smith *et al.* (2009) highlight the important role of the boundary layer in the spin-up process of the inner core of a tropical-cyclone. Their new findings question the longstanding view that increasing the surface drag coefficient,  $C_D$ , leads to both lower intensification rates and lower maximum tangential wind speeds. Montgomery *et al.* (2010) addressed this issue by performing numerical experiments with a modified<sup>2</sup> version of the MM5 model used by Nguyen *et al.* (2008) and showed that both intensification rate and maximum intensity of the model vortex increase with increasing  $C_D$  until a certain threshold and then decrease. More precisely, their calculations show that the maximum tangential wind speed increases with the surface drag coefficient until a value of  $C_D = 2.0 \times 10^{-3}$ . By increasing the drag coefficient further,  $v_{max}$  is shown to be relatively insensitive to  $C_D$  up to a very high value of  $5.2 \times 10^{-3}$ . As  $C_D$  increases beyond  $13.0 \times 10^{-3}$ ,  $v_{max}$  begins to decrease, but the magnitude still exceeds hurricane-strength. The authors state that the largest value of  $C_D$  considered in their study is more typical over land.

Motivated by the findings of Montgomery *et al.* (2010), it is interesting to investigate the sensitivity of the three-layer axisymmetric model to the surface drag coefficient.

### 6.3.2 The calculations

Five experiments are carried out. These are listed in Table 6.3. The first two experiments compare a control calculation that uses Shapiro’s (1992) formula for  $C_D$  with a calculation in which  $C_D$  is calculated from a recent sensitivity study by Smith *et al.* (2011a). These authors modified the surface drag coefficient to fit the results of the coupled boundary layer air-sea transfer experiment (CBLAST: see Black *et al.* 2007, Drennan *et al.* 2007,

<sup>1</sup>If the transfer coefficients for sensible and latent heat are the same, then the total heat transfer is equivalent to the transfer of moist enthalpy (Emanuel 1995). This assumption has been made throughout the thesis.

<sup>2</sup>In each simulation of Montgomery *et al.* (2010),  $C_D$  was set to a constant value.

French *et al.* 2007, Zhang *et al.* 2008). Their formula is given by:

$$C_D = (0.7 + 1.4(1 - \exp(-0.055R_F |\mathbf{u}_b|))) \times 10^{-3}. \quad (6.1)$$

Shapiro's formula for  $C_D$  is given by Eq. 2.11 in Chapter 2. Henceforth, these experiments are referred to as experiments C1 and C2. Because of the lack of better observational guidance,  $C_K$  has often been assumed to be equal to  $C_D$  (e.g. Rotunno and Emanuel 1987, Zhu *et al.* 2001, Nguyen *et al.* 2002). This assumption was made also in the calculations of the previous chapters and in Sections 6.1 and 6.2. However, recent observations (e.g. Drennan *et al.* 2007) suggest that the exchange coefficient for surface enthalpy fluxes does not show a systematic variation with the near-surface wind speed. Therefore, in the calculations presented here,  $C_K$  is set to a constant value of  $1.3 \times 10^{-3}$ .

In order to examine the model sensitivity to the drag coefficient (or to the ratio  $C_K/C_D$ ), and in order to compare the results with those of Montgomery *et al.* (2010), three experiments are carried out in which  $C_D$  is set to one of three constant values. The values for  $C_D$  decrease from 1.86 to 1.3, and  $1.0 \times 10^{-3}$ , respectively. Henceforth, these calculations are referred to as experiments C3, C4 and C5.

Table 6.3: List of experiments that investigate the model sensitivity to the surface drag coefficient.

Series of experiments	Description
C1 and C2	Comparison of two calculations using different formulae for the surface drag coefficient: C1) $C_D$ as suggested by Shapiro (1992), and C2) $C_D$ as suggested by Smith <i>et al.</i> (2011a), respectively. $C_K = 1.3 \times 10^{-3}$ .
C3, C4 and C5	Comparison of three calculations in which the surface drag coefficient, $C_D$ , is decreased from $1.86 \times 10^{-3}$ ( $C_K/C_D = 0.7$ ), to $1.3 \times 10^{-3}$ ( $C_K/C_D = 1.0$ ), and $1.0 \times 10^{-3}$ ( $C_K/C_D = 1.3$ ). $C_K = 1.3 \times 10^{-3}$ .

Figure 6.7 shows the dependence of the surface drag coefficient on the near-surface wind speed from Equations (2.11) and (6.1). Equation (2.11) gives a linear increase with  $|\mathbf{u}_b|$ . Previous numerical studies have assumed also a linear increase of  $C_D$  with the wind speed using similar formulae (e.g. Deacon relationship in Rosenthal 1971, Rotunno and Emanuel 1987, Craig and Gray 1996). However, that based on the CBLAST measurements is relatively insensitive to  $|\mathbf{u}_b|$  for values exceeding about  $30 \text{ m s}^{-1}$ . For all near-surface wind speeds, the value for  $C_D$  is larger if Shapiro's formula is used.

### 6.3.3 Results and interpretation

Figure 6.8 shows time-series of  $v_{max}$  and  $rmax(v_b)$  for the two calculations C1 and C2. The intensification rate during the gestation period is similar in the two simulations. However, the onset of rapid intensification occurs earlier in C1, which uses Shapiro's  $C_D$ , but during

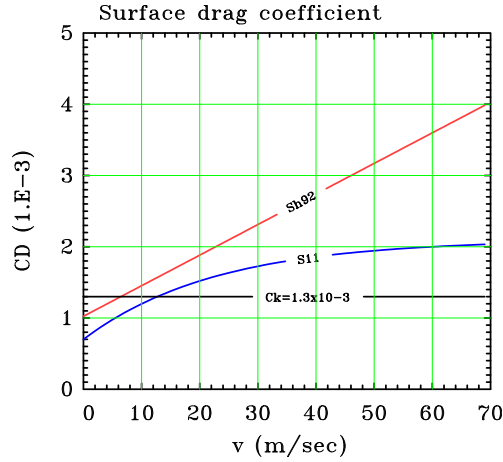


Figure 6.7: Surface drag coefficient as a function of the near-surface wind speed. The red line refers to the formula used in Shapiro (1992) and in the previous chapters of this thesis, the blue line refers to the formula used in Smith *et al.* (2011a). The black line denotes the constant value of  $1.3 \times 10^{-3}$  for  $C_K$  used in the experiments C1 to C5.

the mature stage, the intensity is larger when  $C_D$  is based on CBLAST data (experiment C2). At twelve days,  $v_{max}$  in the latter calculation is  $55.2 \text{ m s}^{-1}$ , compared with only  $45.7 \text{ m s}^{-1}$  in the control calculation. The time-series of  $rmax(v_b)$ , depicted in panel b, show that the differences between the two calculations are most pronounced until about two and a half days, *i.e.* until the end of the period of rapid development. During this time,  $rmax(v_b)$  is smaller in C1 than in C2 by an amount of about 20 km. After the period of rapid intensification, the values for  $rmax(v_b)$  are still smaller in the control simulation, but the differences between the two calculations are minor. The maximum tangential wind speeds in both calculations are smaller than those in the control calculation of Chapter 3 because  $C_K$  is taken here to be constant, which constrains the surface enthalpy flux. Larger values for  $v_{max}$  may still be attained by reducing the level of diffusivity as has been shown in section 6.2.

From a purely dynamical point of view, the role of surface friction in the boundary layer has a dual character with two competing effects. On the one hand, it acts to reduce the tangential wind speed component in the boundary layer. On the other hand, this reduction leads to strong inflow, so that air parcel trajectories undergo fewer revolutions per unit radial displacement and are therefore shorter in length. Thus, friction has less distance over which to slow the parcels down. Consequently, the stronger the inflow in the boundary layer, the less is the reduction of absolute angular momentum,  $M$ , due to surface friction. Therefore, an increase in surface drag may ultimately lead to enhanced vortex spin-up.

So far,  $C_D$  was allowed to vary with wind speed. The additional sensitivity of  $C_D$  to the near-surface wind speed is avoided in the calculations presented next by setting  $C_D$  to constant values.

A number of numerical studies (e.g. Craig and Gray 1996, Braun and Tao 2000, Bryan

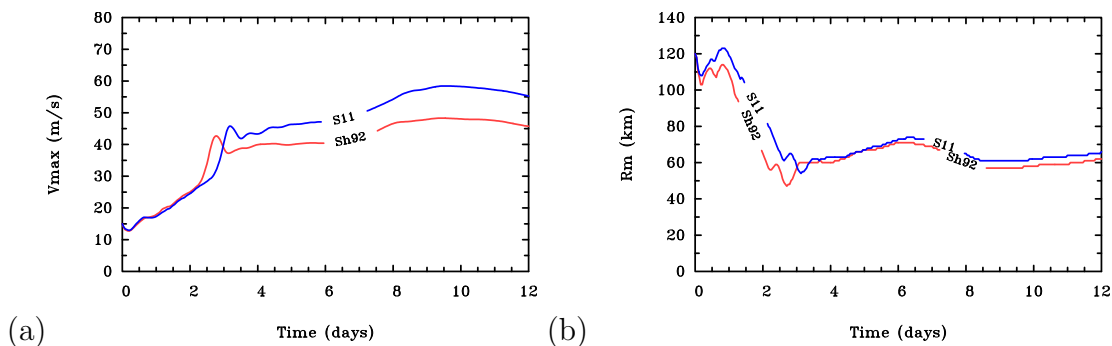


Figure 6.8: Time-series of (a) the maximum tangential wind speed in the lower layer and (b) the corresponding radius of maximum tangential wind speed in the experiments C1 using Shapiro’s formula for  $C_D$  (red curve, label Sh92) and C2 using the formula for  $C_D$  as used in Smith *et al.* (2011a) (blue curve, label S11).

and Rotunno 2009, Montgomery *et al.* 2010) have investigated the dependence of the maximum tangential wind speed on the ratio  $C_K/C_D$ , rather than on the magnitude of either  $C_D$  or  $C_K$ . The perceived importance of the dependence of tropical-cyclone intensification on this ratio stems from Emanuel’s axisymmetric theory, in which the maximum swirling winds are proportional to the square root of the ratio  $C_K/C_D$ . According to Emanuel (1995b), an incipient vortex does not intensify when the ratio  $C_K/C_D$  is below a threshold of 0.75. The dependence of the maximum tangential wind speed on the ratio  $C_K/C_D$  is investigated now in a second series of experiments (see Table 6.3).

The drag coefficient in the experiments C3 to C5 is decreased from  $1.86 \times 10^{-3}$  to  $1.3 \times 10^{-3}$  and then to  $1.0 \times 10^{-3}$ . These calculations use the same constant value for  $C_K$  as before ( $1.3 \times 10^{-3}$ ). Figure 6.9 shows time-series of  $v_{max}$  and  $rmax(v_b)$  for these experiments. During the gestation period, the intensification rate becomes slightly larger as the surface drag coefficient is increased (panel a). A more prominent feature is the different onset time of rapid intensification: as  $C_D$  is increased, the vortex starts to rapidly intensify earlier. A larger value for  $C_D$  leads to stronger inflow, and thus, to earlier grid-scale saturation on account of enhanced moisture convergence. As shown in Chapter 3, rapid intensification coincides with saturation on the grid-scale in the inner core. In the mature stage, however, the final intensity attained decreases as  $C_D$  is increased. At twelve days,  $v_{max}$  in the three calculations is  $54.2 \text{ m s}^{-1}$  ( $C_D = 1.86 \times 10^{-3}$ ),  $62.9 \text{ m s}^{-1}$  ( $C_D = 1.3 \times 10^{-3}$ ) and  $68.3 \text{ m s}^{-1}$  ( $C_D = 1.0 \times 10^{-3}$ ). A common feature of the vortex evolution in the three calculations is the period of reintensification that occurs after about six days. The intensity reaches a peak shortly after and eventually, the vortices start to slowly decay. With minor exceptions, throughout the whole time period,  $rmax(v_b)$  become smaller as the surface drag coefficient is increased. Only between about three and six days of integration, the values for  $rmax(v_b)$  become close to each other. During this time, the dependence of  $v_{max}$  on  $C_D$  reverses, *i.e.* the intensities become smaller as  $C_D$  is increased. However, the dependence of  $rmax(v_b)$  on  $C_D$  does not reverse.

Montgomery *et al.* (2010) showed that, when the ratio  $C_K/C_D$  is reduced from 1.3 to 0.7

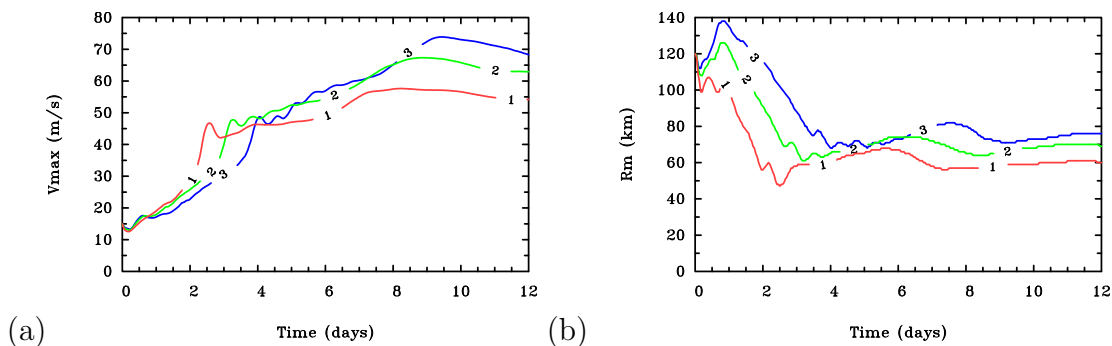


Figure 6.9: Legend as in Fig. 6.8, but in the experiment C3 (curve 1,  $C_D = 1.86 \times 10^{-3}$ ), C4 (curve 2,  $C_D = 1.3 \times 10^{-3}$ ), and C5 (curve 3,  $C_D = 1.0 \times 10^{-3}$ ).

(equivalent to increasing  $C_D$  from  $1.0 \times 10^{-3}$  to  $1.86 \times 10^{-3}$ ), the intensification rate and the maximum mean tangential wind speed increase noticeably. During the gestation period in the experiments presented herein, the intensity does increase with  $C_D$ . However, as mentioned above, this is due to enhanced moisture convergence associated with increased frictionally-induced inflow. During the mature stage, the dependence of  $v_{max}$  on  $C_D$  is reversed, *i.e.*  $v_{max}$  decreases as  $C_D$  is increased. Numerical experiments presented by Bryan and Rotunno (2009) with an axisymmetric numerical model show similar results to those here (see their Fig. 6). An interesting question is, why the sensitivity of  $v_{max}$  to  $C_K/C_D$  is opposite to the results from Montgomery *et al.* (2010).

In their introduction, Montgomery *et al.* (2010) explain that “in an inertial regime, where the inward advection of absolute angular momentum outweighs the frictional loss, an increase in drag could lead to an increase in intensity rather than a decrease because of an increase in the frictionally-induced inflow.” This explanation is based on the results of Smith *et al.* (2009) who showed that significant vortex spin-up can occur in the boundary layer, if the radial inflow is sufficiently large to bring the air parcels to small radii with minimal loss of angular momentum. It has been shown in Chapter 3 that this mechanism is responsible to spin up the inner core of the vortex in the axisymmetric model used herein. The time-series of the radius of maximum tangential wind speed show that, during the whole time period, as  $C_D$  is increased,  $v_{max}$  is located closer to the axis. However, such an inertial regime does not appear to prevail.

Montgomery *et al.* (2010) offer two reasons why their newly discovered functional relationship of  $v_{max}$  on  $C_D$  has gone unnoticed hitherto. As a first reason, they note that numerous numerical studies relied on models that assume a balanced boundary layer. It is clear that, in such models, the only dynamical role of the surface drag is to spin the vortex down. Therefore, using a balance model, the intensity decreases with an increasing drag coefficient. The second reason lies in the choice of the boundary-layer height. “If the slab boundary layer is too deep, [...], the gradient force in the frictional layer will be suitably small (Smith *et al.* 2008, Smith and Vogl 2008) and the dynamics will be slaved to behave like a balanced boundary layer.” In fact, this is presumably the reason why the functional relationship between  $v_{max}$  and  $C_K/C_D$  in Bryan and Rotunno (2009, their Fig. 6) and also

in the study herein is opposite to the relationship shown in Montgomery *et al.* (2010). The axisymmetric model used in this study has only one layer for the boundary layer, whose depth is about 900 m. Bryan and Rotunno (2009) use a vertical grid spacing of 250 m, whereas the vertical resolution in the study by Montgomery *et al.* (2010) is significantly larger with seven  $\sigma$ -levels below 850 mb (about 1.5 km). This fact motivates a future study addressing the following question: how would the results change as the vertical resolution of the present model is increased?

## 6.4 Capped surface enthalpy flux

### 6.4.1 Introduction

A recent study by Montgomery *et al.* (2009) addressed the challenging question as to whether the widely-accepted paradigm for tropical-cyclone intensification, WISHE, is essentially important for the spin-up process. In fact, these authors showed in a variety of numerical experiments using both a three-dimensional model and the axisymmetric model of Rotunno and Emanuel (1987), that a vortex can still intensify even if the surface wind speed in the formulae for the surface enthalpy fluxes is capped at a nominal (trade-wind) value of  $10 \text{ m s}^{-1}$  (see section 1.3.4). Following Montgomery *et al.*, it is interesting to investigate to what extent simulated vortices can intensify in the three-layer axisymmetric tropical-cyclone model used in this study when capping the surface enthalpy flux. The following experiments are carried out to address this question.

### 6.4.2 The calculations

In order to investigate the issue raised above, three calculations are carried out in which the wind-speed dependence of the surface enthalpy fluxes is capped at  $10 \text{ m s}^{-1}$ ,  $15 \text{ m s}^{-1}$  and  $20 \text{ m s}^{-1}$ , respectively. These calculations are compared to a control calculation, in which the wind-speed dependence of the surface fluxes is uncapped. Henceforth, the calculations with a cap in the surface enthalpy flux are referred to as D10, D15, and D20, respectively. One may conclude from section 6.2, that a calculation in which the radial diffusion is parameterized by the biharmonic damping term only (experiment B9) simulates a tropical cyclone of realistic strength. Accordingly, in order to reduce diffusive effects, the second-order diffusion scheme is not included here. In addition, in line with recent observations (see section 6.3),  $C_D$  is calculated as in Smith *et al.* (2011a) and  $C_K$  is set to  $1.3 \times 10^{-3}$ .

### 6.4.3 Results and interpretation

Figure 6.10 shows time-series of  $v_{max}$  in the four calculations. The vortex in the control calculation (with uncapped surface enthalpy flux) rapidly intensifies at about 62 hours of integration to approximately  $50 \text{ m s}^{-1}$ . Thereafter, the maximum intensity fluctuates a

little and temporarily levels out before being followed by another period where the intensity gradually increases before again levelling out. An approximate steady state is achieved after about seven days. At the end of the integration,  $v_{max}$  is  $74.9 \text{ m s}^{-1}$ . Capping the wind-speed dependence in the formulae for the surface enthalpy flux reduces the maximum tangential wind speed at any time. Nevertheless, the vortices undergo rapid intensification and the maximum tangential wind speed reaches hurricane-strength after 69 hours in D20, after 79 hours in D15, and after 149 hours in D10, respectively. The vortex evolution in both D20 and D15 is similar to that in the control calculation with a period of reintensification occurring after about eight days. Simulations in which the integrations are carried out beyond twelve days (not shown), however, reveal that  $v_{max}$  levels out shortly after. At twelve days, the maximum tangential wind speed is  $65.9 \text{ m s}^{-1}$  in D20 and  $56.9 \text{ m s}^{-1}$  in D15. Even when the wind-speed dependence in the formulae for the surface enthalpy flux is capped at  $10 \text{ m s}^{-1}$ , the vortex attains a maximum tangential wind speed greater than hurricane strength ( $37.8 \text{ m s}^{-1}$  at twelve days).

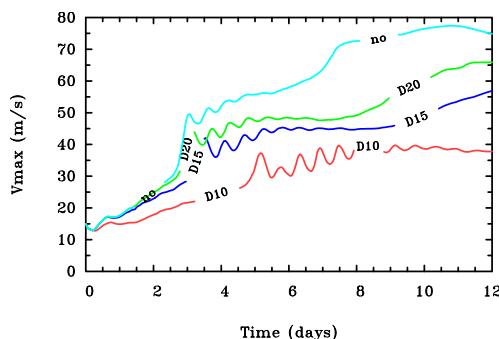


Figure 6.10: Time series of the maximum tangential wind speed in the lower layer. The curves labelled with D10, D15 and D20 correspond to the calculations where the wind-speed dependence in the formulae for the surface enthalpy flux is capped at  $10 \text{ m s}^{-1}$ ,  $15 \text{ m s}^{-1}$  and  $20 \text{ m s}^{-1}$ , respectively. The curve labelled with ‘no’ refers to the calculation where no corresponding cap is set.

Figure 6.11 shows radial profiles of the surface latent heat flux after 66 hours ( $\approx 2 \frac{3}{4}$  days) and at twelve days in the four calculations. Capping the wind speed at  $20 \text{ m s}^{-1}$  reduces the magnitude of the latent heat flux in the inner-core region to almost half of the values of the control run. However, at this stage, the vortices in these two simulations rapidly intensify at almost the same rate. The maximum values of the latent heat flux are about  $500 \text{ W m}^{-2}$  in D10,  $1000 \text{ W m}^{-2}$  in D15, and  $1400 \text{ W m}^{-2}$  in D20 after twelve days of integrations. Despite the fact that these values are very much smaller than the maximum values of about  $3400 \text{ W m}^{-2}$  in the control calculation at this time, the final intensities in these simulations exceed hurricane-strength.

The results presented in this section show that the three-layer axisymmetric model is able to produce storms that reach maximum tangential wind speed greater than hurricane-strength, even if the wind-speed dependence of the surface enthalpy flux is capped at nominal values as small as  $10 \text{ m s}^{-1}$ . Nevertheless, the mature intensity is smaller when



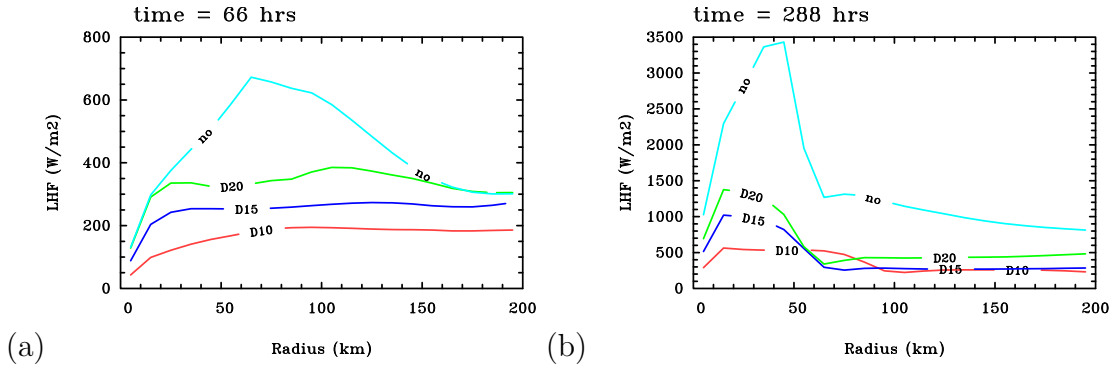


Figure 6.11: Radial profiles of the surface latent heat flux at (a) 66 hours and at (b) twelve days. Labels as in Fig. 6.10. Note the different scales in each panel.

the enthalpy flux is capped. These results are consistent with the axisymmetric results presented by Montgomery *et al.* (2009). However, in their three-dimensional calculations with capped and uncapped surface fluxes, the differences in  $v_{max}$  are not as large as in two-dimensional calculations. In the former case, the intensification proceeds by a pathway associated with vortical hot towers (see section 1.3.4). Nguyen *et al.* (2008) state that “the WISHE feedback mechanism that has previously been proposed to explain tropical-cyclone intensification in an axisymmetric framework has been found to be much less of a constraint in three dimensions.” They suppose “that this is partly because the VHTs are able to extract surface moisture fluxes that are locally sufficient for their growth without the wind-moisture feedback that typifies WISHE.” Montgomery *et al.* conclude that, although WISHE is not essential for tropical-cyclone intensification, in an axisymmetric framework WISHE “adds a considerable augmentation to the spin-up on time-scales of a few hours.” This conclusion is consistent with the findings presented herein.



# Chapter 7

## Summary and conclusions

This study has sought to develop a fundamental understanding of tropical-cyclone evolution in a minimal axisymmetric model. Although the scientific modelling of tropical cyclones has reached a high level of sophistication, a minimal numerical model has been regarded as the appropriate tool for basic research as it helps to separate crucial from incidental mechanisms.

It has been found recently that tropical-cyclone intensification is intrinsically a three-dimensional (asymmetric) process in which deep convective vortex structures, or “vortical hot towers” (VHTs), play a central role. However, one can usefully apply arguments based on the evolution of axisymmetric mean fields bearing in mind that the collective role of VHTs is to generate low-level convergence. In this spirit, and to retain maximum simplicity, this study examined axisymmetric aspects of tropical-cyclone dynamics.

An important part of the thesis sought to examine the rotational influences on the intensity and size of tropical cyclones, as characterized by the maximum tangential wind speed and the radius of gales, respectively. The classical Turner-Lilly-Morton ideas provided a helpful starting point for these investigations. These ideas are based on the premise that there are two fundamental requirements for vortex amplification: a source of rotation and some forcing mechanism to generate an overturning circulation to amplify the rotation. When switched on, the forcing mechanism acts to draw fluid parcels inwards, thereby increasing the tangential wind speed by conservation of absolute angular momentum. The increasing centrifugal and Coriolis forces associated with the increasing tangential velocity component tend to resist these displacements. The ultimate degree of amplification of the angular velocity during this adjustment period depends on how far rings of fluid can be drawn inwards and on the background rotation rate. How far rings of fluid can be drawn inwards depends, *inter alia*, on the forcing strength. If the forcing is sufficiently large for a given rotation rate, rings of fluid may be drawn in to relatively small radii before the centrifugal and Coriolis forces balance the radial pressure gradient induced by the forcing. If the forcing is comparatively weak, or if the rotation rate is sufficiently strong, this balance may be achieved before the radial displacement is very large, so that a significant amplification of the background rotation will not be achieved. Of course, if there is no background rotation, there will be no amplification, and if the background rotation is very

weak, the centrifugal and/or Coriolis forces may never become large enough to balance the radial pressure gradient.

Tropical cyclones have a large quasi-balanced component to their evolution and the forcing mechanism, rather than being impulsive, is associated with the radial gradient of the diabatic heating rate that results from the collective effects of deep vortical convective clouds. In this situation, the resistance to radial motion is associated more with the inertial stability of the vortex plus the ambient rotation.

Using a suite of idealized calculations with the minimal axisymmetric tropical-cyclone model, it has been shown that there is an optimum ambient rotation, characterized by the Coriolis parameter, for the largest vortex intensity and for the largest vortex size. The optimum ambient rotation corresponds to latitudes that lie between  $20.0^\circ\text{N}$  and  $30.9^\circ\text{N}$ , respectively. The former finding is consistent with earlier results of DeMaria and Pickle, but the latter is not. At first sight these findings appear to be broadly consistent with expectations from the Turner-Lilly-Morton ideas. However, a number of reasons have been identified why these ideas are of limited applicability to tropical cyclones. For one thing, the interpretations in the calculations described herein are complicated by the fact that the effective forcing is found to change with latitude, making it difficult to anticipate the outcome in a simple way.

For this reason, a second set of experiments was carried out with the vortex forced by a prescribed radial profile of diabatic heating rate typical of that in the first set of experiments and other moist processes excluded. For this distribution of heating, the maximum intensity increases monotonically with increasing rotation rate, even for unrealistically large rotation rates. However, there *is* an optimum rotation rate at about  $30^\circ\text{N}$  to produce the vortex with the largest size.

A more serious limitation of the Turner-Lilly-Morton ideas when applied to tropical cyclones is the fact that the spin-up of the maximum tangential winds in the tropical-cyclone inner core occurs in the boundary layer, where, because of friction, there is a net inward force, irrespective of the perceived inertial resistance to radial motion. In the boundary layer, absolute angular momentum is not conserved so that the Turner-Lilly-Morton ideas do not strictly apply. In consequence of this spin-up mechanism, a *simple* interpretation for the dependence of intensity and size of tropical cyclones remains elusive. However, this thesis offered an articulation of the key components of the dynamics, which helped to interpret the foregoing dependence. Because of several competing effects, one has to do the relevant calculation to determine which effects outweigh the others for a particular level of ambient rotation. When the forcing is held fixed, it has been shown that there are primarily two competing effects that provide an explanation for the existence of an optimum ambient rotation for the largest vortex size. For small values of the Coriolis parameter,  $f$ , the radial advection of absolute angular momentum,  $M$ , accounts for the largest contribution to the increase in the tangential wind speed with increasing  $f$ . For these values, the reduction of  $M$  by the vertical advection of lower values of  $M$  from the upper layer is correspondingly weak. However, as  $f$  increases, this reduction of  $M$  in the middle layer by downward advection becomes increasingly important. Thus, the radial advection of  $M$  is reduced also resulting in smaller-sized storms. There are two main

opposing effects that determine the radial profile of the tangential wind speed: one is the radial advection of absolute angular momentum and the other is the surface friction. In the fixed forcing calculations, as  $f$  increases, so does the radial gradient of  $M$ , but the radial velocity decreases, thereby increasing the loss of  $M$  to the surface. However, the increased radial gradient of  $M$  dominates, so that the largest values of the maximum tangential wind speed occurs for the largest value of  $f$ .

It has been found that the spin-up of the inner-core in the minimal model occurs in the boundary layer. A prominent feature of the hurricane boundary layer is gradient wind imbalance that implies a net agradiant force. This force generates strong inflow in the boundary layer. An examination of the movement of a passive tracer revealed that radial displacements are very much larger in the lower layer than in the middle layer. Thus, air parcel trajectories undergo only few revolutions per unit radial displacement and are therefore shorter in length so that friction has less distance over which to slow the parcels down. This means that the stronger the inflow in the boundary layer, the less is the reduction of absolute angular momentum. Consequently, although absolute angular momentum is not conserved in the boundary layer, significant spin-up can occur there if air parcels converge quickly enough towards relatively small radii. In fact, radial profiles of the contributions to the tangential momentum equation confirmed that this spin-up process occurs in the present model. Precisely, it acts to intensify the inner-core, where the flow becomes supergradient. Furthermore, it has been shown that the spin-up of the middle layer in the inner-core region occurs by vertical advection of the supergradient winds from below. In the same annular region, there is a strong outward flux of absolute vorticity in the middle layer, equivalent to a negative radial advection of absolute angular momentum, which, by itself would rapidly spin down the vortex.

The radial profiles of the contributions to the tangential momentum equation in the middle layer revealed further that, at radii beyond approximately 80 km, there is an inward flux of absolute vorticity. Thus, the spin-up there, *i.e.* the increase in vortex size, is associated with the radial convergence of absolute angular momentum. It has been shown in this thesis that, during the first few days of vortex evolution, there is little correlation between the evolution of the vortex intensity and the evolution of the vortex size, a result that is consistent with observations by Weatherford and Gray. However, in the ‘moist’ calculations that examined the sensitivity to the Coriolis parameter, it has been shown that for more intense storms ( $v_{max} > 35 \text{ m s}^{-1}$ ), there is an approximate linear increase in the radius of gales with intensity. Due to the occurrence of intense midget storms, one has to be cautious about the generality of this relationship. The intensity and size of the vortex are governed by two different mechanisms that are not completely independent from each other. There must be a degree of coupling through boundary-layer dynamics. Due to the approximate linear increase in vortex size with intensity, one may speculate that this coupling may become more important as the vortex evolves.

It has been shown that, during the development of the vortex, regions develop where a necessary criterion of inertial instability is fulfilled. Due to the coarse vertical resolution of the model, it is highly unlikely that inertially unstable motions occur. However, it was shown that the development of these regions has implications for the evolution of

the vortex size. These regions coincide with regions where the radial gradient of absolute angular momentum becomes negative. Therefore, if there is inflow, the vortex size becomes smaller due to conservation of absolute angular momentum.

A study of the model sensitivity to the horizontal resolution showed that the vortex size is little affected when the grid spacing is varied. The maximum intensity increases only slightly as the horizontal resolution is increased. This finding implies that the results of the sensitivity experiments to the background rotation rate are independent of the horizontal resolution. However, it was shown that there is a strong sensitivity of the maximum tangential wind speed to the turbulent diffusivity, with the maximum intensity increasing as the eddy diffusivity is decreased. These results are consistent with those of Bryan and Rotunno, who show that turbulence in the radial direction leads, *inter alia*, to weaker radial gradients of absolute angular momentum. Consequently, absolute angular momentum has not been advected as far towards the centre as in the less diffusive simulations. Furthermore, it was shown that it is the radial advection of absolute angular momentum *within* the boundary layer that becomes larger in magnitude as the horizontal eddy diffusivity is decreased.

It was shown that increasing the surface drag coefficient leads to an earlier onset of rapid intensification, however, the final intensity is decreased. These findings are consistent with the second aspect of what has been referred to as the conventional view of tropical-cyclone spin-up. From the thermodynamical point of view, an increased value for the surface drag coefficient increases the boundary-layer inflow and thereby the moisture convergence which, in turn, leads to earlier grid-scale saturation in the inner core. It was shown that the grid-scale saturation coincides with the onset of rapid intensification. The conventional view of tropical-cyclone spin-up considers the dynamical role of the boundary layer to be that which spins the vortex down. The results of the sensitivity experiments presented in this thesis are in line with this perception. However, these results are contrary to those of Montgomery *et al.* Using a high-resolution three-dimensional model, these authors showed that increasing the surface drag leads to an *increase* in intensity. They explain that “in an inertial regime, where the inward advection of absolute angular momentum outweighs the frictional loss, an increase in drag could lead to an increase in intensity rather than a decrease because of an increase in the frictionally-induced inflow.” The seemingly paradoxical (dynamical) role of the boundary layer was discussed in the early 1970s by Anthes, and is clearly distinct from the dual role of the boundary layer as perceived in the conventional view of tropical-cyclone spin-up. It has been speculated that the low vertical resolution of the minimal model used for this study explains why the results of the sensitivity experiments presented herein are contrary to those of Montgomery *et al.*

In a final set of experiments, it was shown that the three-layer axisymmetric model is able to produce storms that reach maximum tangential wind speed greater than hurricane-strength, even if the wind-speed dependence of the surface enthalpy flux is capped at nominal values as small as  $10 \text{ m s}^{-1}$ . These results are consistent with those of Montgomery *et al.* and show that the ‘evaporation-wind’ feedback mechanism known as WISHE is not essentially important for tropical-cyclone intensification. However, in this axisymmetric framework, suppressing the WISHE-mechanism leads to considerable weakening of the

final intensities.

The results of this thesis point to the existence of dynamical constraints that are not explicitly included in existing theories for the maximum possible intensity of tropical cyclones. The study of the rotational influences on tropical-cyclone intensification and final intensity is a first step to try to understand hitherto unexplored aspects of tropical-cyclone spin-up. While the use of a minimal model was suitable for this study in order to retain maximum simplicity, it would be worth repeating these calculations using a more sophisticated three-dimensional, nonhydrostatic model. For further future studies, it may prove useful to scale the dependent and independent variables of the model and investigate whether dimensionless parameters exist that govern the intensity and/or size of hurricanes. Further research into the effects of turbulence appears necessary, as these are still poorly understood, but have been shown to have a strong influence on the maximum intensity. The sensitivity experiments that examined the dependence of the maximum intensity on the surface drag coefficient raised the question how the results would change as the vertical resolution of the present model is increased. This issue would be worth investigating. Based on the discussion in this thesis, one may surmise that an inertial regime prevails using a sufficiently high vertical resolution, where an increase in the surface drag coefficient leads to an increase of the vortex intensity.





# Appendix

## APPENDIX A

### *The initial sounding data*

Table 7.1: The initial pressure (p), temperature (T), specific humidity (q), and geopotential height ( $\Phi$ ) in the middle of each layer and at the interface levels in the far field.

$\sigma$	p (hPa)	q (g/kg)	T (K)	$\Phi$ (m <sup>2</sup> s <sup>-1</sup> )
$\sigma_1 = 1/6$	252.5	0.01	230.4	109414
$\sigma_2 = 1/3$	405.0	0.15	256.1	75058
$\sigma_3 = 11/18$	659.2	4.82	278.9	37827
$\sigma_4 = 8/9$	913.3	13.6	293.8	9284
$\sigma_b = 17/18$	964.2	14.0	297.0	4438

## APPENDIX B

### *Diabatic heating calculation*

The maximum magnitude of the negative radial gradient of the diabatic heating rate, i.e.  $\max(-\partial\dot{\theta}/\partial r)$ , has been chosen as an appropriate measure for the effective forcing. The reasons for it are explained in section 4.4. The thermodynamic equation is solved for  $\theta$  without the diabatic term  $Q_\theta$ .

$$\frac{\partial\theta}{\partial t} = -u\frac{\partial\theta}{\partial r} - \dot{\sigma}\frac{\partial\theta}{\partial\sigma} + Q_\theta \quad (7.1)$$

After each time integration step, heating contributions from the cumulus parameterization scheme and explicit condensation on the grid scale are added to  $\theta$ . The diabatic heating rate for each time step is then the difference of both values of  $\theta$  divided by the integration time step, which was taken to be 6 sec for all calculations. From this value, the maximum negative radial gradient can easily be calculated.

APPENDIX C  
*Fixed forcing specification*

In the calculations with a fixed forcing, the diabatic heating rate was prescribed by the formula

$$\dot{\theta} = 2aQ_0 \left( \frac{R - 0.5R_0}{R_0} \right)^4 \exp \left[ - \left( \frac{R - 0.5R_0}{R_0} \right)^4 \right] T(t), \quad (7.2)$$

where  $T(t) = 1 - \exp[-(t/t_0)^2]$ ,  $t$  is the time,  $Q_0 = 600 \text{ K day}^{-1}$ ,  $R_0 = 40 \text{ km}$ ,  $t_0 = 24$  hours, and  $a$  is a factor specific for each model level. This diabatic term was added in the middle ( $a = 1.1$ ) and upper layer ( $a = 1.8$ ). For the boundary layer ( $a = 3.3$ ), a slightly different formula for the diabatic heating rate was used, which takes into account, that its maximum is closer to the storm centre, *i.e.*,

$$\dot{\theta} = 2aQ_0 \left( \frac{R}{R_0} \right)^4 \exp \left[ - \left( \frac{R}{R_0} \right)^4 \right] T(t). \quad (7.3)$$

The spatial variation of  $\dot{\theta}$  is similar to the one used by Möller and Smith (1994). The time dependence,  $T(t)$ , is included to avoid the shock of imposing a finite value of diabatic heating at the initial instant.

# Acknowledgements

I wish to express particular thanks to my supervisor, Prof. Roger Smith for providing me the opportunity to work on this interesting field, tropical cyclones. His support with a wealth of information and fruitful discussions has guided me effectively throughout the completion of this thesis. I am grateful to have had the opportunity to participate in international conferences and to visit meteorological research centres in the US.

Thanks go to Prof. Michael Montgomery for interesting discussions on tropical cyclones.

I am also grateful to Prof. George Craig and Prof. Kerry Emanuel for their useful comments and advice.

I am indebted to my colleague Gerard Kilroy who had a lot of patience and was always willing to help me when I had questions concerning the language.

Thanks go to Heinz Lösslein for his help on any technical problems.

Besonders bedanken möchte ich mich bei meinen guten Freunden Karl Betz und Steffi Vogl, die meinen Blick immer dann auf andere Dinge lenkten, wenn dies nötig war.

Ein sehr persönlicher Dank gilt meiner Familie für ihr Verständnis und ihre Unterstützung während der letzten Jahre.

This work has been generously supported by the German Research Council.





# Lebenslauf

## Persönliche Daten

Name Christoph Wolf Dieter Jakob Schmidt  
geboren am 28. Dezember 1978  
Geburtsort Fürstenfeldbruck  
Familienstand ledig

## Studium/Schulbildung

seit 07/2008	Promotion am Meteorologischen Institut München, Fakultät für Physik, Ludwig-Maximilians-Universität München
10/2004 – 06/2008	Studium der Meteorologie an der Ludwig-Maximilians-Universität München
06/2008	Diplom in Meteorologie Diplomarbeit: Nonlinear waves ahead of fronts in the Great Australian Bight
08/2005 – 06/2006	Studium der Meteorologie, Glaziologie und Ozeanographie am University Centre in Svalbard (UNIS), Norwegen
10/2002 – 10/2004	Studium der Geophysik an der Ludwig-Maximilians-Universität München
10/2004	Vordiplom in Geophysik
10/1999 – 10/2002	Studium der Humanmedizin an der Ludwig-Maximilians-Universität München
09/2001	Physikum
09/1989 – 06/1998	Besuch des Gymnasiums Olching
06/1998	Abitur
09/1985 – 07/1989	Besuch der Grundschule Esting